MECHANISM OF THE HYDROPYROLYSIS OF MANVERS COAL

BY

NAVTEJ SINGH NOOR

A THESIS SUBMITTED FOR THE DEGREE OF
DOCTOR OF PHILOSOPHY
IN THE
UNIVERSITY OF ASTON IN BIRMINGHAM

February 1985

THE UNIVERSITY OF ASTON IN BIRMINGHAM

MECHANISM OF THE HYDROPYROLYSIS OF MANVERS COAL

BY

NAVTEJ SINGH NOOR

A THESIS SUBMITTED FOR THE DEGREE OF DOCTOR OF PHILOSOPHY, FEBRUARY 1985

SUMMARY

Manvers coal has been pyrolysed to 500^{o}C in a stirred autoclave under various pressures of nitrogen (pyrolysis) and hydrogen (hydropyrolysis). All products were investigated.

Pyrolysis of coals involves the transfer of hydrogen atoms from one part of their structure to another. In the above experiments there was no way of labelling the hydrogen or of distinguishing between hydrogen which was initially part of the coal and hydrogen originating in the external atmosphere. Consequently, Manvers coal has been pyrolysed in an atmosphere of deuterium in order to obtain greater insight into the mechanism of hydropyrolysis. In particular it was hoped to distinguish between direct hydrogenation (deuteration!) of the coal and the products of pyrolysis and the 'shuttling' of hydrogen atoms between different parts of the pyrolysing coal.

The addition to the coal of 5% (wt.% of coal) of either tetralin or pyrite was also studied.

A variety of techniques were used to analyse the products of pyrolysis: gas chromatography - mass spectrometry and high performance liquid chromatography for tars; thermal conductivity gas chromatography and high resolution mass spectrometry for gases; methanol densities, microporosities and diffuse reflectance infra red spectroscopy for the cokes (chars); refractive index to determine deuterium in the liquor.

An attempt has been made to apply basic thermodynamics to reactions which are likely to occur in the hydropyrolysis of coals.

Diffusion and effusion rates for hydrogen and tar molecules have also been estimated.

Key words: Coal, Pyrolysis, Hydropyrolysis, Kinetics

ACKNOWLEDGEMENTS

To my supervisor, Dr. A.F. Gaines, I wish to express my sincere thanks for his encouragement, guidance and continual unfailing interest throughout the course of this work.

I am grateful to Dr. M.J. Crook (British Petroleum) for help with the HPLC measurements, to Dr. M. Thorley (British Gas Corporation) who measured the surface areas.

I wish to thank the members of the technical staff in the Department of Chemistry for their assistance, especially Mr. M. Perry for obtaining high resolution mass spectra.

I would like to thank my colleagues, Maureen Davis and Keith Torrence for their help and advice during this work.

I am greatly indebted to my wife, Deborah, for typing the tables.

I would like to thank Mr. E.E. Warner (Wolverhampton Council for Community Relations) for the generous loan of a typewriter.

CONTENTS

LIST OF FIGURES

PAGE

CHAPTER FIVE

CHAPTER SIX

LIST OF PLATES

LIST OF TABLES

PAGE

CHAPTER TWO

CHAPTER THREE

CHAPTER FOUR

LIST OF APPENDICES

CHAPTER ONE

INTRODUCTION

CHAPTER ONE

INTRODUCTION

1.1 Pyrolysis of coal at atmospheric pressure

The pyrolysis of coals at atmospheric pressure may be represented by the sequence of four reactions shown in scheme 1. Hydroaromatic structures dehydrogenate to give an extended aromatic network which becomes incorporated into the coke or char. About as much hydroaromatic material becomes aromatic as aromatic material forms tar[1]. The occurrence of

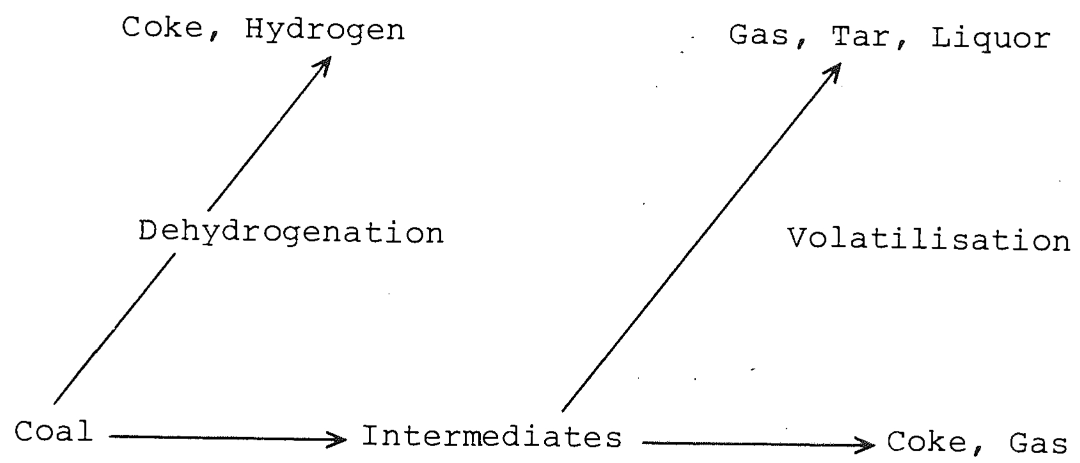

Scheme 1

the dehydrogenation reaction is consistent with the pyrolysis of model compounds and has been observed in lignites by infra red spectroscopy[2].

The hydrogen released diffuses through the solid fuel and causes rupture of aliphatic bonds. Generally this will result in the removal of alkyl groups to form gas, the formation of water from hydroxyl groups and the scission of certain C-C and C-O bonds linking aromatic nuclei and it is not until such reactions are nearly complete that significant quantities of hydrogen gas are evolved from the pyrolysis. The scission of C-C and C-O bonds is accompanied by the creation of free radicals[3,4] some of which recombine to yield extended structures which eventually form coke or char and gas.

The presence of mobile, 'intermediate' material (metaplast) of moderate molecular weight confers fluidity on the coal system[5]. Relatively small changes in the concentration of mobile intermediate make large differences to the fluidity[6]. The viscosity[7] (reciprocal of fluidity) of coal determined by proton magnetic resonance (p.m.r.) suggests that coal becomes fluid due to the depolymerisation of the initially rigid coal structure (followed at a higher temperature and/or time by recondensation of a significant part of the material). However, it should be noted that in the p.m.r. studies of coal only a small sample of coal was used (approximately 500mg) and that p.m.r. measures the molecular properties of a confined sample whereas the Gieseler plastometer measures a bulk viscosity.

In a static bed the reactions in scheme 1 are all diffusion controlled. The scheme is sufficient to describe both the rate of development of fluidity and the loss of weight measured by thermogravimetric analysis. More complex schemes have been reviewed by Howard[8] and by Gavalas[9].

Coal pyrolysis starts at about 350°C; this is considerably lower than the temperature of most gas phase pyrolyses but significantly higher than the temperatures at which weak bonds break and initiate the pyrolysis of polymers. The nature of the initiation of coal pyrolysis remains obscure. However, it may not be a coincidence that the pyrolysis of tetralin also starts at about 350°C[10,11] and it is possible that the pyrolysis of coal is actually started by the dehydrogenation of hydroaromatic structures. This could be initiated by the disruption of trace quantities of hydroperoxides which will inevitably be present in some of the hydroaromatic structures though as yet there is no supporting experimental evidence. It is well established that coals which have been chemically dehydrogenated neither yield volatile products on pyrolysis nor generate coke[1,12], more recently infra red spectra have suggested that coke formation has involved the breaking of ether linkages[13,14,15]. This may be interpreted by supposing that coking coals possess the appropriate combinations of ether linkages and hydroaromatic structures to confer maximum concentrations of low molecular weight intermediates and thus maximum fluidity on the pyrolysing system. The direct determination of ether linkages in coals has led to conflicting results. They should be broken by many reagents consisting of alkaline metals in a solvent containing 'lone pair' electrons. Some workers using such reagents have denied the presence of ether linkages[16], yet if the reagents which form 'coal anions' are followed by treatment with an alkyl iodide[17,18,19] the coal acquires solubility in organic liquids. Evidence suggests that it may be the coking coals which are rendered most soluble in this way.

1.2 Aims of present research

1.2.1 Calculation of thermodynamic and kinetic parameters relating to the hydropyrolysis of coal

Chapter 2 shows the application of basic thermodynamics to reactions which are likely to occur in the hydrogenation of coals. Obviously a more detailed kinetic analysis is necessary to show that the reactions do occur in the solid state at a measurable rate at the temperatures at which coal pyrolyses. Knowledge of the physical structure of coal leads to the realisation that it may well be that diffusion/effusion and not rates of reactions is the slow process during pyrolysis/hydropyrolysis. With this in mind diffusion and effusion rates for hydrogen atoms and tar molecules have been estimated (chapter 2).

1.2.2 Pyrolysis, hydropyrolysis and deuteropyrolysis of a bituminous coal: Manvers

Most of the description of coal pyrolysis outlined in section 1.1 has been based on work conducted at atmospheric pressure. One of the aims of this research is to consider to what extent the description needs altering to account for the effects of pressure (chapter 4), in particular hydrogen pressures (chapter 5).

The hydropyrolysis of coals has been reviewed by Howard[20] and by Furfari[21]. Further experimental work not included in these reviews has been obtained by Cyprès and Furfari[22]. Recently, Geoffrey and his colleagues[23] have studied the pyrolysis and hydropyrolysis of two British coals (a high volatile bituminous and an anthracite) and an Australian brown coal to determine the effects of an increased ratio of hydrogen to coal. However, no attempt was made to distinguish between the effects of increased pressure and of an increased ratio of hydrogen to coal.

The interdependence of the reactions comprising the low temperature carbonisation (pyrolysis) in scheme 1 implies that the hydrogen atoms originally present in the fuels become redistributed amongst the products of pyrolysis. In hydropyrolysis there is an excess of hydrogen in contact with the pyrolysing coal and as hydropyrolysis commences the hydrogen may be consumed and become redistributed amongst the products of pyrolysis. This redistribution of hydrogen is perhaps the key to the mechanism of hydropyrolysis. With this in mind the hydrogen atmosphere was labelled using deuterium instead of hydrogen in the hydropyrolyses. In this way it was possible to follow where the deuterium/hydrogen atoms went on deuteropyrolysis/hydropyrolysis.

A small range of catalysts has been studied so as to determine their effect on the distribution of deuterium amongst the products of deuteropyrolysis.

CHAPTER TWO

THERMODYNAMICS AND THE KINETICS OF THE HYDROGENATION OF BITUMINOUS COALS

CHAPTER TWO

THERMODYNAMICS AND THE KINETICS OF THE HYDROGENATION OF BITUMINOUS COALS

2.1 Thermodynamics

2.1.1 Introduction: Coal Model

Suppose that coal consists of molecules of at least moderately high molecular weight. Let $R_1 - R_2$ be such a coal molecule and let:

$$R_1 - R_2 + H_2 \longrightarrow R_1H + R_2H$$

be a typical hydrogenation reaction. The Gibbs free energy change in such a reaction will be different if the products R_1H and R_2H are volatile or involatile. In general it may be supposed that the molecular weights are so large that the products are involatile.

Typical hydrogenation reactions have been considered and the conditions under which the Gibbs free energy change is less than zero determined. In order to make the reactions precise it has been necessary to consider rather simple models of coal molecules. Thus in the reaction:

$$C_6H_5OH\ (s) + H_2(g) \longrightarrow C_6H_6(s) + H_2O\ (g)$$

it has been assumed that the phenyl group is part of a large coal molecule and that consequently both phenol and benzene may be considered as solids. Similarly in a reaction such as:

$$C_6H_5CH_2C_6H_5\ (s) + H_2\ (g) \longrightarrow C_6H_6\ (s) + C_6H_5CH_3\ (s)$$

all the molecules save hydrogen remain attached to coal and therefore remain solid throughout the hydrogenation.

2.1.2 Thermodynamic calculations

The thermodynamic data of selected molecules is given in appendix 1, table 1 and the thermodynamic analysis (heat of reaction, entropy of reaction and Gibbs free energy change) is given in appendix 1, table 2. A procedure for calculating the thermodynamic quantities presented in appendix 1, table 2 has been included in appendix 1.

2.1.3 Summary of thermodynamic calculations

1. Alkanes + H_2 $\longrightarrow$ Mixture of smaller alkanes

$$CH_3CH_2CH_3\ (g) + H_2\ (g) \longrightarrow C_2H_6\ (g) + CH_4\ (g)$$

$$nC_{18}H_{38}\ (s) + H_2\ (g) \longrightarrow C_{16}H_{34}\ (s) + C_2H_6\ (g)$$

Reactions are exothermic, the entropy change is positive and the reactions can occur under all practical conditions.

2. $C_6H_5CH_3$ (s) + H_2 (g) $\longrightarrow$ C_6H_6 (s) + CH_4 (g)

C_6H_5OH (s) + H_2 (g) $\longrightarrow$ C_6H_6 (s) + H_2O (g)

Reactions are exothermic, the entropy change is positive and the reactions can occur under all practical conditions.

3. $C_6H_5(CH_2)_nCH_3$ (s) + H_2 (g) $\longrightarrow$ $C_6H_5(CH_2)_{n-1}CH_3$ (s) + CH_4 (g)

Reactions are exothermic, the entropy change is positive and the reactions can occur under all practical conditions.

4. $C_6H_5NH_2$ (s) + H_2 (g) $\longrightarrow$ C_6H_6 (s) + NH_3 (g)

C_6H_5SH (s) + H_2 (g) $\longrightarrow$ C_6H_6 (s) + H_2S (g)

$C_6H_5SC_6H_5$ (s) + H_2 (g) $\longrightarrow$ C_6H_6 (s) + C_6H_5SH (s)

No thermodynamic estimates have been made.

5. $C_6H_5CH_2C_6H_5$ (s) + H_2 (g) $\longrightarrow$ C_6H_6 (s) + $C_6H_5CH_3$ (s)

Reaction is exothermic and the entropy change is positive and the reaction can occur under all practical conditions. Increase in pressure causes the Gibbs free energy (ΔG) to become more negative and the reaction becomes even more likely.

6. $C_6H_5CH_2CH_2C_6H_5$ (s) + H_2 (g) $\longrightarrow$ $2C_6H_5CH_3$ (s)

Reaction is exothermic and the entropy change is positive; the reaction can occur under all practical conditions. Increase in pressure causes ΔG to become more negative and therefore making the reaction even more likely.

7. $C_6H_5C_6H_5$ (s) + H_2 (g) $\longrightarrow$ C_6H_6 (s) + C_6H_6 (s)

The reaction is slightly endothermic ($\Delta H^{o}_{R,298}$ = 1.51 KJ mol^{-1}) and the entropy change is negative ($\Delta S^{o}_{R,298}$ = - 42.41 J $mol^{-1}K^{-1}$) which makes ΔG positive and the reaction is not feasible even at moderate pressures ($\leq$ 1000 atmospheres). At very high pressures ($\geq$ 1000 atmospheres) ΔG for the reaction does become negative and therefore the reaction is 'on'.

8. $C_6H_5OC_6H_5$ (s) + H_2 (g) $\longrightarrow$ C_6H_5OH (s) + C_6H_6 (s)

Reaction is exothermic and the entropy change is negative; the reaction can occur under all practical conditions. Increase in pressure causes ΔG to become more negative.

9. Hydroaromatic system $\longrightarrow$ Aromatic system + H_2

Reactions are endothermic and the entropy change is positive. ΔG is positive at 298 K (1 atmosphere) but at about 800 K (1 atmosphere) it becomes negative and with increase in pressure ΔG becomes less negative.

For example:

a. Tetralin (s) $\longrightarrow$ Naphthalene (s) + $2H_2$ (g)

At 1 atmosphere $\Delta G = 0$ when T = 469 K

At 100 atmospheres $\Delta G = 0$ when T = 564 K

At 1000 atmospheres $\Delta G = 0$ when T = 627 K

b. 9,10-Dihydrophenanthrene (s) $\longrightarrow$ Phenanthrene (s) + H_2 (g)

At 1 atmosphere $\Delta G = 0$ when T = 429K

At 100 atmospheres $\Delta G = 0$ when T = 640 K

At 1000 atmospheres $\Delta G = 0$ when T = 848 K

10. $C_6H_5OC_6H_5$ (s) + H_2O (g) $\longrightarrow$ $2C_6H_5OH$ (s)

Reaction is exothermic but the entropy change is negative and ΔG, although negative at 298 K and 1 atmosphere, is markedly positive at 800 K and 1 atmosphere. However, reaction is possible above 455 K at 1 atmosphere and above 658 K at 100 atmospheres and above 848 K at 1000 atmospheres.

2.1.4 Thermodynamic Analysis: Conclusions

The thermodynamic analysis (appendix 1, table 2) indicates that one may hydrogenate coal molecules to remove all peripheral groups as simple gases such as methane and ethane and water as steam and also as simple molecules such as benzene and toluene when these are attached to the coal only by a single bond. One may expect ammonia and hydrogen sulphide to be generated in the same way. Coal molecules may be broken into involatile fragments by hydrogenation only when they contain ether linkages or aromatic groups separated by certain methylene bridges. There is, of course an exception to this when molecules contain strings of fairly simple groups R_1, R_2, R_3 linked by single bonds. Such molecules can be unzipped by hydrogen removing successive volatile groups from the ends of the molecule.

When bituminous coals are heated in excess hydrogen the resulting 'coal liquid' generally resembles a pitch. One expects that the molecules of the pitch will be similar to those of the original coal with peripheral groups removed, with ether linkages broken and probably with the dehydrogenation of hydroaromatic groups.

2.2 Kinetics of the Hydropyrolysis of Coal

2.2.1 Introduction

The thermodynamic treatment has indicated the likelihood of typical reactions (hydrogenation and dehydrogenation) occurring at the pyrolysis temperature of coal. A more detailed kinetic analysis is necessary to show that the reactions do occur in the solid state at a measurable rate at the temperatures at which coal pyrolyses.

Knowledge of the physical structure of coal leads to the realisation that it may well be that diffusion/effusion and not rates of reaction is the slow process during liquefaction and pyrolysis. With this in mind diffusion and effusion rates for hydrogen atoms and tar molecules have been calculated. We have considered the diffusion of hydrogen and tar molecules in softening and nonsoftening coals. When calculating diffusion and effusion rates it has been assumed that there are no heat transfer limitations. The analysis of heat transfer in coal pyrolysis has been reviewed by Gavalas[24].

2.2.2 Diffusion in Softening Coals

Here, the diffusion of hydrogen and tar molecules through the fluid coal will be considered. Diffusion constants have been calculated using the Stokes - Einstein equation:

$$D = kT / 6\pi\mu a \qquad (m^2 s^{-1})$$

Where: D is the diffusion constant, $m^2 s^{-1}$

μ is the viscosity, Kg m^{-1} s^{-1}

a is the radius of the diffusing molecule, m

k is the Boltzmann constant, JK^{-1}

T is the temperature, K

Dividing the Stokes - Einstein equation by L^2 gives units of rate (rate units of s^{-1} have been used throughout this chapter. These units are those of a first order velocity constant.):

$$D/L^2 = kT / 6\pi\mu a L^2 \qquad (s^{-1})$$

Where L is the length, in metres, characteristic of the diffusion, approximately the average distance that hydrogen has to diffuse before reaction. L depends on the effective size of the coal bed: for loose beds L is approximately the size of the particles; for tightly packed beds, L is approximately the size of the bed of coal.

Diffusion through 'fluid coal' is very dependent on temperature because the viscosity (the reciprocal of fluidity) of the system changes rapidly with temperature. There is little data on the viscosity of coals in an atmosphere of hydrogen and consequently data obtained for pyrolysis in an inert atmosphere has been used. A good coking coal has a plastic (fluidity) range of about 80°C and a minimum viscosity of $10^3 - 10^4$ Kg m^{-1} s^{-1} ($10^4 - 10^5$ poise)[25,26]. A highly volatile coal has a minimum viscosity of $10^5 - 10^6$ Kg m^{-1} s^{-1} ($10^6 - 10^7$ poise). The variation of viscosity with temperature for a coking coal [27] is shown in figure 2.1.

Diffusion constants and diffusion rates for hydrogen and tar molecules in a coking coal and a highly volatile coal have been calculated using the following data:

μ	from the plot of viscosity versus temperature, figure 2.1
a	for the hydrogen molecule is: 0.37Å (0.37×10^{-10}m)
	for the tar molecules is : 4Å (4×10^{-10}m)
T	Temperature in Kelvin corresponding to the viscosity, figure 2.1
k	Boltzmann's Constant: 1.38×10^{-23} JK^{-1}
L	for a particle L = 10^{-3}m
	for a bed of coal L = 10^{-2} (1cm bed)
	for a bed of coal L = 10^{-1}(10cm bed)

For estimation purposes the viscosity of a highly volatile coal has been taken as 100 times greater than the viscosity of a coking coal at a particular temperature.

Diffusion constants for hydrogen and tar molecules are shown in tables 2.1a (page 16) and 2.2a (page 18) respectively. Diffusion rates for hydrogen and tar molecules are shown in tables 2.1b (page 17) and 2.2b (page 19) respectively.

Figure 2.1

The Variation of Viscosity with Temperature for a Coking Coal

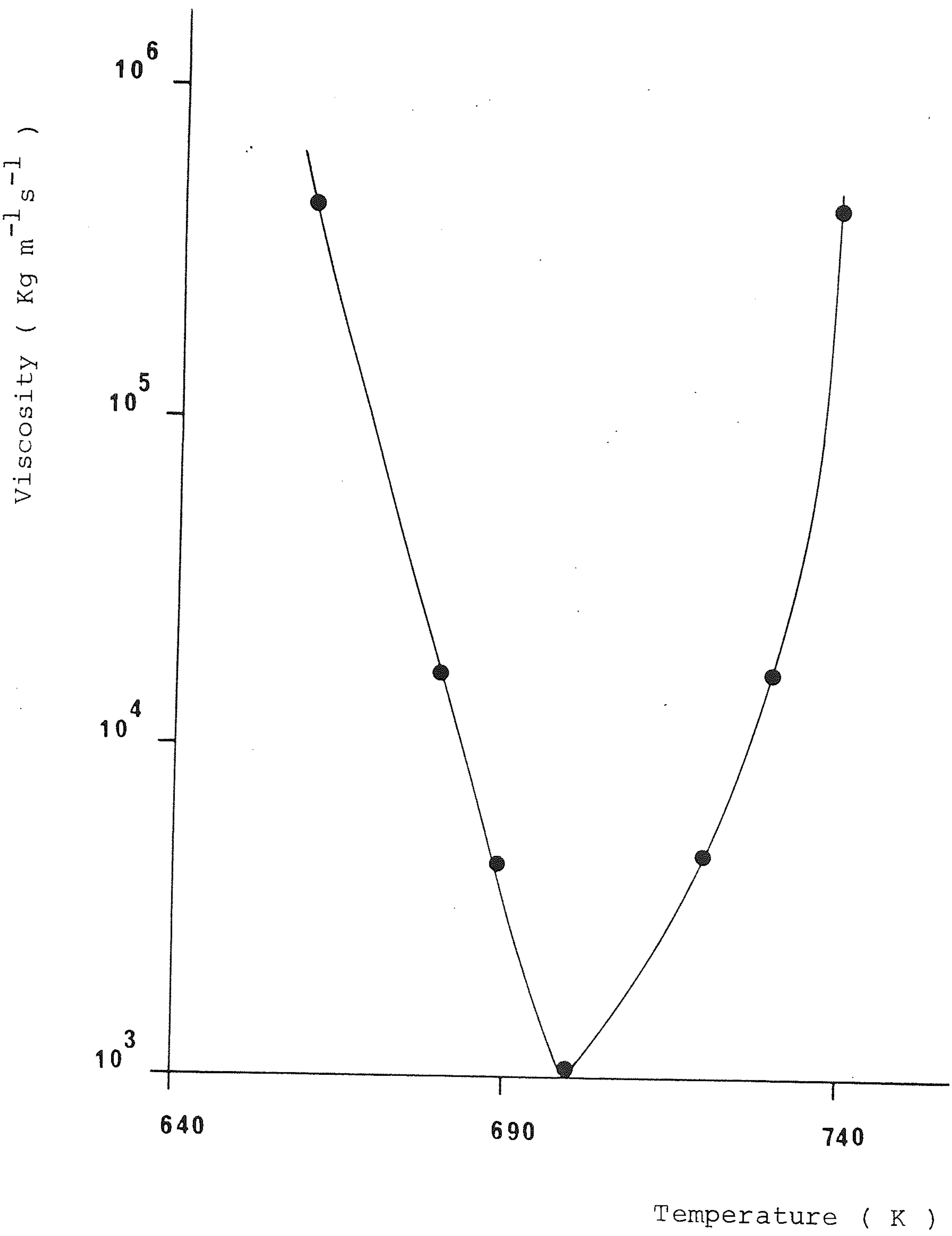

Table 2.1a Diffusion Constants for Hydrogen Molecules in Fluid Coal

Temperature (K)	Coking Coal Diffusion Constant D ($m^2 s^{-1}$)	Highly Volatile Coal Diffusion Constant D ($m^2 s^{-1}$)
660	2.2×10^{-17}	2.2×10^{-19}
670	1.5×10^{-16}	1.5×10^{-18}
680	6.7×10^{-16}	6.7×10^{-18}
700	1.4×10^{-14}	1.4×10^{-16}
720	2.1×10^{-15}	2.1×10^{-17}
730	6.3×10^{-16}	6.3×10^{-18}
740	2.3×10^{-17}	2.3×10^{-19}

Table 2.1b Diffusion Rates for Hydrogen Molecules in Fluid Coal

Temperature (K)	Coking Coal Diffusion Rate D/L^2 (s^{-1})			Highly Volatile Coal Diffusion Rate D/L^2 (s^{-1})		
	$L = 10^{-3}m$	$L = 10^{-2}m$	$L = 10^{-1}m$	$L = 10^{-3}m$	$L = 10^{-2}m$	$L = 10^{-1}m$
660	2.2×10^{-11}	2.2×10^{-13}	2.2×10^{-15}	2.2×10^{-13}	2.2×10^{-15}	2.2×10^{-17}
670	1.5×10^{-10}	1.5×10^{-12}	1.5×10^{-14}	1.5×10^{-12}	1.5×10^{-14}	1.5×10^{-16}
680	6.7×10^{-10}	6.7×10^{-12}	6.7×10^{-14}	6.7×10^{-12}	6.7×10^{-14}	6.7×10^{-16}
700	1.4×10^{-8}	1.4×10^{-10}	1.4×10^{-12}	1.4×10^{-10}	1.4×10^{-12}	1.4×10^{-14}
720	2.1×10^{-9}	2.1×10^{-11}	2.1×10^{-13}	2.1×10^{-11}	2.1×10^{-13}	2.1×10^{-15}
730	6.3×10^{-10}	6.3×10^{-12}	6.3×10^{-14}	6.3×10^{-12}	6.3×10^{-14}	6.3×10^{-16}
740	2.3×10^{-11}	2.3×10^{-13}	2.3×10^{-15}	2.3×10^{-13}	2.3×10^{-15}	2.3×10^{-17}

Table 2.2a Diffusion Constants for Tar Molecules in Fluid Coal

Temperature (K)	Coking Coal Diffusion Constant D ($m^2 s^{-1}$)	Highly Volatile Coal Diffusion Constant D ($m^2 s^{-1}$)
660	2.0×10^{-18}	2.0×10^{-20}
670	1.4×10^{-17}	1.4×10^{-19}
680	6.2×10^{-17}	6.2×10^{-19}
700	1.3×10^{-15}	1.3×10^{-17}
720	2.0×10^{-16}	2.0×10^{-18}
730	5.8×10^{-17}	5.8×10^{-19}
740	2.1×10^{-18}	2.1×10^{-20}

Table 2.2b Diffusion Rates for Tar Molecules in Fluid Coal

Temperature (K)	Coking Coal Diffusion Rate D/L^2 (s^{-1})			Highly Volatile Coal Diffusion Rate D/L^2 (s^{-1})		
	$L = 10^{-3}m$	$L = 10^{-2}m$	$L = 10^{-1}m$	$L = 10^{-3}m$	$L = 10^{-2}m$	$L = 10^{-1}m$
660	2.0×10^{-12}	2.0×10^{-14}	2.0×10^{-16}	2.0×10^{-14}	2.0×10^{-16}	2.0×10^{-18}
670	1.4×10^{-11}	1.4×10^{-13}	1.4×10^{-15}	1.4×10^{-13}	1.4×10^{-15}	1.4×10^{-17}
680	6.2×10^{-11}	6.2×10^{-13}	6.2×10^{-15}	6.2×10^{-13}	6.2×10^{-15}	6.2×10^{-17}
700	1.3×10^{-9}	1.3×10^{-11}	1.3×10^{-13}	1.3×10^{-11}	1.3×10^{-13}	1.3×10^{-15}
720	2.0×10^{-10}	2.0×10^{-12}	2.0×10^{-14}	2.0×10^{-12}	2.0×10^{-14}	2.0×10^{-16}
730	5.8×10^{-11}	5.8×10^{-13}	5.8×10^{-15}	5.8×10^{-13}	5.8×10^{-15}	5.8×10^{-17}
740	2.1×10^{-12}	2.1×10^{-14}	2.1×10^{-16}	2.1×10^{-14}	2.1×10^{-16}	2.1×10^{-18}

2.2.3 Diffusion in Nonsoftening Coals

So far, 'hydrodynamic' diffusion of molecules through coals at their maximum fluidity has been considered. If it is now assumed that the coal remains solid and does not plasticise, we are essentially dealing with diffusion of a gas through a pore system. There are two types of diffusion to consider:

a. diffusion of gas across a boundary to (or from) the exterior surface of the coal

b. diffusion of gas into (or out of) a pore and into (or out of) the interior of coal

These diffusion processes will now be detailed in turn.

2.2.3.1 Diffusion of gas across a boundary

The diffusion constant, D, for the diffusion of gas across a boundary to (or from) the exterior surface of the coal was calculated using the equation[28]:

$$D = {}^{1}/_{3}\,\bar{c}\,\lambda \qquad (m^2 s^{-1})$$

Where: $\bar{c}$ is the average velocity of gas molecules (ms^{-1})

λ is the mean free path of gas molecules (m)

$\bar{C}$ was calculated using the equation[28]:

$$\bar{C} = (8kT / \pi M)^{0.5} \qquad (ms^{-1})$$

Where: k is the Boltzmann's Constant: 1.38×10^{-23} JK^{-1}

T is the temperature, K

M is the mass (Kg) of a diffusing molecule

The mean free path lengh, λ, has been calculated using the equation[28]:

$$= 1/ \pi \sigma^2 n 2^{0.5} \qquad (m)$$

Where: σ is the diameter of the gas molecule which is approximately equal to the molecular diameter; for the hydrogen molecule σ = 0.74Å (0.74×10^{-10}m) for the tar molecule σ = 8Å (8×10^{-10}m)

n is the number of molecules per m^3

'n' was calculated using the equation[28]:

$$n = P / kT \qquad (no./m^3)$$

Where: k is the Boltzmann's Constant: 1.38×10^{-23} JK^{-1}

T is the temperature, K

P is the pressure, Pa

The diffusion rate was calculated using the equation:

$$\text{Diffusion Rate} = D/L^2 \qquad (s^{-1})$$

Where: D is the diffusion constant: $^1/_3\, \bar{c}\lambda$ $(m^2 s^{-1})$

L is the thickness of the absorbed layer on the coal surface (we have considered two thicknesses: 2 and 4Å)

Diffusion constants for hydrogen and tar molecules are shown in tables 2.3a (page 23) and 2.4a (page 25) respectively. Diffusion rates for hydrogen and tar molecules are shown in tables 2.3b (page 24) and 2.4b (page 26) respectively.

2.2.3.2 Diffusion through a Pore

The micropore system has radii of the same order of magnitude as the size of the gas and tar molecules (for Manvers coal these are below about 14Å). X-ray diffraction indicates the presence of pores having diameters of approximately 40Å (4×10^{-9}m) whilst macropores exist in cokes. Common sense suggests that 'rates of diffusion' in the macropore system must be larger than those in the micropore system. Let 10^{-10}m be the gas micropore diameter, d_G and 10^{-9}m be the tar micropore diameter, d_T. Let R_G and R_T be the ratio of the mean free path, λ, to d_G and d_T respectively. The variation of these ratios with temperature and pressure are shown in table 2.5 (page 27).

Table 2.3a Diffusion Constants for Hydrogen Molecules Diffusing through an Absorbed Layer to the Surface of Coal.

Temperature (K)	Diffusion Constant D ($m^2 s^{-1}$)		
	1 Atmosphere	10 Atmospheres	100 Atmospheres
273	0.88×10^{-3}	0.88×10^{-4}	0.88×10^{-5}
503	2.19×10^{-3}	2.19×10^{-4}	2.19×10^{-5}
603	2.88×10^{-3}	2.88×10^{-4}	2.88×10^{-5}
703	3.63×10^{-3}	3.63×10^{-4}	3.63×10^{-5}
803	4.43×10^{-3}	4.43×10^{-4}	4.43×10^{-5}

Table 2.3b Diffusion Rates for Hydrogen Molecules Diffusing through an Absorbed Layer (2-4Å in thickness) to the Surface of Coal

Temperature (K)	Diffusion Rate D/L^2 (s^{-1})					
	1 Atmosphere		10 Atmospheres		100 Atmospheres	
	L = 2Å	L = 4Å	L = 2Å	L = 4Å	L = 2Å	L = 4Å
273	2.20×10^{16}	0.55×10^{16}	2.20×10^{15}	0.55×10^{15}	2.20×10^{14}	0.55×10^{14}
503	5.49×10^{16}	1.37×10^{16}	5.49×10^{15}	1.37×10^{15}	5.49×10^{14}	1.37×10^{14}
603	7.20×10^{16}	1.80×10^{16}	7.20×10^{15}	1.80×10^{15}	7.20×10^{14}	1.80×10^{14}
703	9.07×10^{16}	2.27×10^{16}	9.07×10^{15}	2.27×10^{15}	9.07×10^{14}	2.27×10^{14}
803	11.07×10^{16}	2.77×10^{16}	11.07×10^{15}	2.77×10^{15}	11.07×10^{14}	2.77×10^{14}

Table 2.4a Diffusion Constants for Tar Molecules (Molecular Mass = 512) Diffusing through an absorbed Layer to the Surface of Coal

Temperature (K)	Diffusion Constant D (m^2s^{-1})		
	1 Atmosphere	10 Atmospheres	100 Atmospheres
273	0.47×10^{-6}	0.47×10^{-7}	0.47×10^{-8}
503	1.17×10^{-6}	1.17×10^{-7}	1.17×10^{-8}
603	1.54×10^{-6}	1.54×10^{-7}	1.54×10^{-8}
703	1.93×10^{-6}	1.93×10^{-7}	1.93×10^{-8}
803	2.37×10^{-6}	2.37×10^{-7}	2.37×10^{-8}

Table 2.4b Diffusion Rates for Tar Molecules (Molecular Mass = 512) Diffusing through an Absorbed Layer (2-4Å in thickness) to the Surface of Coal

Temperature (K)	Diffusion Rate D/L^2 (s^{-1})					
	1 Atmosphere		10 Atmospheres		100 Atmospheres	
	L = 2Å	L = 4Å	L = 2Å	L = 4Å	L = 2Å	L = 4Å
273	1.17×10^{13}	0.29×10^{13}	1.17×10^{12}	0.29×10^{12}	1.17×10^{11}	0.29×10^{11}
503	2.93×10^{13}	0.73×10^{13}	2.93×10^{12}	0.73×10^{12}	2.93×10^{11}	0.73×10^{11}
603	3.85×10^{13}	0.96×10^{13}	3.85×10^{12}	0.96×10^{12}	3.85×10^{11}	0.96×10^{11}
703	4.83×10^{13}	1.21×10^{13}	4.83×10^{12}	1.21×10^{12}	4.83×10^{11}	1.21×10^{11}
803	5.92×10^{13}	1.48×10^{13}	5.92×10^{12}	1.48×10^{12}	5.92×10^{11}	1.48×10^{11}

Table 2.5 Ratios of the Mean Free Path, λ, to Gas (R_G) and Tar (R_T) Micropore Diameters

Temperature (K)	1 Atmosphere		10 Atmospheres		100 Atmospheres	
	R_G	R_T	R_G	R_T	R_G	R_T
273	1.5×10^4	13.3	1.5×10^3	13.3×10^{-1}	1.5×10^2	13.3×10^{-2}
803	4.5×10^4	39.0	4.5×10^3	39×10^{-1}	4.5×10^2	39×10^{-2}

Table 2.5 shows that for all temperatures and pressures considered λ is much greater than the smallest pores but at the higher pressures λ is smaller than the diameter of the largest micropores (those in which tar molecules can travel). When λ is much greater than the pore opening there is effusion in the pore. Let us consider the rates of effusion and diffusion of hydrogen molecules. The rate of effusion into the pore was calculated using the equation[28]:

$$\text{Rate of Effusion, } R_E = (0.25n\bar{C})(\text{area of pore}) \qquad ns^{-1}$$

Where: n is the number of molecules per unit volume (no./m^3)

$\bar{C}$ is the mean velocity of gas molecules (ms^{-1})

R_E is the number of particles (molecules) per unit time per unit area of pore. For Manvers coal the pore radius is: 7Å (7×10^{-10}m).

The rate of diffusion down the pore (assuming that λ is equal to 2r, where r is the pore radius) was calculated using the equation:

$$\text{Rate of Diffusion} = \tfrac{1}{3}\,\bar{C}\,(2r)\ /\ \text{area of pore} \qquad (s^{-1})$$

Where: r is the pore radius (for Manvers coal r = 7Å, 7×10^{-10}m)

Rates of effusion and diffusion for hydrogen molecules are shown in table 2.6.

Table 2.6 Rates of Effusion and Diffusion (mean free path length of gas molecules is assumed to be much greater than pore opening) for Hydrogen Molecules

Temperature (K)	Effusion Rate (ns^{-1})			Diffusion Rate (s^{-1})
	1 Atmosphere	10 Atmospheres	100 Atmospheres	
273	1.74×10^{10}	1.74×10^{11}	1.74×10^{12}	5.15×10^{11}
503	1.28×10^{10}	1.28×10^{11}	1.28×10^{12}	7.00×10^{11}
603	1.17×10^{10}	1.17×10^{11}	1.17×10^{12}	7.67×10^{11}
703	1.08×10^{10}	1.08×10^{11}	1.08×10^{12}	8.27×10^{11}
803	1.01×10^{10}	1.01×10^{11}	1.01×10^{12}	8.87×10^{11}

The orders of magnitude of the mean free paths demonstrated that for gas molecules λ was much greater than the pore radius, r, whilst for tar molecules $\lambda > r$. Therefore, if the diffusion of the tar molecules through the pores is taken as being one dimensional diffusion, then:

$$\text{Diffusion Constant for Tar Molecules} = {}^1/_3\, \bar{c}\lambda \qquad (m^2 s^{-1})$$

and to obtain units of rate (s^{-1}) the above equation has to be divided by the area of a pore (r = 7Å). Therefore, the rate of diffusion was calculated using the following equation:

$$\text{Rate of Diffusion of Tar Molecules} = {}^1/_3\, \bar{c}\lambda /\ \text{area of pore} \qquad (s^{-1})$$

Table 2.7 shows the diffusion rates for tar molecules (molecular mass = 512) for the case where the pore opening is much greater than λ.

2.2.4 Kinetic Analysis: Conclusions

1. Diffusion constants calculated for hydrogen and tar molecules (tables 2.1a and 2.2a respectively) diffusing through the 'fluid coking coal' at minimum viscosity are 3 to 4 orders of magnitude greater than those obtained by Gavalas[29]. However, Gavalas has used a larger minimum viscosity and a larger tar molecule radius.

Table 2.7 Rates of Diffusion for Tar Molecules (Molecular Mass = 512)

Temperature (K)	Diffusion Rate (s^{-1}) 1 Atmosphere	10 Atmospheres	100 Atmospheres
273	3.05×10^{11}	3.05×10^{10}	3.05×10^{9}
503	7.60×10^{11}	7.60×10^{10}	7.60×10^{9}
603	10.00×10^{11}	10.00×10^{10}	10.00×10^{9}
703	12.60×10^{11}	12.60×10^{10}	12.60×10^{9}
803	15.40×10^{11}	15.40×10^{10}	15.40×10^{9}

2. Diffusion through the fluid coal is many orders of magnitude slower than diffusion through the solid, porous coal (see tables 2.1b and 2.6).

3. At 100 atmospheres the mean free paths of permanent gases are greater than the diameters of the micropores but the mean free paths of gaseous tar molecules are smaller than the diameters of the micropores. This suggests that the transport of the permanent gases and of gaseous tar molecules follow different mechanisms. Effusion of permanent gases in and out of the micropore system seems to be the slow process (see tables 2.6 and 2.7).

4. Diffusion through the fluid coal and through the micropore system of solid coal is obviously complex and steps towards more detailed kinetics have been taken by Gavalas[30] and Howard[31].

CHAPTER THREE

EXPERIMENTAL

CHAPTER THREE

EXPERIMENTAL

3.1 Introduction

Manvers coal, a fuel which has been well characterised by technological properties, petrographic and ultimate analysis (table 3.1) has been used throughout the study. This coal has been stored under nitrogen and was crushed, when needed, to pass a 124 micron mesh and dried for two hours in a rotary evaporator at 373 K.

3.2 The Autoclave

Pyrolyses have been performed in a one litre, stainless steel, vertical, stirred (60 revolutions per minute) autoclave (plate 1). Temperatures were measured by a thermocouple (Ni-Cr/Ni-Al) placed in the centre of the autoclave. The autoclave and its contents were heated by an external furnace and as the temperature rose a maximum difference of 30^{o}C developed across the coal. Pressures were measured by a calibrated Bourdon gauge. After pyrolysis at 500^{o}C the autoclave was cooled to room temperature in one hour by passing cold water through a pipe network welded to the outside of the autoclave.

3.3 Typical Pyrolysis Run

Dried coal was placed in the autoclave which was then flushed

Table 3.1 CHARACTERISATION OF MANVERS COAL

Ultimate Analysis (% d.a.f.)

Carbon	Hydrogen	Oxygen	Nitrogen	Sulphur (total)
83.26	5.3	8.5	1.8	1.7

Proximate Data (% d.b.)

Moisture	Ash	Volatile Matter
5.10	5.6	37.1

Coking Properties

B.S. Swelling Number	Gray-King Coke Type
5	F

Low Temperature Dilatometry data

Softening Temperature (°C)	Maximum Dilatation Temperature (°C)	Dilatation %
346	446	2.0

Maceral Group Composition

Vitrinite	Exinite	Inertinite
80.0	8.0	11.0
0.74 max. reflectance		

Plate 1

The Autoclave

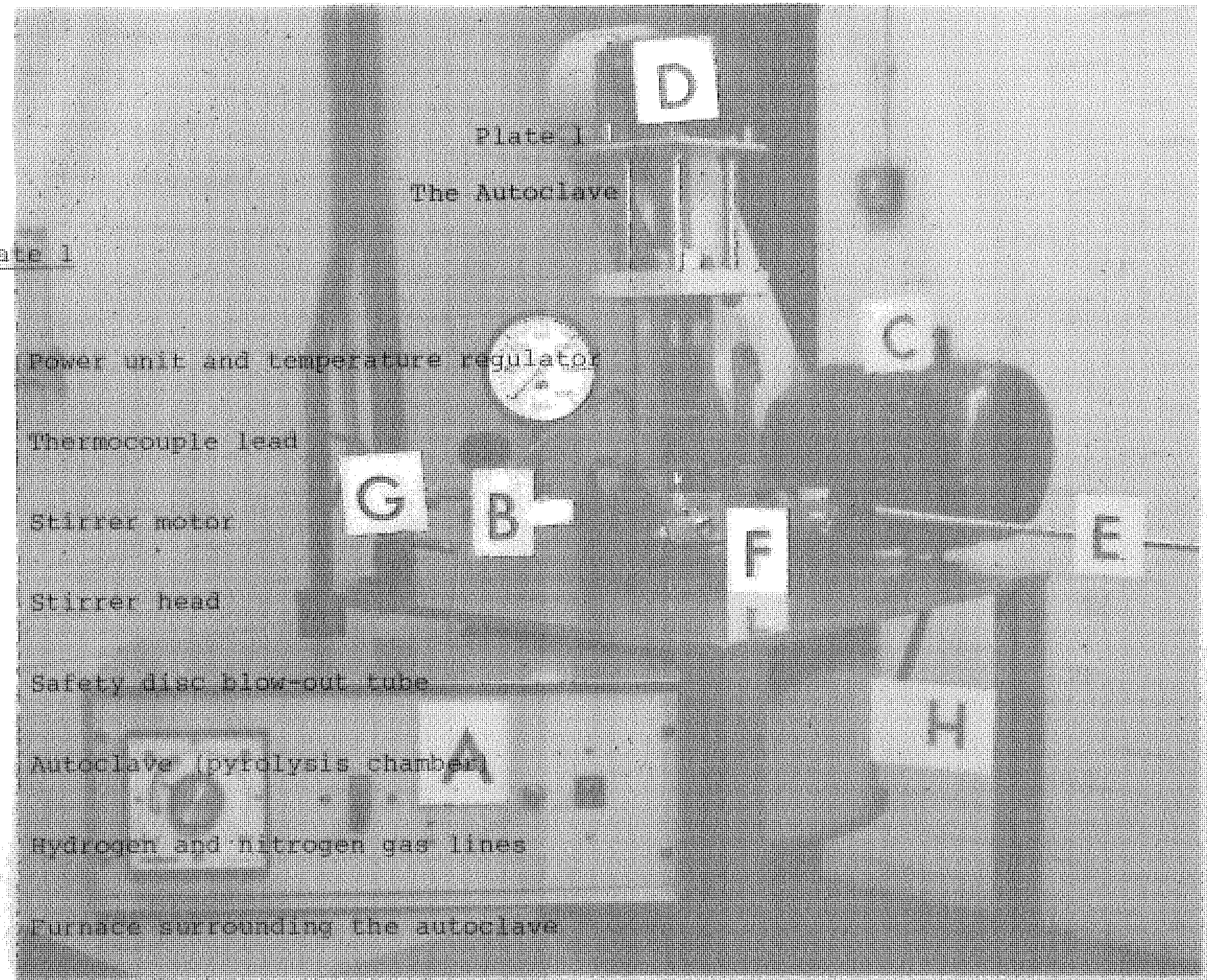

Key to Plate 1

A	Power unit and temperature regulator
B	Thermocouple lead
C	Stirrer motor
D	Stirrer head
E	Safety disc blow-out tube
F	Autoclave (pyrolysis chamber)
G	Hydrogen and nitrogen gas lines
H	Furnace surrounding the autoclave

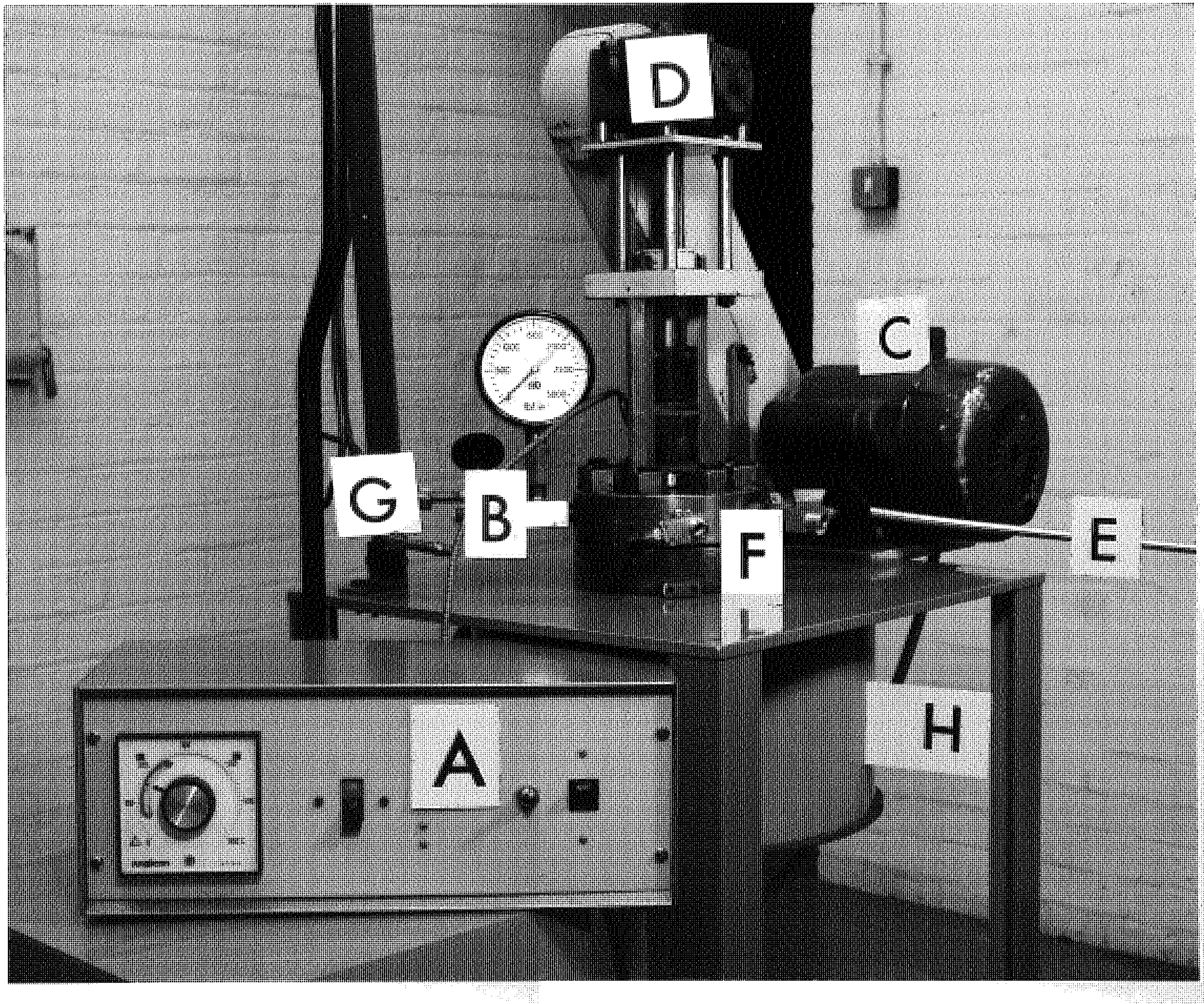
D
C
G
B
F
E
A
H

and filled with gas (nitrogen or hydrogen/deuterium) to the desired initial pressure. The principal variables were the initial quantity of coal (and thereby the final pressure achieved) and the initial pressure of the nitrogen or hydrogen/deuterium atmosphere. The sealed autoclave was invariably heated to 500°C in about two hours (average heating rate was 4.2°C min.$^{-1}$) and maintained at that temperature for a further two hours. Temperature and pressure readings were taken at 5 minute intervals during the pyrolysis run. Typical graphs for the increase in pressure with temperature for pyrolyses in nitrogen and hydrogen/deuterium atmospheres are shown in figure 3.1.

After pyrolysis the autoclave was cooled to room temperature and the pressure noted. A gas sample was taken by displacement of water from a gas bottle. The cooled autoclave was washed thoroughly first with toluene and then with tetrahydrofuran (THF). All pyrolyses were repeated at least three times.

3.4 Liquor Determination

The toluene solution contained tar and liquor (water containing dissolved gases such as NH_3 and H_2S). In addition, care was taken to wash out all the coke into the toluene solution. A Dean and Stark apparatus[32] was used to separate the liquor from the toluene solution.

Figure 3.1 Typical Pressure versus Temperature graphs for Pyrolyses performed in Nitrogen (■) and Hydrogen (●) atmospheres

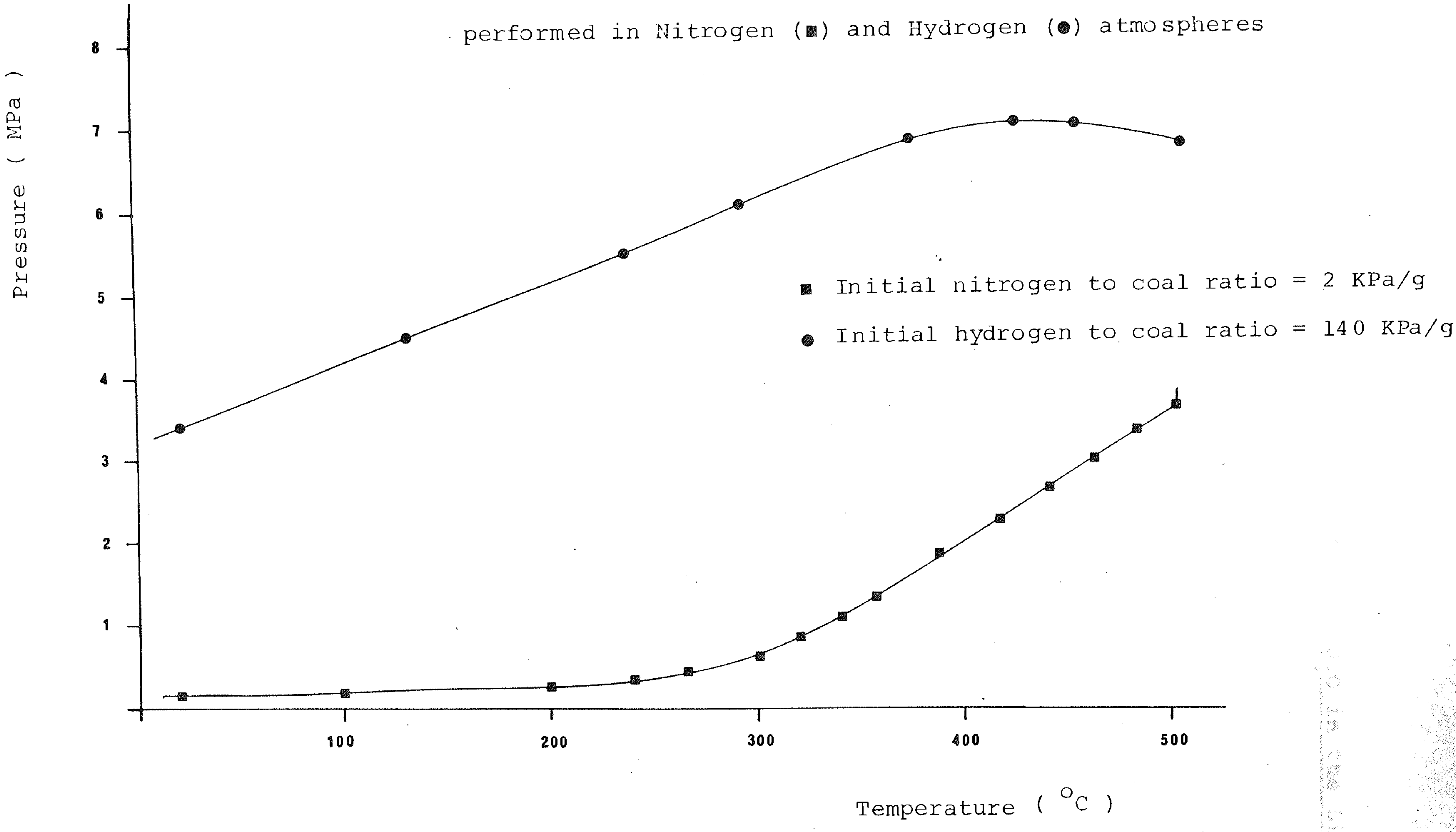

3.5 Use of Abbé Refractometer to Measure D_2O in the Liquor

The refractive index of liquor was measured at 298 K and then compared with a calibration curve (% D_2O in water versus refractive index) to determine the percentage of D_2O in the liquor. Dissolved gases such as NH_3 and H_2S were removed by passing nitrogen through the sample until the refractive index became constant. The presence of these dissolved gases would increase the observed refractive index.

3.6 Soxhlet Extraction of Coke : Preliminary Separation of Tars

Having removed the liquor from the toluene solution, only tar and coke remained to be separated. This was achieved by extracting the coke with the toluene solution in a Soxhlet apparatus. Subsequently the coke was further Soxhlet extracted with the THF solution obtained previously from washing out the autoclave. The coke was then dried. Toluene and THF were then removed from the tar solutions by rotary evaporation at reduced pressure. The residual toluene tar was liquid whereas the THF tar was a solid. Both tars were weighed.

3.7 Separation of Tars into Neutral, Acidic and Basic Fractions

Tars (THF and toluene) obtained from nitrogen and hydrogen pyrolyses were separated into neutral, acidic and basic fractions according to their solubilities in 10% NaOH and 20% H_2SO_4. The procedure for the separation[33] of tars is shown in figure 3.2. Deuterated tars were not separated.

3.8 Analysis of Tars by Gas Chromatography-Mass Spectrometry (G.C.- M.S.)

The neutral, acidic and basic fractions were analysed by G.C.- M.S. . Such analyses used a 40m glass capillary column coated with OV-1 for neutral and acidic material and with SE-54 for the bases. Acidic fractions were silylated, prior to injection, by shaking with NO-Bis(trimethylsilyl) acetamide ($CH_3C(OSi(CH_3)_3)NSi(CH_3)_3$).

Both columns were heated from 100°C to 250°C at 8°C $min.^{-1}$ and maintained at the upper temperature for 5 minutes. The outlet of the G.C. column led to a VG Micromass 12/12 quadrupole mass spectrometer in which positive ions were generated by 70eV electrons at an ultimate vacuum of approximately 0.13 - 13 mPa. Deuterated tars were injected whole (not separated into neutral,acidic and basic fractions) on to the OV-1 column. Again the THF tar (mainly acidic) was silylated prior to injection.

Figure 3.2

Procedure for the Separation of Tars into Acidic, Basic and Neutral Fractions

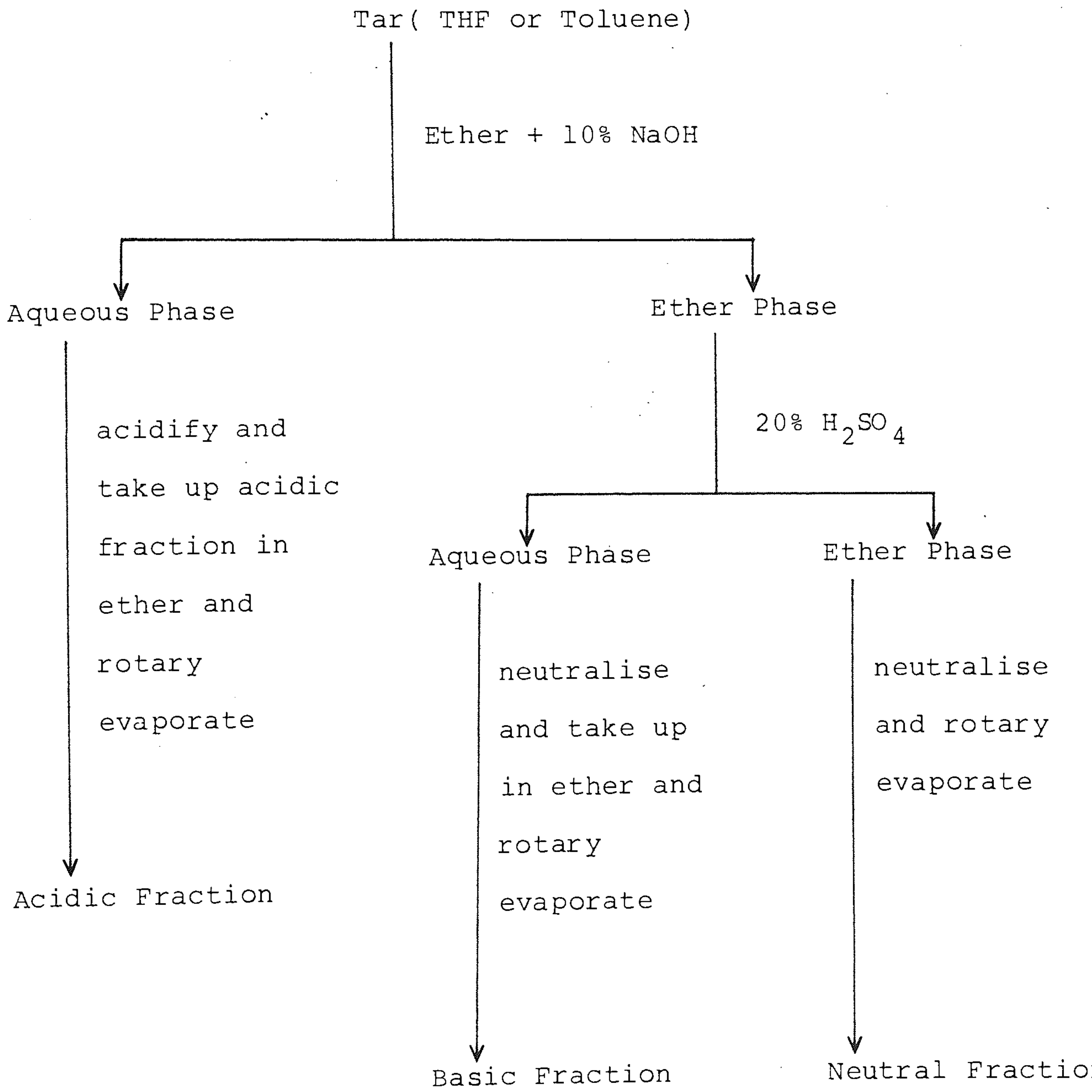

3.9 Separation of Whole Tars (THF and Toluene) Obtained from Nitrogen Pyrolyses by High Performance Liquid Chromatography (HPLC) into Alkane, Aromatic and Polar Fractions

HPLC analyses were performed on a Perkin Elmer Series 2 Liquid Chromatograph which was coupled to a Perkin Elmer LC-75 Spectrophotometric detector using the following experimental conditions:

Column Temp.	:	Ambient
Column	:	SiO_2 Preparation Lichro 15-25 microns (250mm long and 22.5mm(i.d.))
Solvent	:	n-heptane at 15ml/min.
Detector	:	UV Absorption (254nm), Attenuation X 1024
Chart Speed	:	12cm/h
Injection	:	100 micro litres (Tar sample in dichloromethane-concentrated)
Pressure	:	6.85 MPa

When the alkanes (not detected by UV) and the aromatics had been eluted from the column the n-heptane was replaced by a methanol/chloroform (1:9) solvent mixture to elute the polar compounds. Again, the flow rate was maintained at 15ml/minute.

3.10 Separation of Toluene Solubles Obtained from Nitrogen and Hydrogen Pyrolyses by Gradient Mode HPLC

HPLC analyses were performed using analytical and preparative columns. The UV trace obtained from an analytical column was a series of peaks whose retention time was dependant on the number of aromatic rings present in the molecules. To identify the contents of each peak a preparative column was used because this provided enough material for GC-MS. The compounds present under each peak were collected separately and a GC-MS analysis obtained. The following experimental conditions were used:

Analytical Column

Column Temp.	: Ambient
Column	: NH_2 Spherisorb-5 microns; 250mm x 8mm (i.d.)
Solvents	: n-Heptane at 3ml/min. (dichloromethane added at 3% per minute)
Detector	: UV Absorption (254nm)
Chart Speed	: 1cm/min.
Injection	: 20 micro litres (containing 2×10^{-6}g of tar) of very dilute tar in n-heptane
Pressure	: 10.27 MPa

Preparative Column

Column Temp. : Ambient

Column : NH_2 Lichrosorb - 5 microns; 250mm x 22.5 (i.d.)

Solvent : n-Heptane at 15ml/min. (only n-Heptane used)

Detector : UV Absorption (254nm); Attenuation x1024

Chart Speed : 1cm/min.

Injection : 100 micro litres (tar in n-heptane: concentrated)

Pressure : 10.27 MPa

3.11 Gas Analyses

Gas samples were analysed by a Gow Mac Series 552 Gas Chromatograph (thermal conductivity detector) and peak areas were compared with those of standards.

Experimental Conditions

Column Temp. : $70^{o}C$.

Column : 1.5m (6mm i.d.) Stainless Steel filled with Porapak N

Gas Flow Rate : Nitrogen at $30cm^3$/min.

Detector Temp.: $80^{o}C$

Bridge Current : 120mA

Injection : $0.5cm^3$

Chart Speed : 3cm/min.

Additionally, gas samples obtained by pyrolysis in an atmosphere of deuterium were analysed by a high resolution electron - impact mass spectrometer (Metropolitan Vickers MS 9) using a tungsten filament and a nominal ionizing voltage of 16eV. An ultimate vacuum of 10^{-5}Pa was obtained prior to injection of the gas sample.

3.12 Porosity Measurements on Cokes and Manvers Coal

Carbon dioxide adsorption isotherms have been measured on cokes and coal at 298 K to obtain the limiting micropore volumes, V_o(cm^3/g), in the adsorbed state, the corresponding micropore surface areas, S_{micro}(m^2/g), and the mean eqivalent micropore radii, $\bar{r}_e$(nm). The samples were outgassed for a minimum of 16 hours at 423 K and an ultimate vacuum of 1.33×10^{-2}Pa. The following experimental readings were taken: coke sample weight, free space volume, equilibrium pressure (P_e), volume adsorbed at equilibrium pressure (V), saturation vapour pressure of CO_2 at 298 K (P_o) and the time elapsed in hours. The results were calculated using the Dubinin equation[34]:

$$\ln V = \ln V_o - (RT/E)^n (\ln (P_0/P_e))^n$$

Where: V is the volume adsorbed (cm^3/g) at equilibrium pressure

V_o is the limiting micropore volume (cm^3/g)

E is the characteristic energy (KJ/mole)

n is the exponent, which is not necessarily integral

R is the Gas constant (8.314 $JK^{-1}mol^{-1}$)

T is the temperature (K)

The exponent n was optimised using standard regression techniques. ln V was plotted against $(\ln (P_o/P_e))^n$ to obtain $\ln V_o$ from the intercept on the ln V axis. The antilogarithm of $\ln V_o$ gives V_o in cm^3/g. The slope of the graph is equal to $(RT/E)^n$ and hence the characteristic energy, E, can be calculated.

The effective surface area of the micropores, S_{micro}, was calculated using the equation[34]:

$$S_{micro} = 2V_o \quad (E/K)^{1/3} \, \Gamma((3n + 1)/3n)$$

Where: Γ is the gamma function[35] (variation of this function with the exponent n is given in reference 35)

K is a constant, $K_{CO_2} = 3.145$ KJ nm^3 $mole^{-1}$

The mean equivalent pore radius, $\bar{r}_e$, was calculated using the equation[34]:

$$\bar{r}_e = 2V_o / S_{micro} = (K/E)^{1/3} / \Gamma((3n+1)/3n)$$

Pore size distribution curves (frequency (number of pores) versus equivalent pore radius, $\bar{r}_e$) have been inferred. The maximum pore radius on the frequency distribution curve is called the mode equivalent pore radius, r_e, and is given by the following equation[34]:

$$r_e = ((3n/(3n+1))^{1/n} (K/E))^{1/3}$$

The maximum frequency corresponding to r_e is called the mode frequency, f_{mode}, and this is given by the following equation[34]:

$$f_{mode} = 3(n+1) \ ((3n+1)/3n)^{1/3n} \ V_o (E/K)^{1/3} \ \exp(-(3n+1)/3n)$$

3.13 Methanol Densities of Cokes and Coal

Coke and coal densities were determined by measuring the displacement of methanol in stoppered, 5ml grade A ($\pm$0.02ml at 293 K) volumetric flasks. Approximately one gram of coke or coal (crushed to pass a 124 micron sieve) was used. Consistent densities were obtained by allowing the coke (or coal) and methanol to stand for 24hours. The density, d, was calculated using the equation :

$$d = \text{grams of coke} / ((m_1/d_1)-(m_2/d_2))$$

Where: d is the density of the coke or coal (cm^3/g)

m_1 is the weight (g) of methanol (at temperature T_1) needed to make up to 5ml mark in absence of coke

m_2 is the weight (g) of methanol (at temperature T_2) needed to make up to 5ml mark in presence of coke

d_1 is the density (cm^3/g) of methanol at temperature T_1

d_2 is the density (cm^3/g) of methanol at temperature T_2

The variation of methanol density with temperature is given by the following equation[36]:

$$d_m = 0.80999 - 9.253 \times 10^{-4}T - 4.1 \times 10^{-7}T^2$$

Where: d_m is the density of methanol (cm^3/g)

T is the temperature (^oC)

3.14 Elemental Analysis

The carbon, hydrogen and nitrogen content of the cokes and coal, was determined by micro analytical techniques carried out in the micro analytical laboratories in the chemistry department of Aston university using a Perkin Elmer 240B Elemental Analyser and a Carlo Erba 1106 Elemental Analyser.

3.15 Diffuse Reflectance Infra Red Spectroscopy of Coal and Cokes

Infra red spectra were recorded on a Perkin Elmer 683 spectrophotometer which was fitted with a Harrick DRA 35P diffuse reflectance module and interfaced to a Perkin Elmer 3500 data station.

Diffuse reflectance spectra of mixtures containing approximately 5% of coke/coal in KBr, crushed to -100 microns +50 microns, were measured in atmospheres of nitrogen. The powders were loosely close packed in a disc of 0.5cm depth. Each sample was scanned six times (3min./scan) and the average of the six scans stored on disc. A reference spectra of pure KBr was subtracted from each of the sample spectra.

Diffuse reflectance spectra at 'infinite' depth are obtained by ratioing the averaged spectrum of the sample to that of the KBr reference sample and converting to the Kubelka-Munk[37,38] function:

$$\text{Kubelka-Munk Function} = (1 - r_\infty)^2 / 2r_\infty$$

Where: $r_\infty = R_o / I_o$; R_o is the intensity of reflected radiation at the surface of the infinitely deep sample (bed) and I_o is the incident radiation at the surface of the sample.

The Kubelka-Munk function is proportional to the concentration of absorbing species; the computer interfaced to the infra red spectrometer calculates $(1 - r_{\infty})^2 / 2r_{\infty}$ and a plot of the result as a function of wavelength is a diffuse reflectance spectrum. This function is valid for an infinitely deep bed. 'Infinitely deep' may be defined as ' so deep that further increase in depth produces no further change in R_o or r_{∞} '. It is commonly found, certainly with coal, that a depth of approximately 0.5cm is infinite and comparatively small amounts of powdered sample are required to obtain a spectrum.

3.16 Fluidised Sandbath Heater

Some pyrolyses were performed in small (8 cm^3), brass bombs heated rapidly to a temperature of 500^{o}C in a fluidised bed of sand. A rate of heating of approximately 83^{o}C/min. was obtained from the Techne SBS-4 fluidised sandbath heater.

CHAPTER FOUR

PYROLYSIS OF MANVERS COAL IN AN ATMOSPHERE OF NITROGEN

CHAPTER FOUR

PYROLYSIS OF MANVERS COAL IN AN ATMOSPHERE OF NITROGEN

4.1 Experimental Conditions

The experimental conditions for nitrogen pyrolyses are shown in table 4.1 . Typical graphs for the increase in pressure with temperature for nitrogen pyrolyses are shown in figure 4.1 . It is clear from these graphs that pyrolysis starts at about 270^{o}C. Between room temperature and 270^{o}C the graphs depict the steady heating of the initial nitrogen atmosphere and the water in the coal (the coal was dried prior to pyrolysis but obviously some intrinsic moisture will remain). The final pressure at 500^{o}C is determined by the initial quantity of coal introduced into the autoclave.

4.2 Yields

Yields from pyrolyses are shown in tables 4.2, 4.3a, 4.3b, 4.4, 4.5 and 4.6, pages 65, 66, 67, 68, 72 and 73 respectively. Table 4.2 shows the expected effects of pressure on coal pyrolysis in an inert atmosphere. The tar yield decreased exponentially (figure 4.2, page 59) with an increase in pressure while the yield of liquor was unaffected. Gas yields appeared to increase (figure 4.3, page 60) and the yield of coke, though increased by mild pressure was unaffected by further increase. It is clear that the major change produced by pressure was the 'cracking' of the tar to give gas and some char.

Table 4.1 Experimental Conditions for Nitrogen Pyrolyses Performed in the Autoclave

Initial Nitrogen Pressure	=	0.1 MPa
Average Rate of Heating	=	$4.2^{o}C\ min^{-1}$
Final Coal Pyrolysis Temperature	=	$500^{o}C$
Heat Soak Time at $500^{o}C$	=	2 hours

Experiment	Grams of Coal used	Initial Nitrogen to Coal Ratio KPa/g	Final Pressure at $500^{o}C$ in MPa
N0	1	125	0.10 ± 0.00
N1	6.25	16	0.85 ± 0.00
N2	12.5	8	1.28 ± 0.02
N3	25.0	4	1.90 ± 0.05
N4	50.0	2	3.88 ± 0.05
N5	100.0	1	7.32 ± 0.14

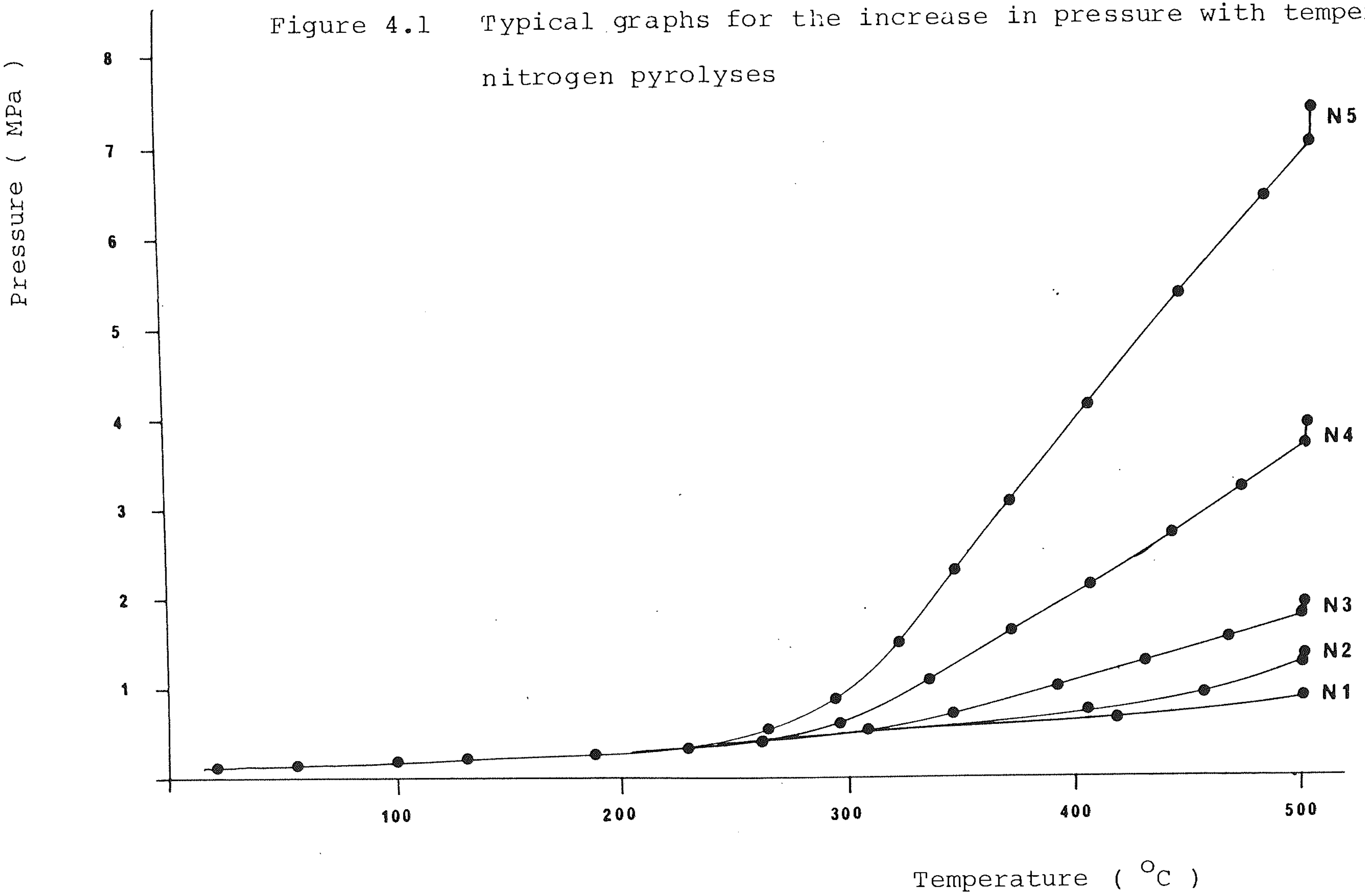

Figure 4.1 Typical graphs for the increase in pressure with temperature for nitrogen pyrolyses

4.3 Tars

In terms of reaction scheme 1 (chapter 1) nitrogen pressure may be presumed to have diminished tar yields by inhibiting the dehydrogenation of hydroaromatic systems thereby decreasing the subsequent bond scission by hydrogenation and also by decreasing the ratio of volatilisation to polymerisation of low boiling material. The inhibition of tar formation means that at the upper temperatures of pyrolysis there is more aliphatic material which cracks to give gas.

Table 4.3a (page 66) shows the separation of the total tar into a toluene soluble fraction and a THF soluble fraction. Table 4.3b (page 67) shows that whereas the toluene soluble tar was predominantly neutral, the THF soluble tar consisted mainly of phenols and in fact GC-MS analysis showed the THF soluble material to be composed of polyhydric phenols (dihydroxybenzenes), naphthols and high boiling phenolic material.

Table 4.4 (page 68) lists the components present in the tars obtained from pyrolysis under nitrogen. These are clearly 'coal tars' having similar compositions to those recorded in the literature[39]. The neutrals in these tars contained little paraffinic material and somewhat similar quantities of substituted and non-substituted aromatics. Thus the neutral tar material may be thought of as being midway between the compositions of 'low' and 'high' temperature tars. Moderate pressure has had a similar cracking effect to a slow increase in temperature.

4.3.1 Separation of Whole Tars into Alkane, Aromatic and Polar Fractions by High Performance Liquid Chromatography (HPLC)

A typical HPLC trace showing the separation of a whole tar into alkane, aromatic and polar fractions is shown in figure 4.4 (page 61). Since the fractions were detected by their UV absorption, at 254 nm, there is no peak for the alkane fraction. Table 4.5 (page 72) gives the yields of the alkanes, aromatics and polars obtained by HPLC separation. The aromatic and polar fractions decrease exponentially with an increase in pressure (figure 4.5, page 62). This effect was in fact demonstrated in table 4.3a (page 66).

GC-MS analysis shows that the alkanes have a chain length of C_{11}- C_{24}. The aromatic fraction contained essentially all the components found previously in the neutral toluene tar in table 4.4 (page 68). The polar fraction contained all the acids and bases found in the toluene tars (table 4.4) and polyhydric phenols, naphthols and high boiling phenols found in the THF tar (table 4.4).

Figure 4.6 (page 63) is a typical HPLC trace showing the separation of a toluene soluble neutral material. The HPLC trace shows that there are higher molecular weight materials (perylene, dibenzopyrene and coronene) than those identified by GC-MS in the toluene neutral material. Table 4.6 (page 73) summarises HPLC analyses of the toluene soluble neutral material. Since the fractions were detected by their UV absorption at 254 nm the results overemphasised the importance of the larger polynuclear aromatic molecules. The table shows that nitrogen pressures reduced the yields of all neutral fractions. The overall effect, of course, was that shown in table 4.2 (page 65). These results require confirmation since it is possible that changes in the composition of the neutral material may have changed the extinction coefficients controlling the absorption of 254 nm light though GC-MS analysis of the tars suggests this is unlikely. Table 4.7 (page 74) shows the extinction coefficients of selected molecules[40,41] (molecules similar to those found in toluene neutral tar) at a UV absorption of approximately 254 nm.

4.4 Cokes

Table 4.8 (page 75) shows the atomic carbon, hydrogen and nitrogen content of the cokes and Manvers coal. Table 4.9 (page 76) shows the atomic hydrogen to carbon ratios and the methanol densities of the cokes. The densities of the cokes were nearly twice those of cokes produced at atmospheric pressure but showed little variation with pressure. Presumably only very moderate pressures are required to compress the coke structure. The micropore volume surface areas, volumes and the mean equivalent pore radii of the cokes deduced from carbon dioxide adsorption isotherms are shown in table 4.10 (page 77). Carbon dioxide adsorption isotherm data for Manvers coal and a nitrogen coke is given in appendix 2. The micropore volumes and surface areas of cokes prepared in nitrogen were slightly larger than those of the parent coal. When pyrolysis produces little fluidity, as here with slow rates of heating in nitrogen, volatilisation unlocks the pore structure and leads to an increase in microporosity. That the microporosity of the cokes (chars) increased with nitrogen pressure demonstrates that the cracking of the tar generated more gas than coke (table 4.2, page 65). Table 4.10 (page 77) shows that the mean equivalent pore radii of the nitrogen cokes were similar to the mean equivalent pore radius of the parent coal. Figure 4.7 (page 64) shows the pore size distribution for Manvers coal and nitrogen cokes.

4.5 Gases

Table 4.11 (page 78) shows the composition of the gases obtained by pyrolysis. As one would expect the gases were comprised of hydrogen and simple hydrocarbons, presumably formed by the action of hydrogen on alkyl chains[1]. Traces of ammonia and hydrogen sulphide were also found. No oxides of carbon were found. Propane yields increased with the increasing nitrogen pressure whilst the yields of hydrogen decreased. The decrease in the yield corresponds to the increase in gas formation with increasing nitrogen pressure. Methane yields remained constant at moderate pressures but did increase at higher nitrogen pressures. Table 4.12 (page 79) shows the percentage gas volumes in table 4.11 converted into gas weights (grams). This is easily done: suppose there are four gases in a gas sample A, B, C and D respectively. Then the weight of any gas in the sample is given by the formula:

$$\text{Weight of gas A in grams} = \frac{(\text{M.M. of gas A})(\%\ \text{gas volume of gas A})}{\sum_{N=A}^{D} (\text{M.M.})_N \ (\%\ \text{gas volume})_N} \times W_g$$

Where : M.M. is the molecular mass

W_g is the total weight of gas generated by pyrolysis in grams

Tables 4.13 (page 80) and 4.14 (page 81) give the hydrogen and carbon content of each gas (in grams) respectively.

4.6 Hydrogen and Carbon Mass Balance

Table 4.15 (page 82) shows the hydrogen mass balance. The effect of nitrogen pressure on hydrogen distribution in the gas, coke and liquor was negligible. However, the hydrogen content of the tar decreased as the nitrogen pressure increased. Table 4.16 (page 83) shows the carbon mass balance. The carbon content of the coke remains approximately constant with increasing nitrogen pressure. As the nitrogen pressure increased the carbon content of the gas increased.

4.7 Fluidised Sandbath Experiments

Table 4.17 (page 84) compares the formation of coke in the autoclave and in a closed bomb heated in a few minutes to the same final pressure and temperature. It will be seen that whereas there were small differences in the yields of coke, the densities of the cokes and the yields of tar were very similar.

Figure 4.2

Total tar (wt%) versus final pressure for nitrogen pyrolyses

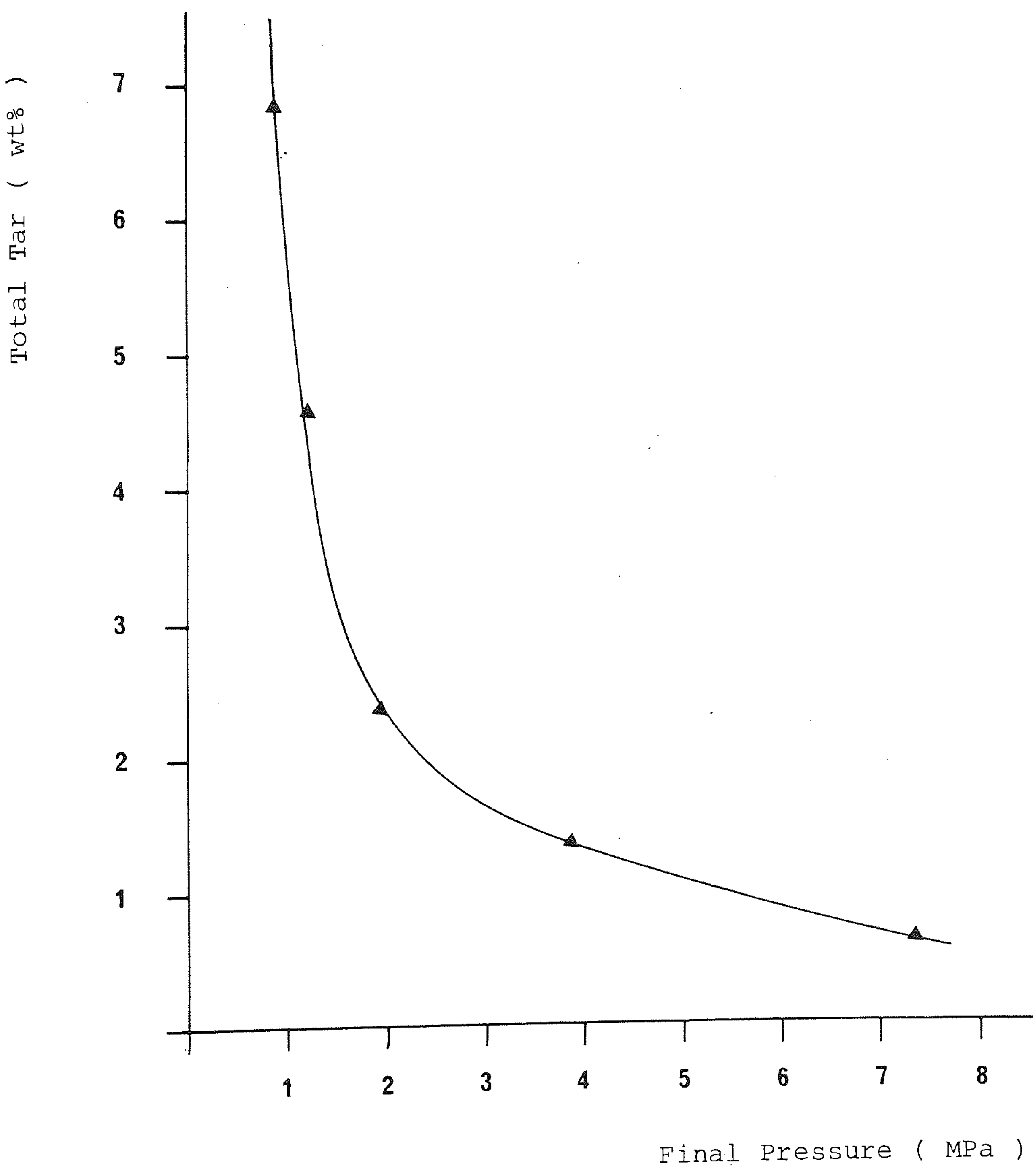

Figure 4.3

Gas yield (by difference) versus final pressure for nitrogen pyrolyses

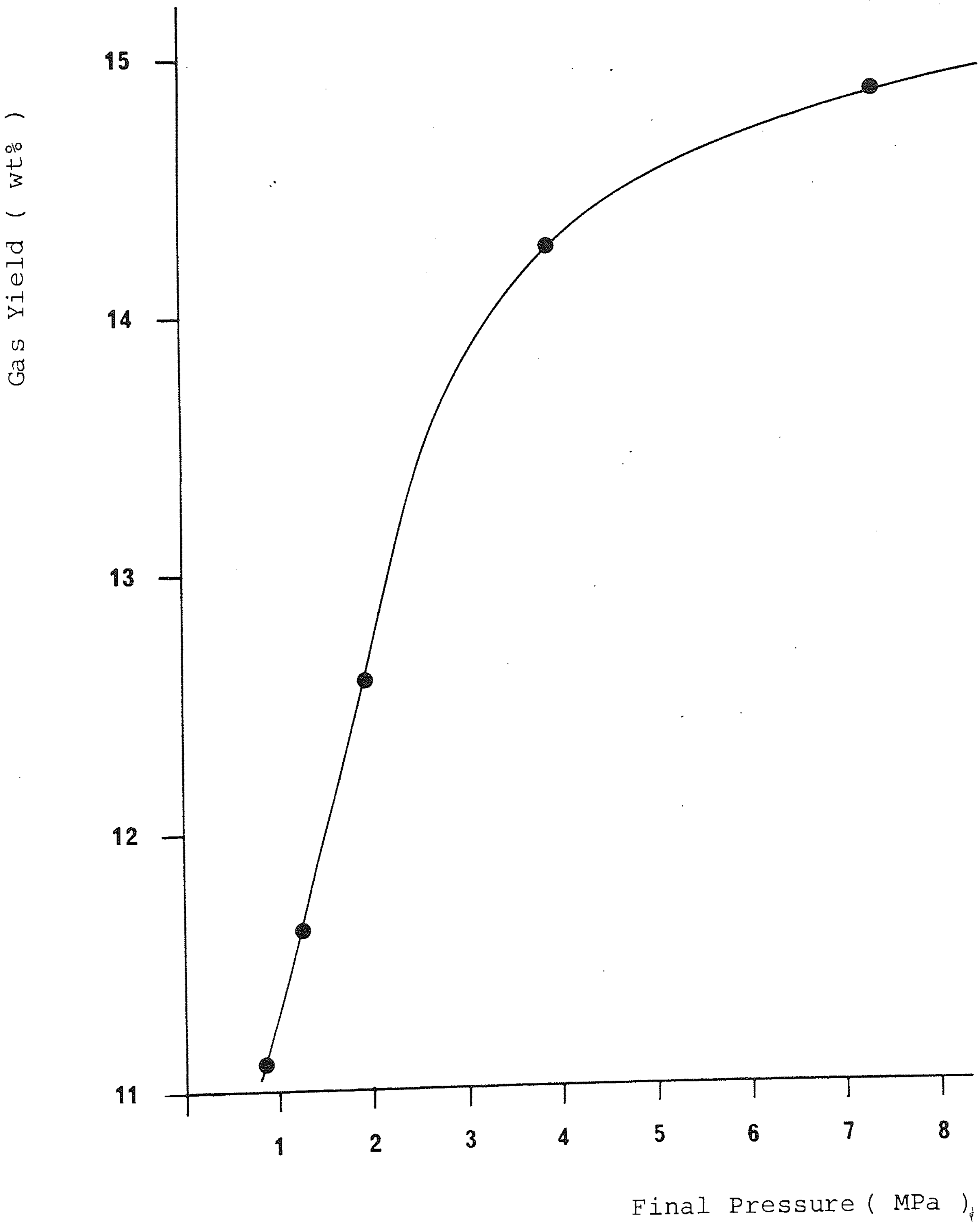

Figure 4.4

Typical HPLC trace showing the separation of a 'whole' tar, obtained by pyrolysis in a nitrogen atmosphere, into alkane, aromatic and polar fractions

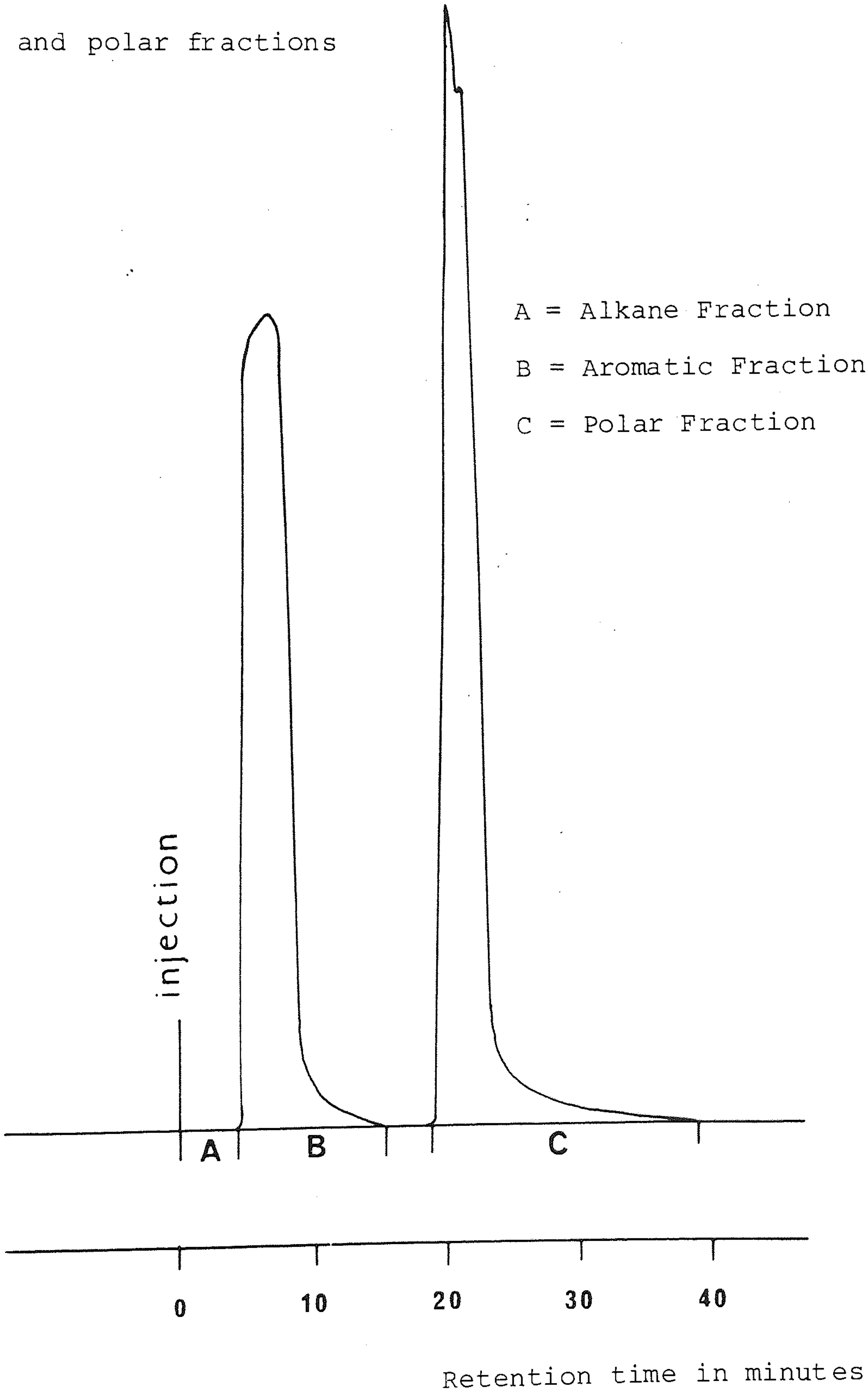

Figure 4.5

Yield of aromatic (■) and polar (●) fractions, obtained by HPLC separation, versus final pressure

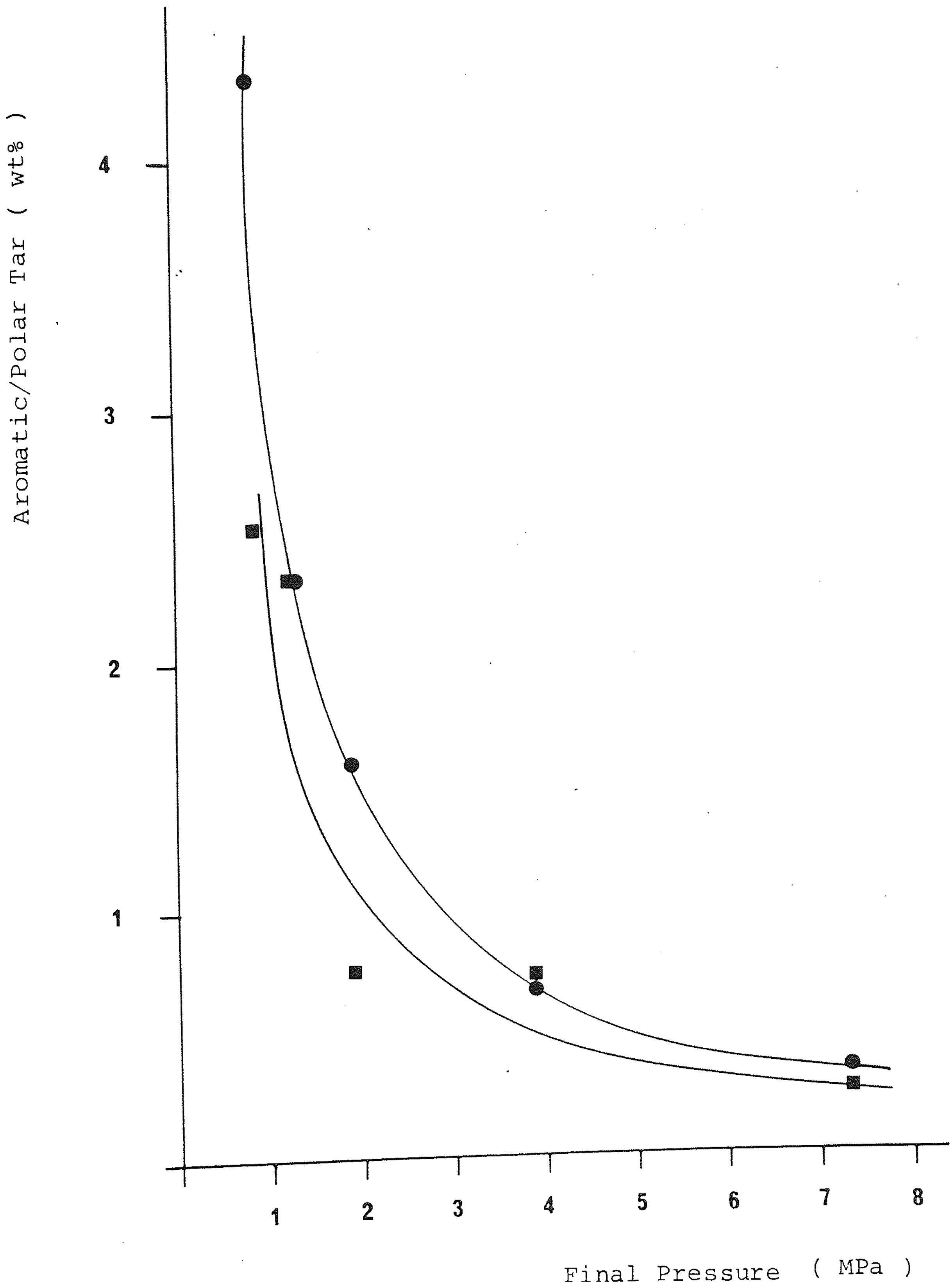

Figure 4.6

Typical HPLC trace for a toluene tar (produced under a nitrogen pressure) showing the aromatic region and the typical compounds present in HPLC fractions A-H

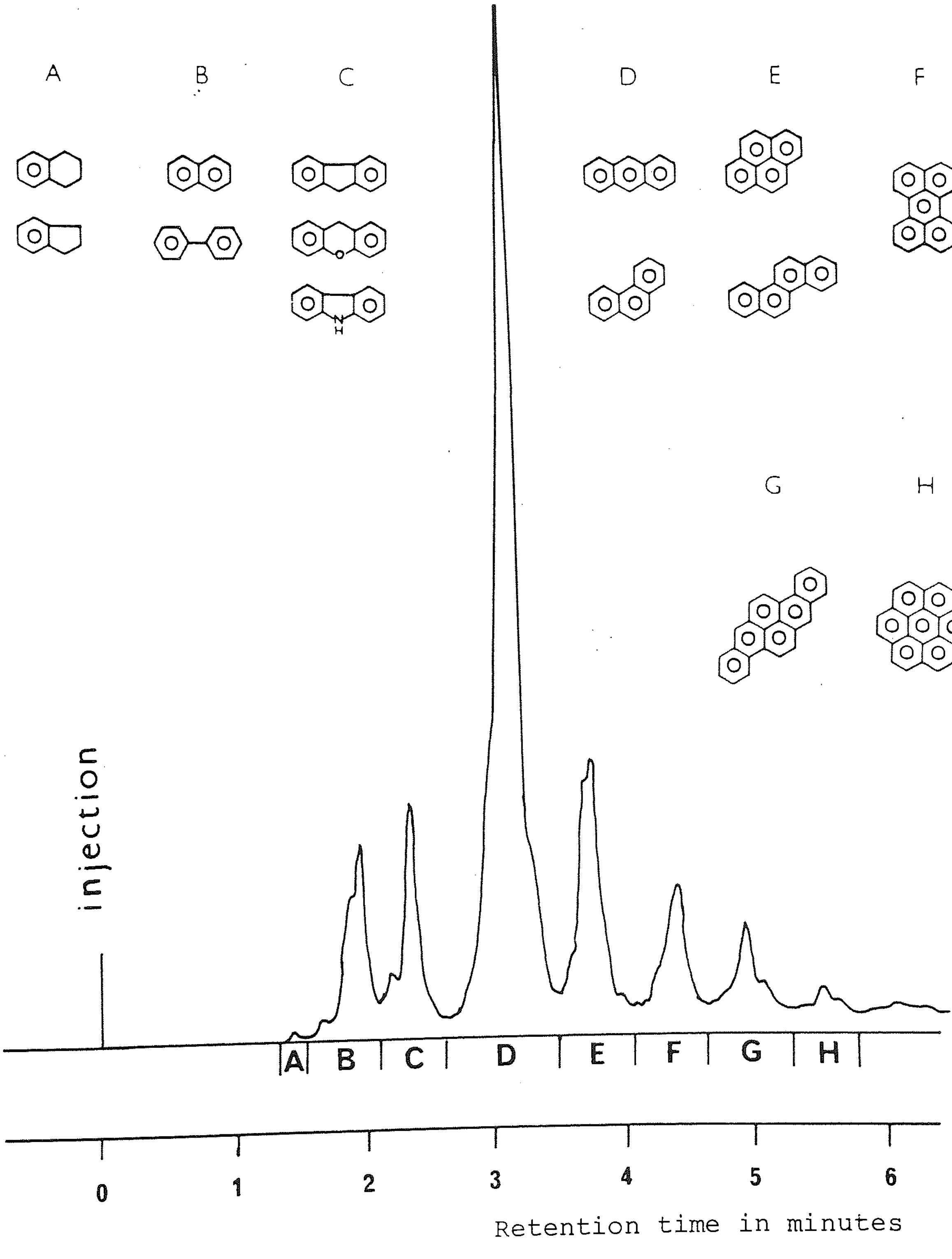

Figure 4.7

Pore size distribution for Manvers coal and nitrogen cokes

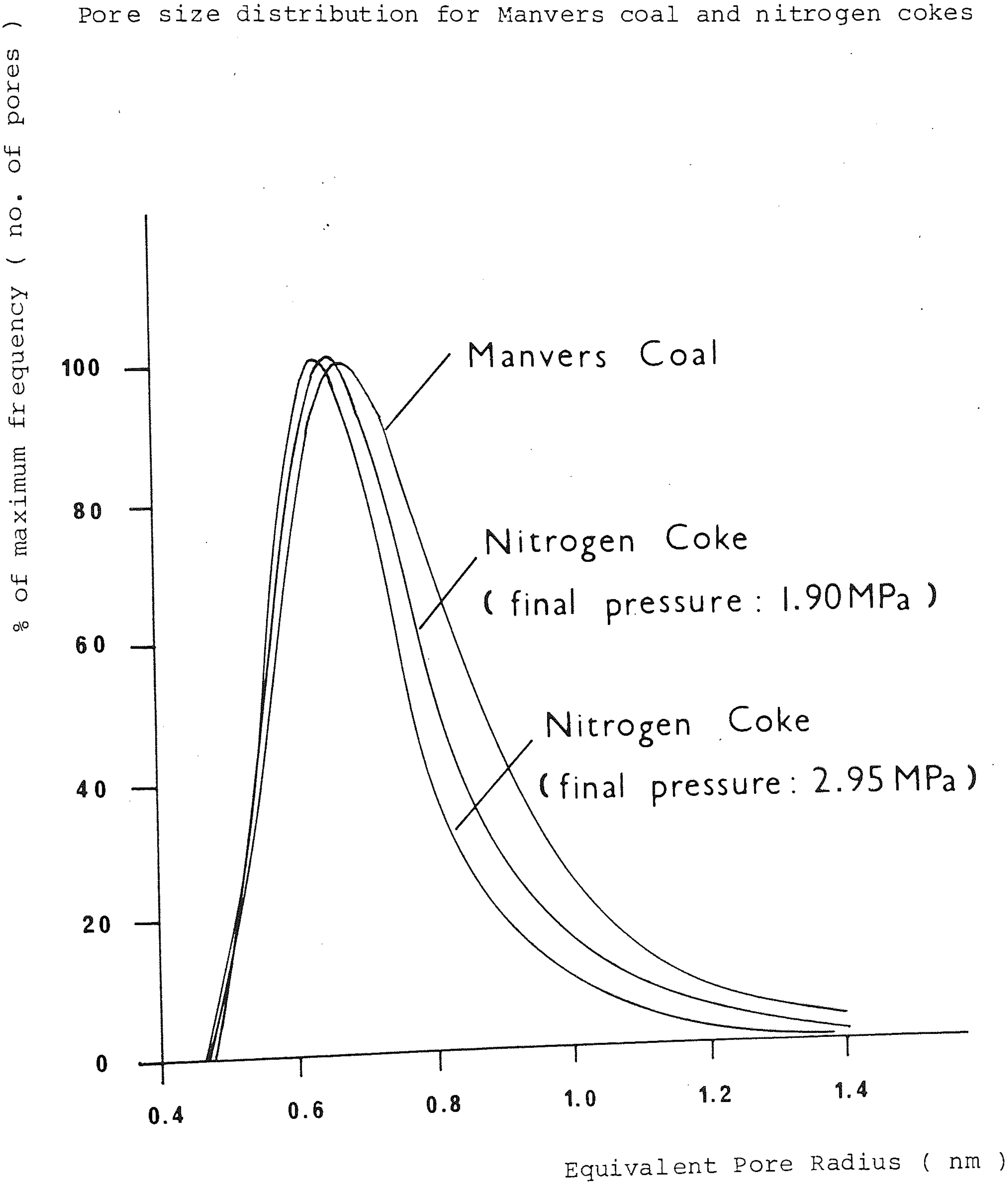

Table 4.2 Yields of Coke, Tar, Liquor and Gas at 500°C in Nitrogen

Final Pressure at 500°C (MPa)	Coke Wt.%	Tar Wt.%	Liquor Wt.%	Gas (by difference) Wt.%
0.85 ± 0.00	76.0 ± 0.5	6.87 ± 0.40	6.0 ± 0.5	11.1 ± 1.4
1.28 ± 0.02	78.0 ± 0.6	4.60 ± 0.28	5.8 ± 0.5	11.6 ± 1.4
1.90 ± 0.05	79.5 ± 0.5	2.36 ± 0.21	5.5 ± 0.5	12.6 ± 1.2
3.88 ± 0.05	78.3 ± 0.3	1.38 ± 0.05	6.0 ± 0.2	14.3 ± 0.6
7.32 ± 0.14	77.9 ± 0.3	0.65 ± 0.06	6.5 ± 0.3	14.9 ± 0.6

Table 4.3a Composition of Tars formed at 500°C in Nitrogen

Final pressure at 500°C MPa	Tar (Wt.% of coal)	
	Toluene Tar	THF Tar
0.85 ± 0.00	3.5	3.3
1.28 ± 0.02	2.4	2.1
1.90 ± 0.05	1.8	0.5
3.88 ± 0.05	1.1	0.3
7.32 ± 0.14	0.5	0.2

Table 4.3b Composition of Tars Formed at 500°C

Final Pressure Range at 500°C = 0.85 ± 0.00 - 7.32 ± 0.14 MPa

Composition of Tar					
Toluene Tar (Wt.%)			THF Tar (Wt.%)		
Neutrals	Acids	Bases	Neutrals	Acids	Bases
83 ± 4	9 ± 1	6 ± 1	5 ± 0.5	90 ± 5	1 ± 0.1

Table 4.4 Composition of Tar obtained from Pyrolysis under Nitrogen

Initial Nitrogen/Coal Ratio = 1 KPa/g

Final Pressure = 7.32 ± 0.14

Toluene Soluble Neutral Fraction

Molecule	Relative Concentration
Indan	0.02
Methylindan	0.11
Tetrahydronaphthalene	0.02
Naphthalene	0.98
Ethylindan	0.02
Dimethylindan	0.04
Methyltetrahydronaphthalene	0.03
Methylnaphthalene	1
Biphenyl	0.29
Dihydrophenalene	0.20
Dimethyl/Ethylnaphthalene	0.59
Phenalene	0.03
Methylbiphenyl	0.18
Dimethylbiphenyl	0.06
Trimethylnaphthalene	0.07
Dibenzofuran	0.10
Ethylbiphenyl	0.05
Fluorene	0.49
Xanthene	0.06
Methyldibenzofuran	0.08

Table 4.4 Continued

Toluene Soluble Neutral Fraction-Continued

Molecule	Relative Concentration
Dihydrophenanthrene/Anthracene	0.08
Methylfluorene	0.17
Anthracene/Phenanthrene	0.32
Carbazole	0.02
Methylanthracene/Phenanthrene	0.06
Dihydropyrene	0.04
Pyrene	0.02
Methylpyrene	0.04
Benzanthracene	0.01
Chrysene	0.03
Alkanes C_{11} - C_{24}	Trace

Toluene Soluble Acidic Fraction

Molecule	Relative Concentration
Phenol	0.40
Methylphenol	0.81
Trimethylphenol	0.17
Ethyl/Dimethylphenol	1
Methylethylphenol	0.65
Diethylphenol	0.63
Methylindanol	0.32
Dimethylindanol	0.01
Hydroxybiphenyl	0.25

Table 4.4 Continued

Toluene Soluble Basic Fraction

Molecule	Relative Concentration
Aniline	0.24
Methylaniline	0.30
Ethyl/Dimethylaniline	0.50
Quinoline	1
Methylquinoline	4.5
Tetrahydroquinoline	5.7
Ethyl/Dimethylquinoline	3.9
Acridine	6.0
Methylacridine	1.3
Naphthalamine	0.35
Diphenylamine	0.60

THF Neutral Fraction

Molecule
Phenalene
Methylbiphenyl
Dimethylbiphenyl
Trimethylnaphthalene
Dibenzofuran
Ethylbiphenyl
Fluorene
Xanthene
Methyldibenzofuran
Dihydrophenanthrene/ anthracene
Methylfluorene

Table 4.4 Continued

THF Neutral Fraction - Continued

Molecule

Anthracene/Phenanthrene

Carbazole

Methylanthracene/Phenanthrene

Dihydropyrene

Pyrene

Methylpyrene

Benzanthracene

Chrysene

THF soluble Acidic Fraction

Molecule

Catechol

Resorcinol

Hydroquinone

Naphthols

High Boiling Phenols

THF Soluble Basic Fraction

Too weak a tar solution for GC-MS

Table 4.5 Separation of Whole Tars (THF + Toluene) Obtained from Nitrogen Pyrolyses by High Performance Liquid Chromatography (HPLC) into Alkane, Aromatic and Polar Fractions

Final Pressure MPa	Alkanes Wt.%	Aromatics Wt.%	Polars Wt.%
0.85 ± 0.00	Trace Amount	2.54 ± 0.07	4.33 ± 0.07
1.28 ± 0.02	"	2.30 ± 0.23	2.30 ± 0.23
1.90 ± 0.05	"	0.75 ± 0.07	1.60 ± 0.07
3.88 ± 0.05	"	0.70 ± 0.04	0.67 ± 0.04
7.32 ± 0.14	"	0.26 ± 0.03	0.38 ± 0.03

Table 4.6 Variation of Yields of HPLC Fractions of Toluene Soluble Neutral Tars (Figure 4.6) with Pressure

Experiment	Final Pressure MPa	Typical Compounds present in HPLC Fractions A - H and the Relative Yields of the HPLC Fractions							
		A	B	C	D	E	F	G	H
		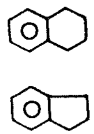	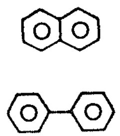	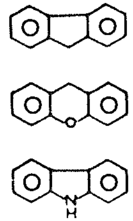	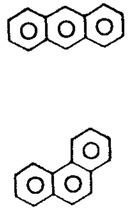	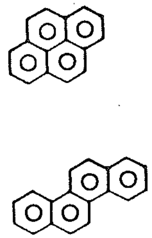	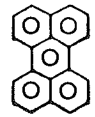	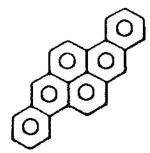	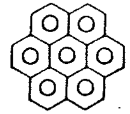
N1	0.85 ± 0.00	1	1	1	1	1	1	1	1
N2	1.28 ± 0.02	0.39	0.94	0.63	0.63	0.77	0.69	0.61	0.71
N3	1.90 ± 0.05	0.28	0.44	0.53	0.49	0.48	0.48	0.54	0.47
N4	3.88 ± 0.05	0.56	0.25	0.27	0.31	0.32	0.25	0.21	0.24
N5	7.32 ± 0.14	0.22	0.31	0.20	0.14	0.16	0.10	0.09	0.12

Table 4.7 Extinction Coefficients (ϵ) of Selected Molecules Present in Neutral Toluene Tar at a UV Absorption Wavelength (λ) of Approximately 254 nm

Molecule	Solvent	λmax. (nm)	logϵ
Indan	Isooctane	259.5	2.91
1,2,3,4-tetrahydro-naphthalene	Isooctane	259.5	2.54
Benzene	Isooctane	254	2.40
Naphthalene	Isooctane	256.5	3.50
Biphenyl	Isooctane	247	4.30
Fluorene	Isooctane	249	4.11
Xanthene	Isooctane	250	3.90
Carbazole	Ethanol	255	4.20
Anthracene	Isooctane	251.5	5.29
Phenanthrene	Isooctane	250.5	4.82
Pyrene	Cyclohexane	252	4.10
Chrysene	Heptane	255	4.90
Perylene	Isooctane	252.5	4.78
Dibenzo(a,l)pyrene	Ethanol	253	4.80
Coronene	Ethanol	252	3.88

Table 4.8 Elemental Analyses for Cokes and Manvers Coal (as received)

Experiment	Final Pressure MPa	% Carbon	% Hydrogen	% Nitrogen
N1	0.85 ± 0.00	82.0 ± 0.05	2.7 ± 0.05	1.8 ± 0.1
N2	1.28 ± 0.02	81.9 ± 0.2	2.7 ± 0.05	1.9 ± 0.1
N3	1.90 ± 0.05	82.0 ± 0.05	2.8 ± 0.05	1.9 ± 0.1
N4	3.88 ± 0.05	83.5 ± 0.1	2.9 ± 0.05	2.0 ± 0.1
N5	7.32 ± 0.14	82.8 ± 0.3	2.7 ± 0.05	1.9 ± 0.1
Manvers Coal	-	78.6 ± 0.4	5.0 ± 0.1	1.6 ± 0.1

Table 4.9 Atomic H/C Ratios and Methanol Densities of Cokes

Initial Nitrogen to Coal Ratio (KPa/g)	Final Pressure (MPa)	Atomic H/C Ratio	Methanol Density (g/cm^3 at $25^{\circ}C$)
125	0.1	0.41 ± 0.01	0.88 ± 0.03
1 - 16	0.85 - 7.32	0.39 ± 0.01	1.59 ± 0.005

Table 4.10 Microporosities and Surface Areas of Cokes

Sample	Final Pressure MPa	Surface Area m^2/g	Micropore Volume cm^3/g	Mean Equivalent Pore Radius $\bar{r}_e$ (nm)
Coal	-	162	0.061	0.75
Nitrogen Coke	1.90 ± 0.05	181	0.063	0.69
Nitrogen Coke	2.95 ± 0.07	206	0.074	0.72

Table 4.11 Variation in Percentage Gas Volumes at 500°C with Final Pressure for Nitrogen Pyrolyses

Experiment	Final Pressure MPa	Hydrogen	Methane	Ethane	Propane
N1	0.85 ± 0.00	18.80 ± 0.20	74.95 ± 0.65	3.30 ± 0.30	2.95 ± 0.15
N2	1.28 ± 0.02	18.85 ± 0.65	74.55 ± 0.45	3.35 ± 0.15	3.25 ± 0.35
N3	1.90 ± 0.05	17.55 ± 0.25	73.20 ± 0.00	3.80 ± 0.20	5.45 ± 0.05
N4	3.88 ± 0.05	12.75 ± 0.25	73.10 ± 0.80	3.90 ± 0.20	10.20 ± 0.80
N5	7.32 ± 0.14	9.40 ± 0.10	70.80 ± 1.20	6.90 ± 0.60	12.85 ± 0.65

Table 4.12 Yields of gas in grams per 100 grams of coal for nitrogen pyrolyses

Experiment	Final Pressure MPa	Hydrogen	Methane	Ethane	Propane
N1	0.85 ± 0.00	0.29 ± 0.03	9.1 ± 1.3	0.74 ± 0.03	0.98 ± 0.08
N2	1.28 ± 0.02	0.30 ± 0.02	9.4 ± 1.1	0.79 ± 0.05	0.78 ± 0.07
N3	1.90 ± 0.05	0.28 ± 0.02	9.5 ± 0.9	0.92 ± 0.13	1.9 ± 0.2
N4	3.88 ± 0.05	0.21 ± 0.01	9.5 ± 0.6	0.95 ± 0.10	3.6 ± 0.1
N5	7.32 ± 0.14	0.15 ± 0.01	8.8 ± 0.6	1.6 ± 0.1	4.4 ± 0.1

Table 4.13 Hydrogen content of gas in grams per 100 grams of coal for nitrogen pyrolyses

Experiment	Final Pressure (MPa)	Hydrogen	Methane	Ethane	Propane	Total Hydrogen
N1	0.85 ± 0.00	0.29 ± 0.03	2.3 ± 0.2	0.14 ± 0.00	0.18 ± 0.02	2.9 ± 0.3
N2	1.28 ± 0.02	0.30 ± 0.02	2.3 ± 0.3	0.15 ± 0.02	0.14 ± 0.02	2.9 ± 0.4
N3	1.90 ± 0.05	0.28 ± 0.02	2.4 ± 0.2	0.19 ± 0.03	0.35 ± 0.04	3.2 ± 0.3
N4	3.88 ± 0.05	0.21 ± 0.01	2.4 ± 0.2	0.19 ± 0.02	0.66 ± 0.01	3.5 ± 0.2
N5	7.32 ± 0.14	0.15 ± 0.01	2.2 ± 0.2	0.32 ± 0.01	0.80 ± 0.01	3.5 ± 0.2

Table 4.14 Carbon content of gas in grams per 100 grams of coal for nitrogen pyrolyses

Experiment	Final Pressure MPa	Methane	Ethane	Propane	Total Carbon
N1	0.85 ± 0.00	6.8 ± 0.9	0.59 ± 0.03	0.80 ± 0.06	8.2 ± 1.0
N2	1.28 ± 0.02	7.0 ± 0.8	0.63 ± 0.04	0.64 ± 0.06	8.3 ± 0.9
N3	1.90 ± 0.05	7.1 ± 0.6	0.74 ± 0.10	1.6 ± 0.2	9.4 ± 0.9
N4	3.88 ± 0.05	7.1 ± 0.4	0.76 ± 0.08	3.0 ± 0.1	10.9 ± 0.5
N5	7.32 ± 0.14	6.6 ± 0.5	1.30 ± 0.04	3.6 ± 0.2	11.5 ± 0.7

Table 4.15 Hydrogen mass balance in grams per 100 grams of coal for nitrogen pyrolyses

Experiment	Final Pressure MPa	Quantity of Coal used (grams)	Hydrogen in Coke	Hydrogen in Tar based on Naphthalene	Hydrogen in Liquor	Hydrogen in Gas	Total Hydrogen	Total Hydrogen Expected
N1	0.85 ± 0.00	6.25	2.24	0.43	0.67	2.9	6.2	5
N2	1.28 ± 0.02	12.5	2.16	0.29	0.65	2.9	6.0	5
N3	1.90 ± 0.05	25	2.24	0.15	0.60	3.2	6.2	5
N4	3.88 ± 0.05	50	2.28	0.09	0.66	3.4	6.4	5
N5	7.32 ± 0.14	100	2.10	0.04	0.72	3.5	6.4	5

Total Hydrogen Expected: Hydrogen content of a given amount of Manvers coal at the start of pyrolysis.

Table 4.16 Carbon mass balance in grams per 100 grams of coal for nitrogen pyrolyses

Experiment	Final Pressure MPa	Quantity of Coal used (grams)	Carbon in Coke	Carbon in Tar based on Naphthalene	Carbon in Gas	Total Carbon	Total Carbon Expected
N1	0.85 ± 0.00	6.25	61.8	6.4	8.2	76.4	78.6
N2	1.28 ± 0.02	12.5	61.8	4.3	8.3	74.4	78.6
N3	1.90 ± 0.05	25	65.2	2.2	9.4	76.8	78.6
N4	3.88 ± 0.05	50	65.4	1.3	10.9	77.6	78.6
N5	7.32 ± 0.14	100	64.5	0.6	11.5	76.6	78.6

Total Carbon Content: Carbon Content of a given amount of Manvers coal at the start of pyrolysis.

Table 4.17 Effect of Rate of Heating on Coke and Tar Formation

Experiment	Final Pressure (MPa)	Coke Yield (Wt.%)	Tar Yield (Wt.%)	Density of Coke (g/cm^3)
A	7.32	77.9 $\pm$ 0.3	0.65	1.585 $\pm$ 0.005
B	7.32	75.0 $\pm$ 0.5	0	1.595 $\pm$ 0.005

A = Autoclave experiment, average rate of heating: 4.2 $^{\circ}$C/min and held at 500 $^{\circ}$C for 2 hours.

B = Sandbath experiment, average rate of heating: 83 $^{\circ}$/min and held at 500 $^{\circ}$C for 30 minutes.

CHAPTER FIVE

HYDROPYROLYSIS OF MANVERS COAL

CHAPTER FIVE

HYDROPYROLYSIS OF MANVERS COAL

5.1 Pyrolysis Under Hydrogen Pressure

Chapter four describes how nitrogen pressures have modified the original pyrolysis scheme (chapter 1, scheme 1, page 1) and now the effects of hydrogen pressures on this reaction scheme will be examined. In considering hydropyrolysis it is desirable to distinguish between the effects of increased pressure and of an increased ratio of hydrogen to coal. Nitrogen pyrolyses have shown that pressure has had a marked effect on the yields of tar and in hydropyrolysis the presence of hydrogen is expected to enhance tar yields. Therefore, it is necessary to know whether it is the pressure or the hydrogen to coal ratio which is affecting the yields of pyrolysis. To achieve this, Manvers coal has been pyrolysed at a constant hydrogen to coal ratio (140 KPa/g) and also at various hydrogen to coal ratios (4 - 190 KPa/g).

5.2 Experimental Conditions

The experimental conditions for hydropyrolyses are shown in table 5.1. Typical graphs showing the increase in pressure with temperature during hydropyrolysis are shown in figures 5.1 (page 87) and 5.2 (page 88). Figure 5.1 shows the pressure - temperature graphs for the various hydrogen to coal ratios used and figure 5.2 shows the pressure -

Table 5.1 Experimental Conditions for Hydrogen Pyrolyses Performed in the Autoclave

Average Rate of Heating = $4.2^{o}C\ min^{-1}$

Final Coal Pyrolysis Temperature = $500^{o}C$

Heat Soak Time at $500^{o}C$ = 2 hours

Experiment	Grams of Coal used	Initial Hydrogen/Coal Ratio (KPa/g)	Final Pressure (at $500^{o}C$) MPa
H0	25	4	1.85 ± 0.06
H1	50	20	4.45 ± 0.10
H2	25	80	5.75 ± 0.16
H3	25	140	6.66 ± 0.14
H4	25	190	10.03 ± 0.24
H5	6.25	140	2.50 ± 0.10
H6	12.5	140	4.50 ± 0.10
H7	25	140	6.66 ± 0.14
H8	50	140	13.20 ± 0.30

Figure 5.1 Typical graphs showing the increase in pressure with temperature during hydropyrolysis for varying hydrogen to coal ratios

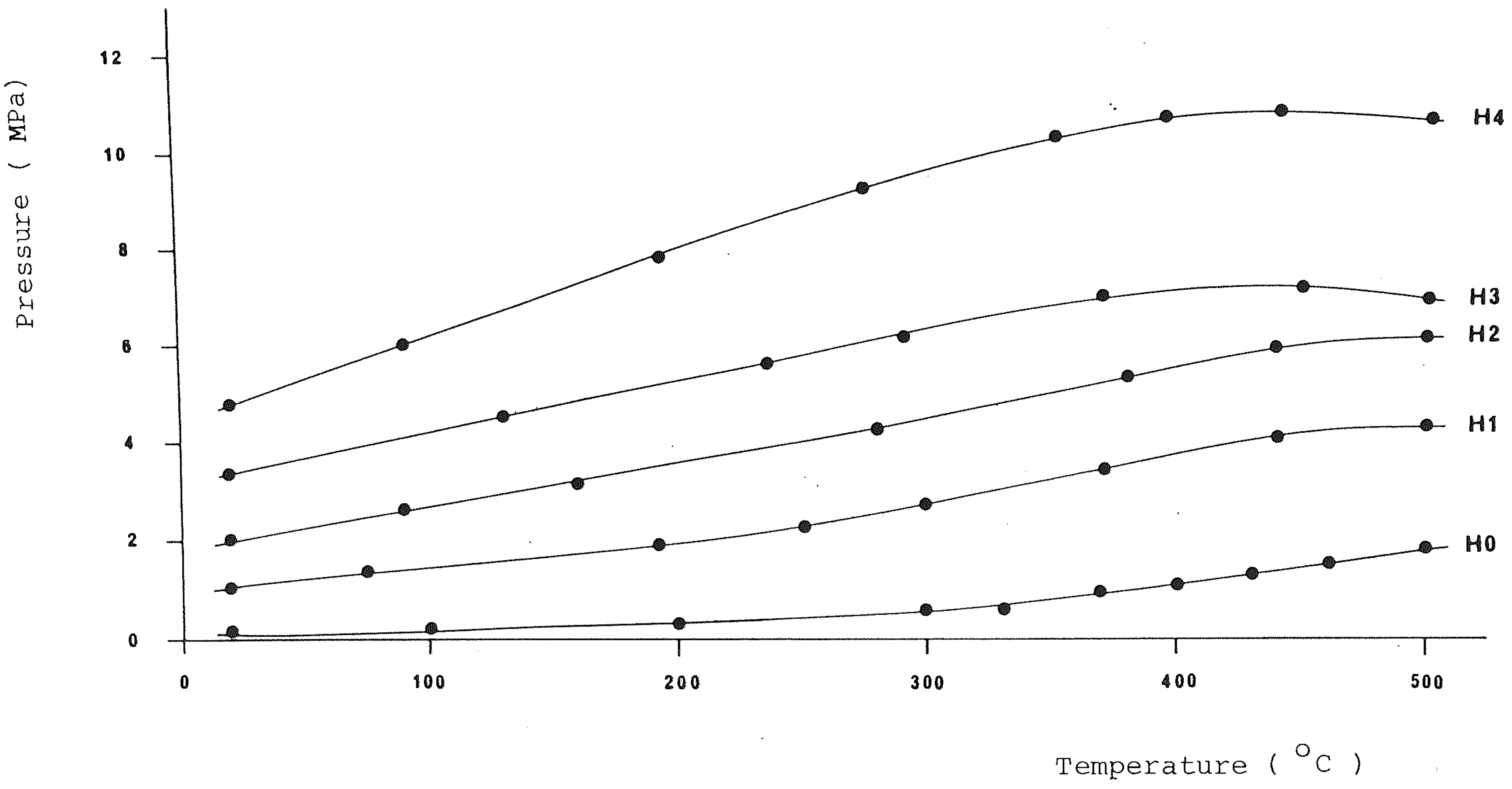

Figure 5.2 Typical graphs showing the increase in pressure with temperature during hydropyrolysis (initial hydrogen to coal ratio maintained constant: 140 KPa/g)

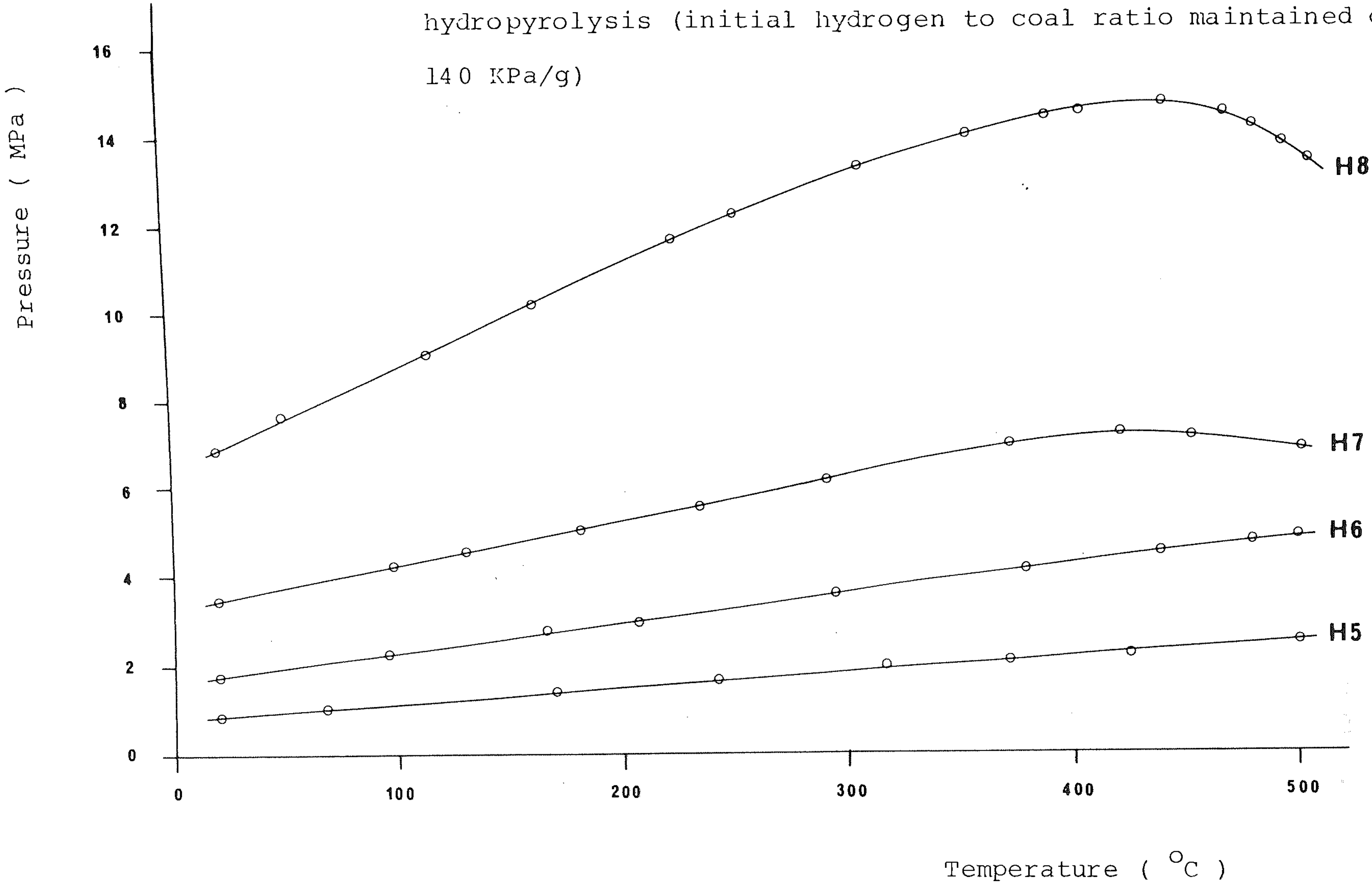

temperature graphs obtained for hydropyrolyses performed at a constant hydrogen to coal ratio (140 KPa/g). Further experimental details have been outlined in chapter 3.

5.3 Yields

Yields from hydropyrolyses are shown in tables 5.2 (page 105) and 5.3 (page 106). Table 5.2 emphasises the effect of pressure at a constant high ratio of hydrogen to coal. Comparison with table 4.2 (page 65) shows that, unsurprisingly, the presence of hydrogen increased the yield of tar and in terms of reaction scheme 1 (page 1) this was presumably because of the increased scission of aliphatic linkages between aromatic nuclei and the increased formation of comparatively low molecular weight volatile material. The presence of hydrogen also increased the yield of liquor and indeed at least 90% of the oxygen present in the initial coal was evolved as liquor. Table 5.2 (page 105) shows that increase in pressure caused a great increase in the yield of gas (figure 5.3, page 95), a dramatic fall in the yield of THF soluble tar (figure 5.4, page 96) and a significant reduction in the yield of coke (figure 5.5, page 97), but had comparatively little effect on the yields of either liquor or of toluene soluble tar.

Table 5.4 (page 107) shows that whereas the toluene soluble tar was predominantly neutral, the THF soluble tar consisted mainly of phenols and in fact GC-MS analysis showed the THF soluble material to be composed of polyhydric phenols, naphthols and high boiling phenolic material. Thus increasing hydrogen pressure caused loss of polyhydric and high boiling phenols (including naphthols) during pyrolysis.

Comparison of tables 5.2 (page 105) and 5.3 (page 106) suggests that as the ratio of hydrogen to coal was increased the yields of tar (figure 5.6, page 98) and liquor increased correspondingly to a maximum value which was obtained when there was an initial pressure of between 140 and 190 KPa of hydrogen per gram of coal (viz. the hydrogen initially present was about 14% of the weight of coal). The presence of such a maximum value has already been demonstrated by Cyprès and his colleagues[22] and indicates that not only does hydrogen promote tar formation but it must also promote some reactions in which tar is cracked to evolve gas. The gas yield increased (figure 5.7, page 99) with increasing hydrogen to coal ratio whereas the coke yield decreased (figure 5.8, page 100).

5.4 Tars

Figure 5.9 (page 101) shows a typical HPLC trace for a toluene soluble neutral tar produced by hydropyrolysis. The HPLC trace indicates that there are small amounts of higher molecular weight materials (perylene, dibenzopyrene and coronene) than those identified by GC-MS. Table 5.5 (page 108) summarises HPLC analyses of the toluene soluble neutral material. Since the fractions were detected by their UV absorption at 254 nm the results overemphasised the importance of the larger polynuclear aromatic molecules. Comparison of tables 4.6 (page 73) and 5.5 (page 108) shows that whereas nitrogen pressures reduced the yields of all neutral fractions, hydrogen pressure (at constant hydrogen to coal ratio) increased the yields of the smaller and moderate sized molecules but diminished the yields of the larger molecules. The overall effect, of course, was that shown in tables 4.2 (page 65) and 5.2 (page 105) respectively. The results confirmed that the yields of all HPLC fractions increased with values of the initial hydrogen to coal ratio to 140 KPa per gram but that, allowing for the effect of change in the final pressure, the initial hydrogen to coal ratio of 190 KPa per gram produced no further increase in yields. These results require confirmation since it is possible that changes in the composition of the neutral material may have changed the extinction coefficients controlling the absorption of 254 nm light though GC-MS analysis of the tars suggests this is unlikely. Table 5.6 (page 109) lists the components present in the tars obtained from hydropyrolysis. Comparison of tables 4.4 (page 68) and table 5.6 shows that the tars produced under hydrogen pressure are very similar to those produced under nitrogen pressure.

Perhaps the most interesting result shown by tables 5.2 (page 105) and 5.3 (page 106) is that the conditions for maximum yields of tar and gas are entirely different. Maximum yields of tar requires an optimum ratio of hydrogen to coal but not high pressures; maximum yields of gas appear to be generated by high ratios of hydrogen to coal and by high pressures.

5.5 Cokes

Table 5.7 (page 113) shows the elemental analyses for the cokes. Table 5.8 (page 114) shows the atomic hydrogen to carbon ratios and the methanol densities of the cokes. The densities of the cokes were nearly twice those of cokes produced at atmospheric pressure but showed little variation with pressure. The methanol densities of cokes obtained from pyrolyses having a liquor yield of more than 10% must be close to the true density of the coke since under these circumstances the cokes could not have retained many polar groups[42]. In fact the methanol densities of all the cokes were reasonably similar suggesting that their chemical structures were determined more by the temperatures than the pressures at which pyrolysis occurred.

The micropore surface areas, volumes and the mean equivalent pore radii of the cokes deduced from carbon dioxide adsorption isotherms are shown in table 5.9 (page 115). Carbon dioxide adsorption isotherm data for a coke prepared under hydrogen are given in appendix 2. Cokes prepared under hydrogen were much stronger and more coherent than those prepared in nitrogen and a more fluid intermediate was obviously formed during pyrolysis. Pyrolysis generated fluidity and decreased the microporosity of the resulting coke. The microporosity diminished with increasing hydrogen pressure (figure 5.10, page 102). It is not clear whether this was due to the collapse of the original pore structure of the rigid coal when it became fluid and the inhibition of volatilisation by pressure or whether it occurred because blocking of the pore structure by viscous material and cracking of mobile material trapped within the micropores diminished the accessible micropore surface. Both explanations imply that the large tar yields one expects to be obtainable in the presence of excess hydrogen at low pressures had been diminished very significantly by cracking in all the hydropyrolyses reported here. Figure 5.11 (page 103) shows the typical pore - size distribution curve for a hydropyrolysis coke. The pore size distribution of the hydrogen cokes resembled that of the nitrogen cokes.

Finally, one notes that during pyrolysis with hydrogen, but not with nitrogen, the pressure increased to a maximum close to the final temperature (figures 5.1 (page 87) and 5.2 (page 88)), 500°C, and then decayed slowly showing that hydrogenation reactions were continuing. The rate of decrease of pressure was approximately proportional to the square of the maximum pressure obtained which is consistent with the occurrence of such reactions as:

$$\text{Carbonaceous Solids} + 2H_2 \longrightarrow CH_4$$

Thus we appear to have been observing the hydrogasification of the residual char and tar which, at 500°C, was slow.

5.6 Gases

Tables 5.10 (page 116) and 5.11 (page 117) show the composition of the gases obtained by hydropyrolysis. There was a tendency, at a constant hydrogen to coal ratio of 140 KPa/g, for the proportion of simple alkanes to increase with the pressure of the hydropyrolysis. However, as the ratio of hydrogen to coal was increased the proportion of simple alkanes decreased. Traces of ammonia and hydrogen sulphide were also found. No oxides of carbon were found. The gas volumes given in tables 5.10 and 5.11 have been converted into gas weights (grams) in table 5.12 (page 118). Tables 5.13 (page 119) and 5.14 (page 120) show the hydrogen and carbon content of each gas (in grams) respectively. Table 5.15 (page 121) shows the hydrogen mass balance which indicates that the hydrogen in each gram of coke was constant (similar to nitrogen cokes). There appears to be no mechanism whereby the cokes can readily be partially hydrogenated at these temperatures. The table also shows that the overwhelming majority of the hydrogen is in the pyrolysis gas and it is this fraction which accounts for most of the hydrogen consumption. Table 5.16 (page 122) shows the carbon mass balance. Table 5.17 (page 123) shows the hydrogen consumption for all the hydropyrolyses performed. It is clear that for a constant hydrogen to coal ratio the effect of increased pressure on hydrogen consumption is negligible. As the ratio of hydrogen to coal was increased the hydrogen consumption increased correspondingly to a maximum value (figure 5.12, page 104) which was obtained when there was an initial pressure of between 140 and 190 KPa of hydrogen per gram of coal.

Figure 5.3

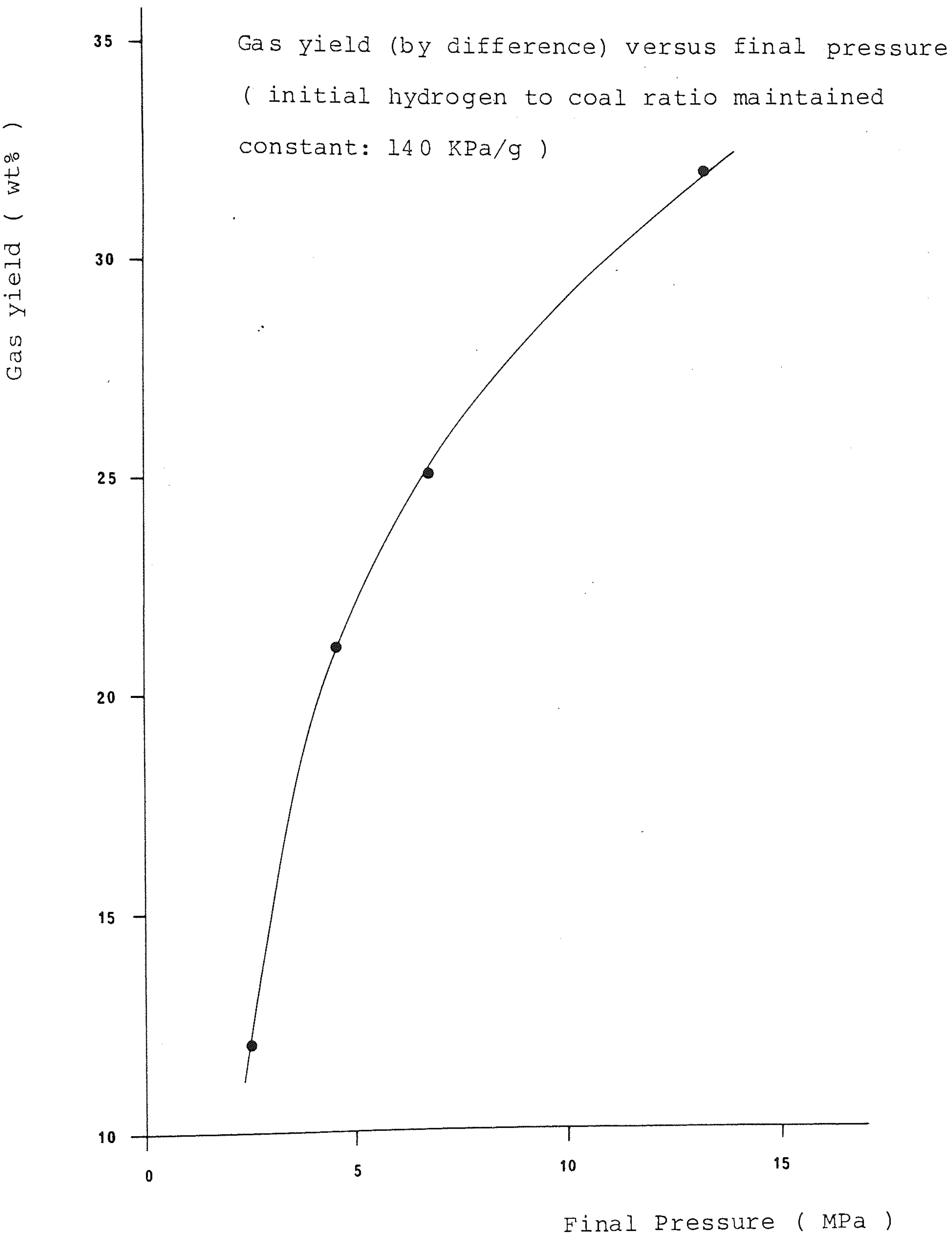
Gas yield (by difference) versus final pressure
(initial hydrogen to coal ratio maintained
constant: 140 KPa/g)
Gas yield (wt%)
35
30
25
20
15
10
0
5
10
15
Final Pressure (MPa)

Figure 5.4

Yield of THF tar versus final pressure (initial hydrogen to coal ratio maintained constant: 140 KPa/g)

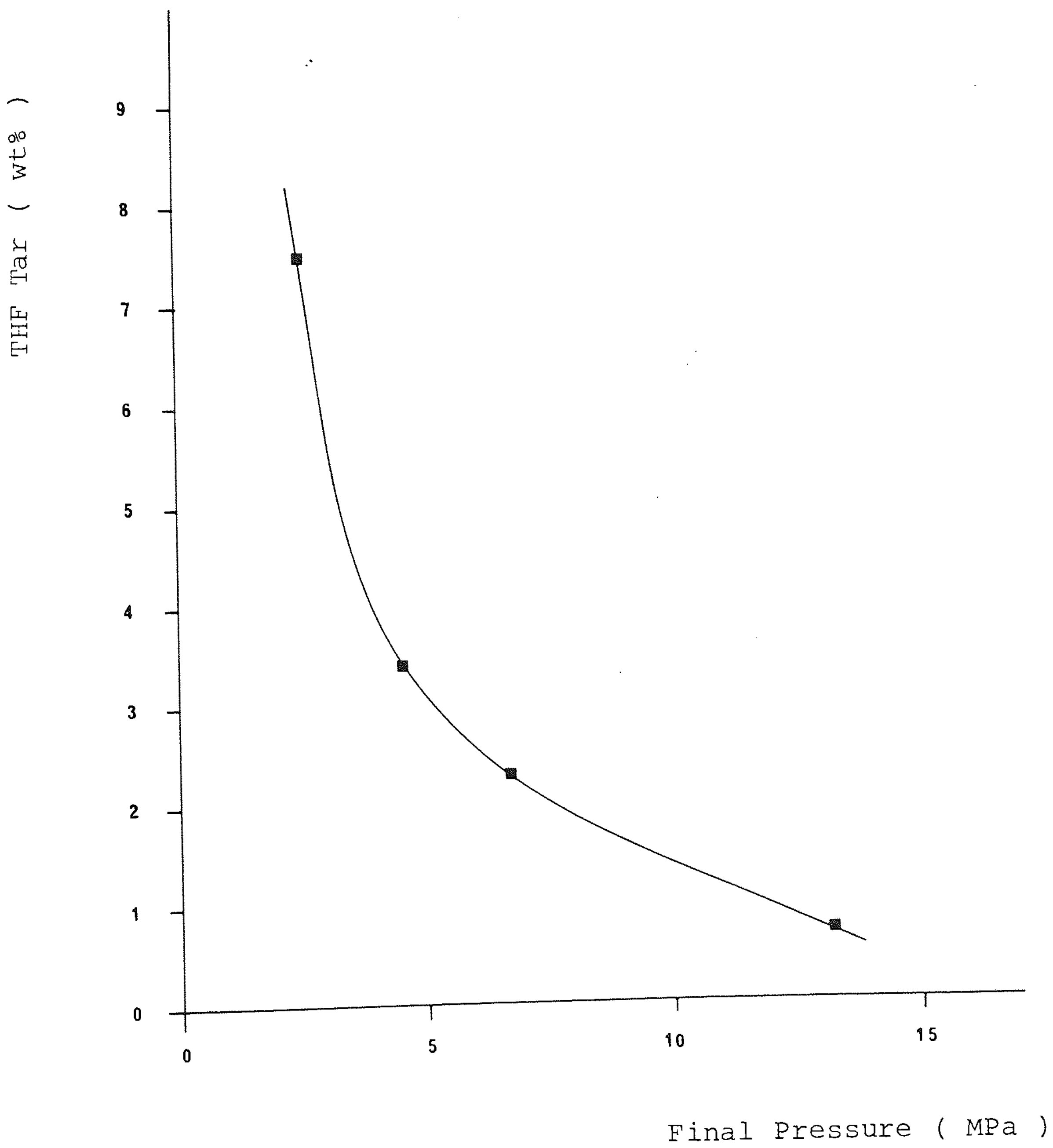

Figure 5.5

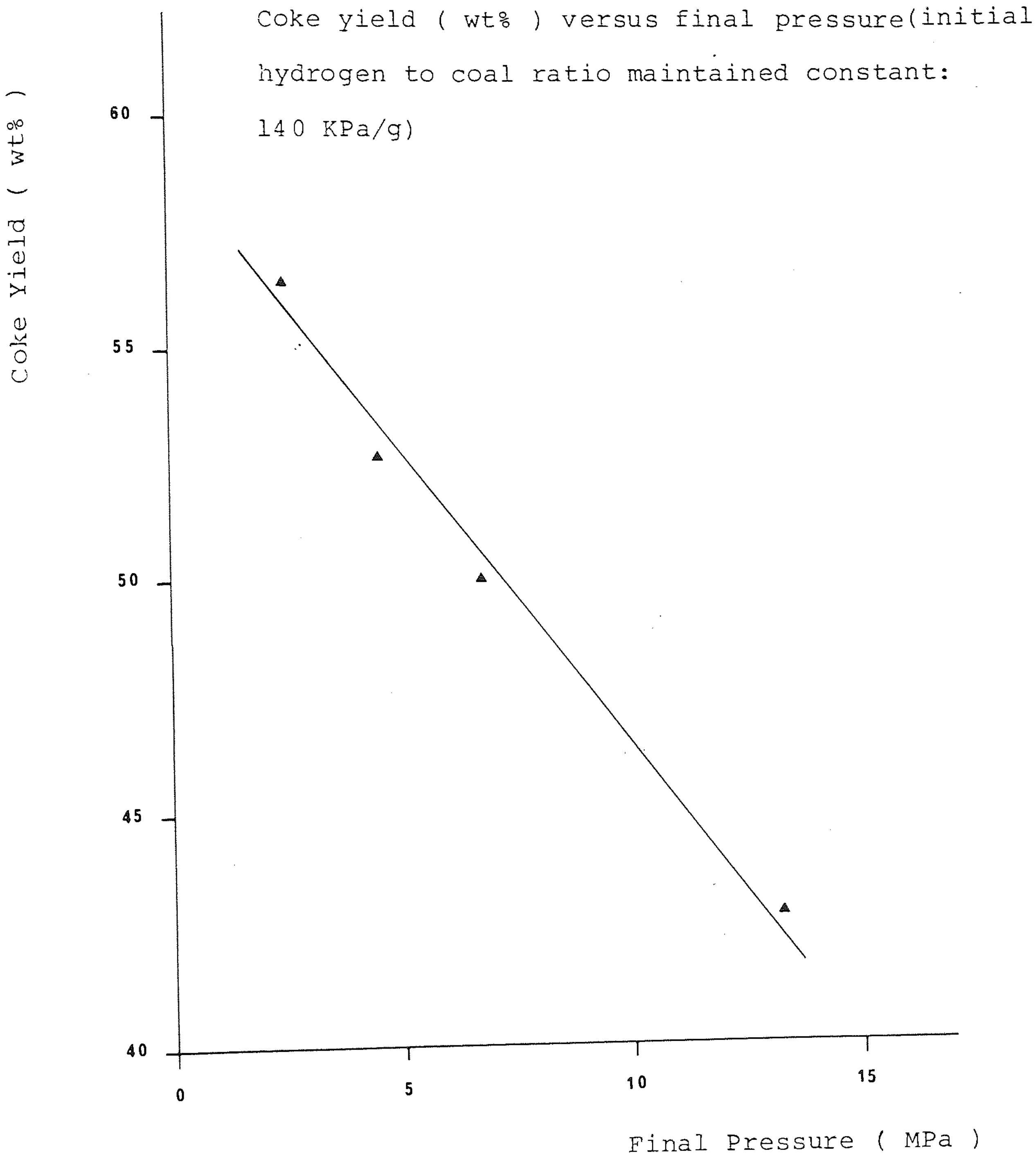
Coke yield (wt%) versus final pressure(initial
hydrogen to coal ratio maintained constant:
140 KPa/g)
Coke Yield (wt%)
60
55
50
45
40
0
5
10
15
Final Pressure (MPa)

Figure 5.6 Toluene tar yield (wt%) versus initial hydrogen to coal ratio

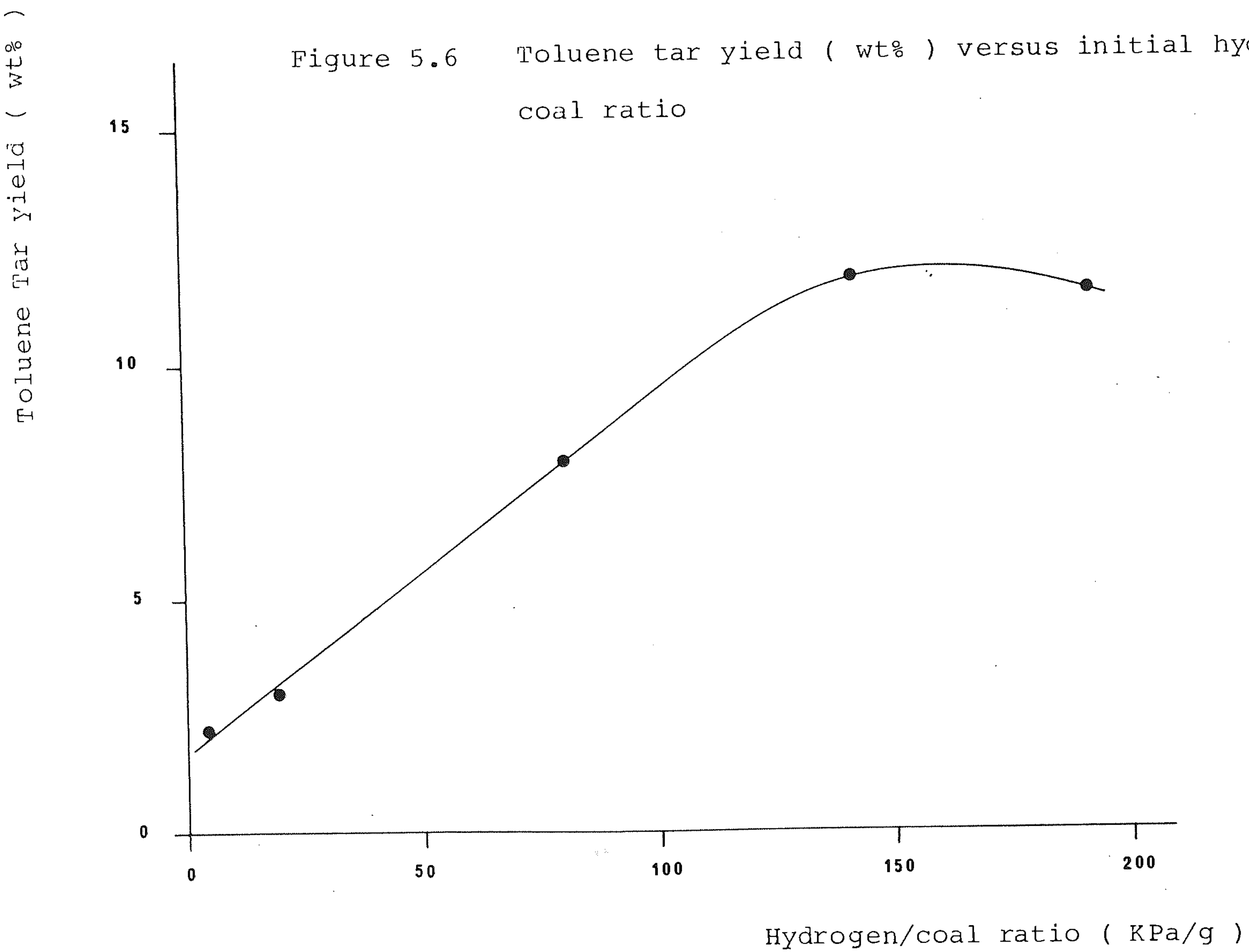

Figure 5.7 Gas yield (by difference) versus initial hydrogen to coal ratio

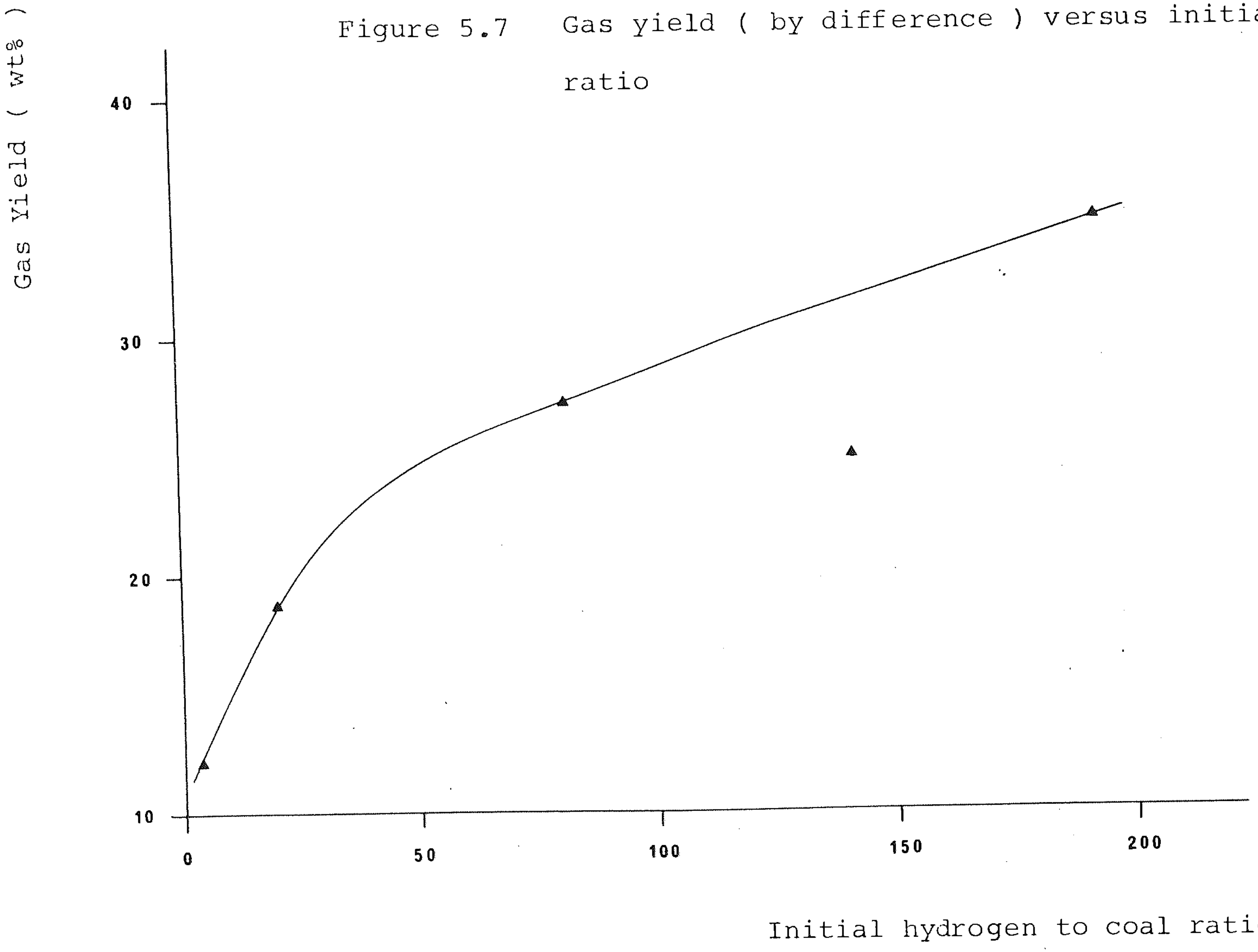

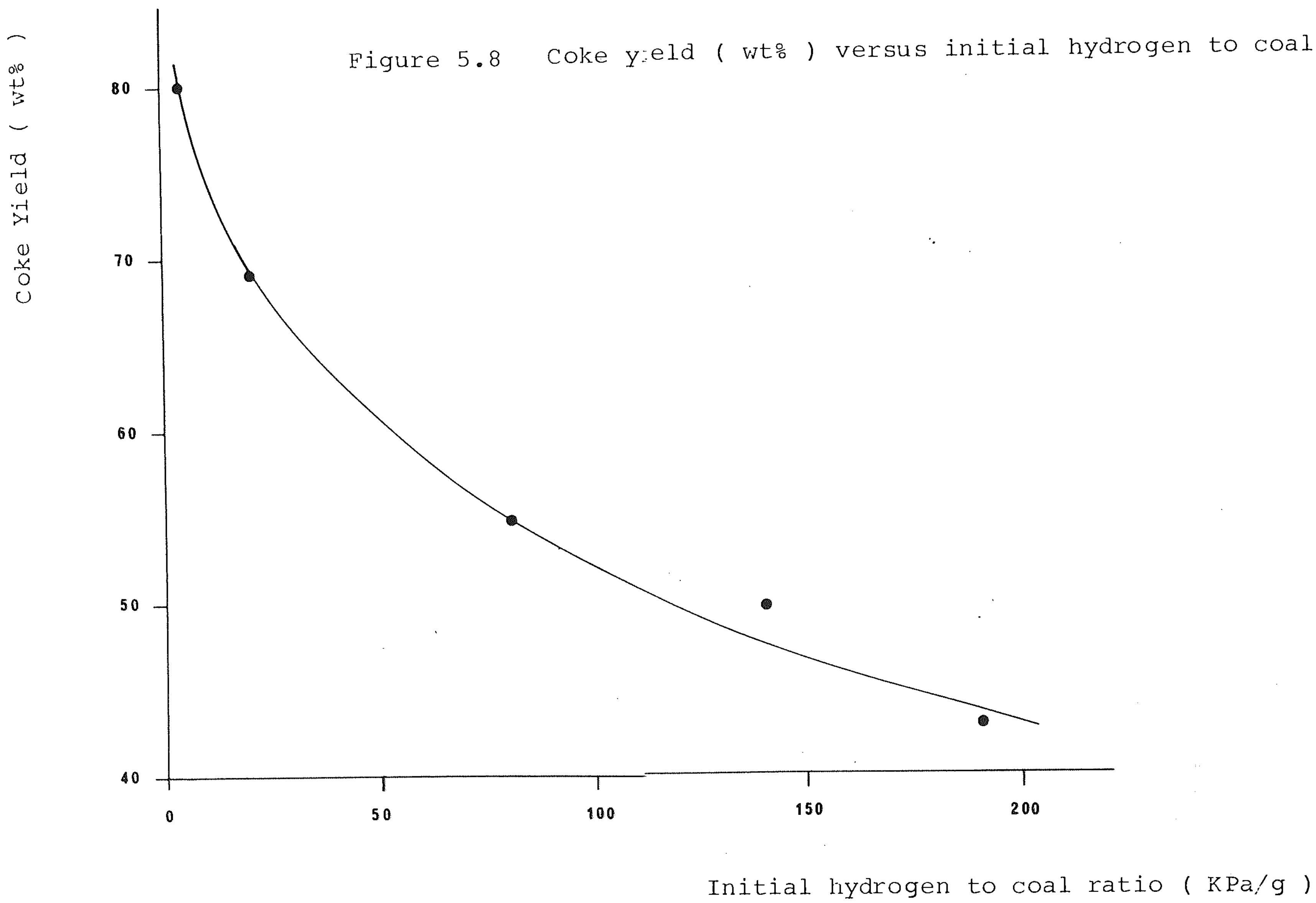

Figure 5.8 Coke y:eld (wt%) versus initial hydrogen to coal ratio

Figure 5.9

Typical HPLC trace for a toluene tar (produced under a hydrogen pressure) showing the aromatic region and the typical compounds present in HPLC fractions A-H

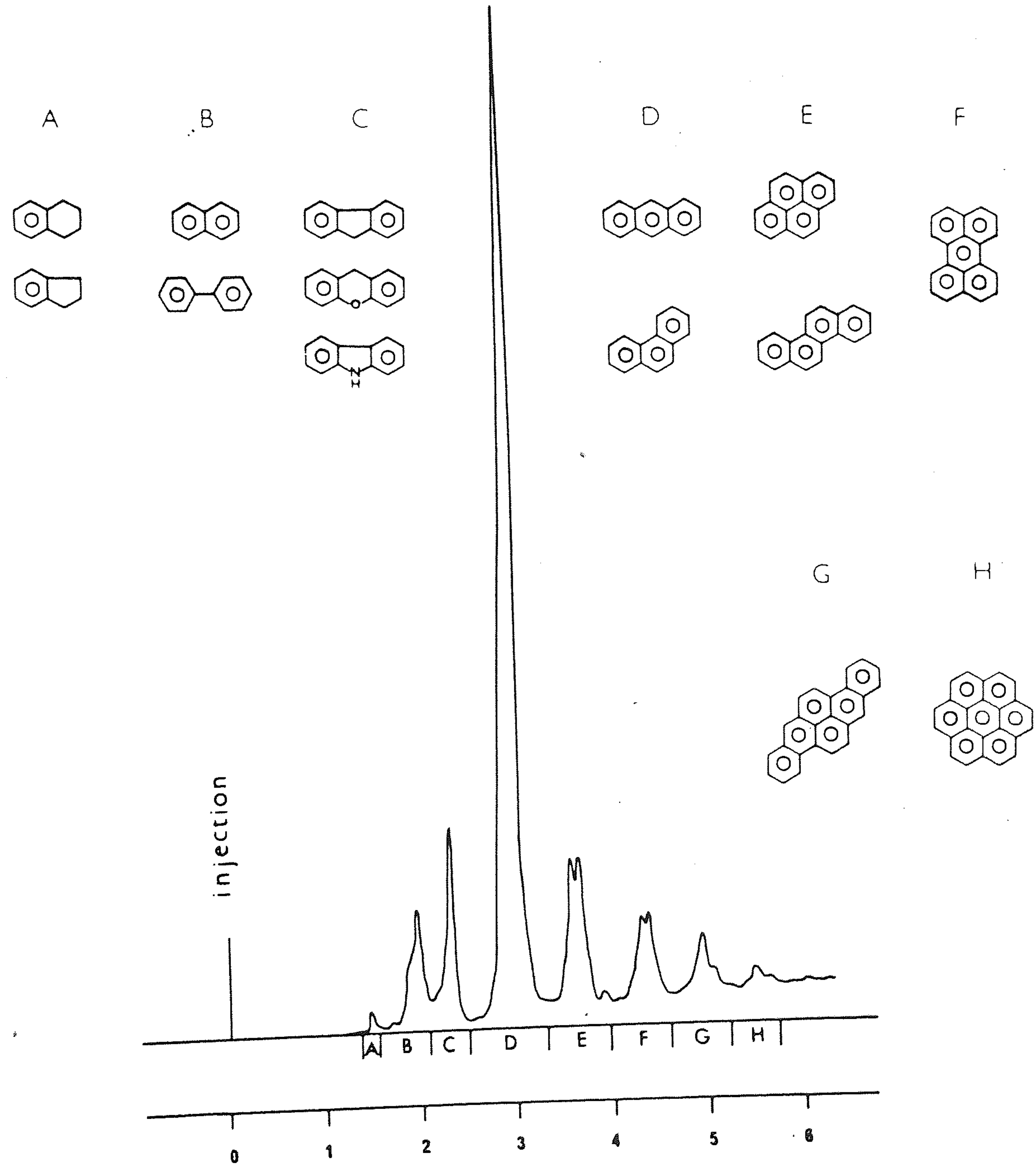

Retention time in minutes

Figure 5.10 Micropore volume (V_o) versus Final Pressure

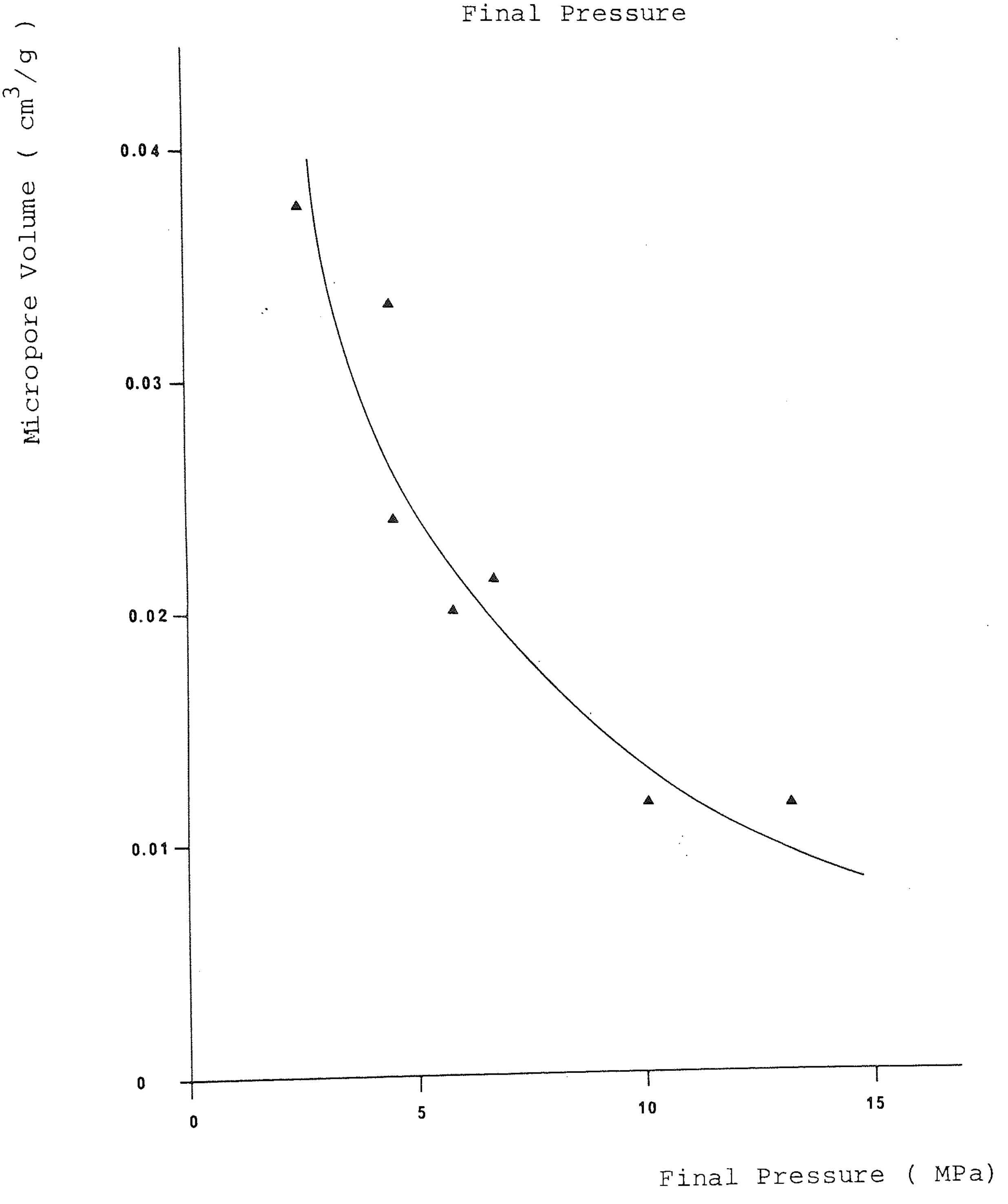

Figure 5.11

Typical pore size distribution for a hydrogen coke

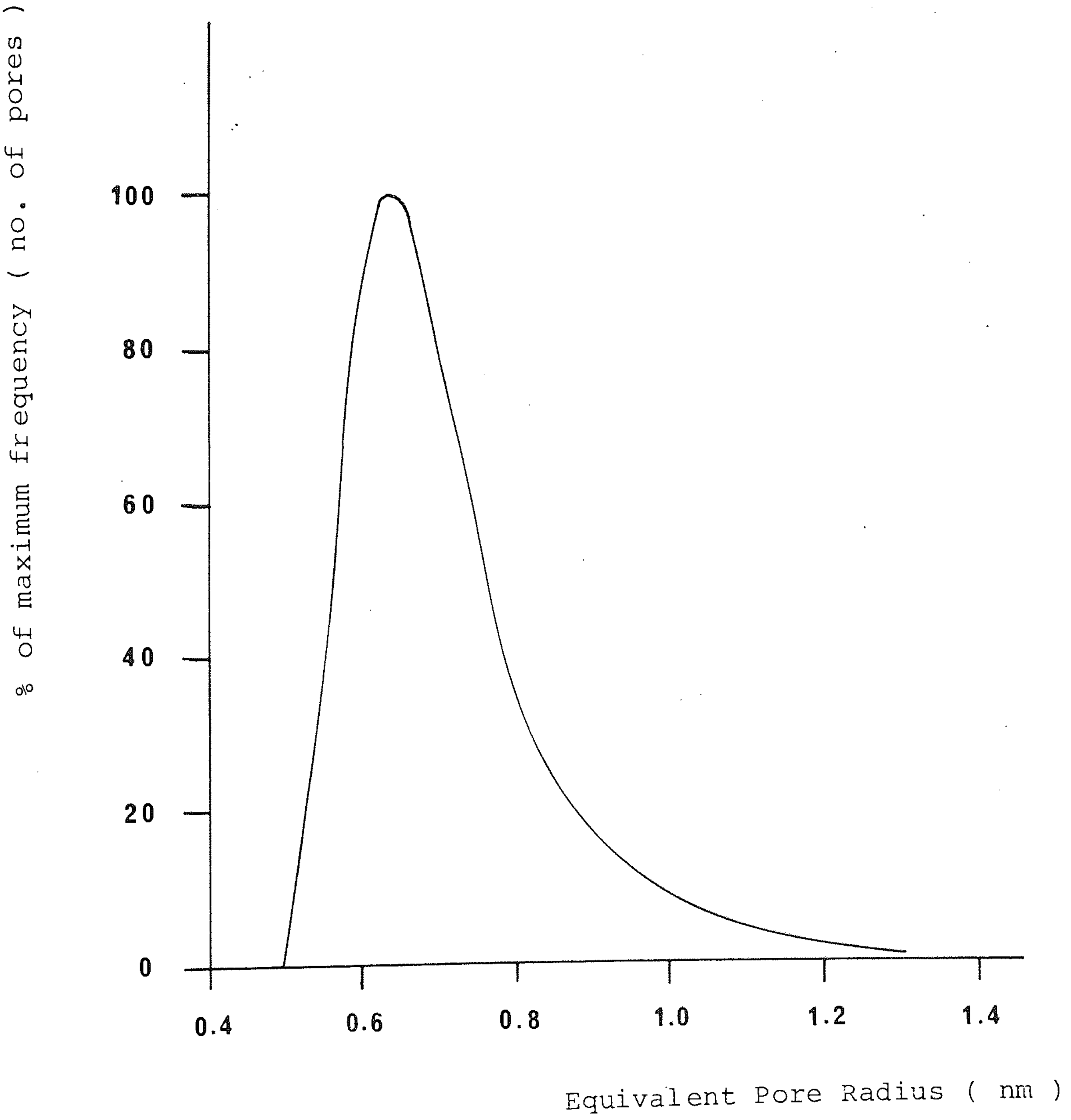

Figure 5.12 Hydrogen consumption versus initial hydrogen to coal ratio

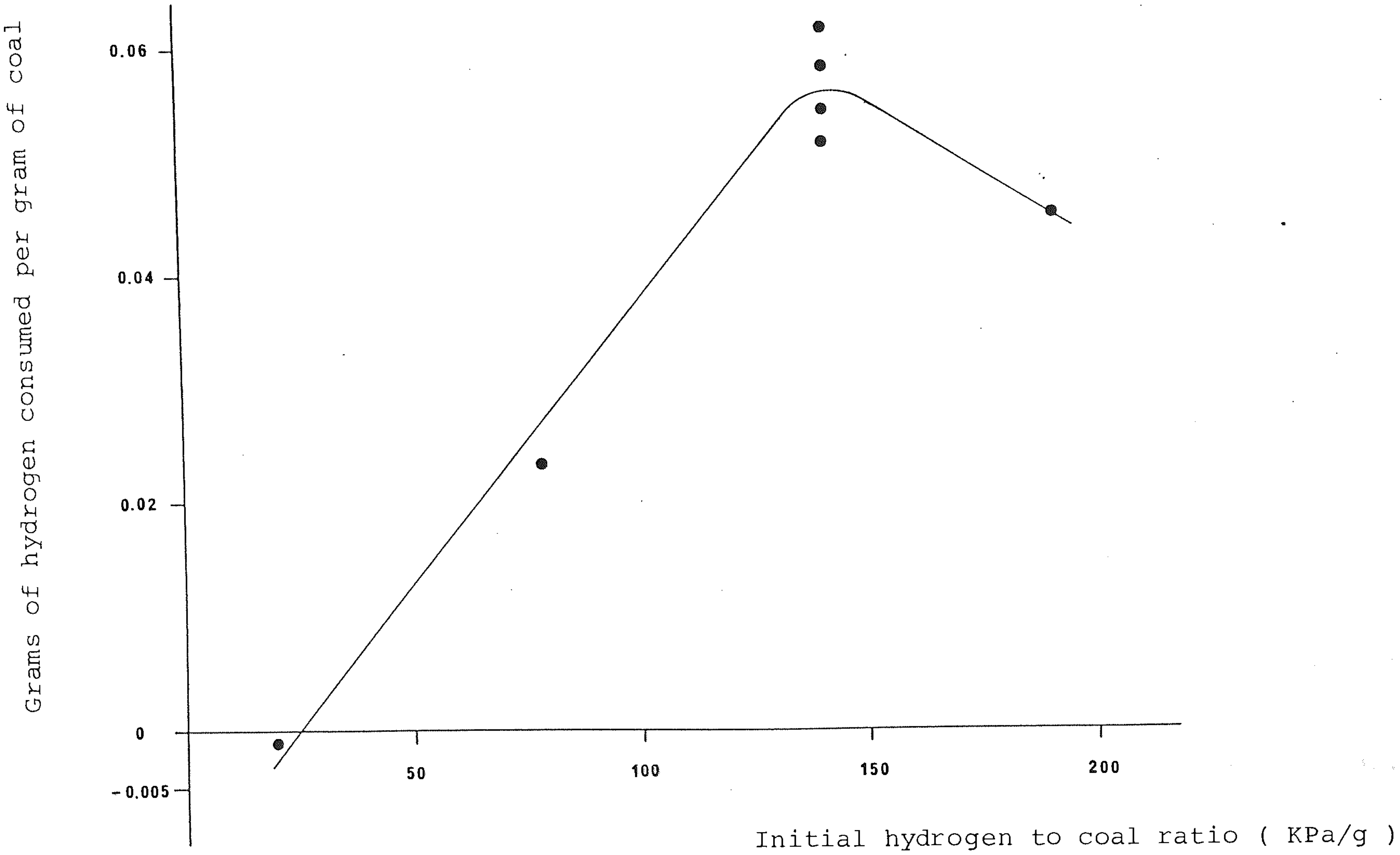

Table 5.2 Variation in Yields of Products at 500°C with Final Pressure

(Initial Hydrogen/Coal Ratio maintained Constant: 140 KPa/g)

Experiment	Final Pressure MPa	Coke Wt.%	Toluene Soluble Tar Wt.%	THF Soluble Tar Wt.%	Liquor Wt.%	Gas (by Difference) Wt.%
H5	2.5 ± 0.10	56.5 ± 0.5	13.5 ± 0.2	7.5 ± 0.4	10.5 ± 0.4	12.0 ± 1.5
H6	4.5 ± 0.10	52.7 ± 1.2	12.6 ± 0.1	3.4 ± 0.2	10.2 ± 0.5	21.1 ± 2.0
H7	6.66 ± 0.14	50.0 ± 0.5	11.8 ± 0.1	2.3 ± 0.1	10.8 ± 0.5	25.1 ± 1.2
H8	13.20 ± 0.30	42.8 ± 2.0	13.6 ± 0.2	0.7 ± 0.1	10.7 ± 0.5	32.2 ± 2.8

Table 5.3 Variation in Yields of Products at 500°C with Initial Hydrogen/Coal Ratios

Experiment	Initial Hydrogen/Coal Ratio KPa/g	Final Pressure MPa	Coke Wt.%	Toluene Soluble Tar Wt.%	THF Soluble Tar Wt.%	Liquor Wt.%	Gas (by difference) Wt.%
H0	4.0	1.85 ± 0.06	80.0 ± 0.2	2.10 ± 0.30	0.26 ± 0.02	5.5 ± 0.5	12.1 ± 1.0
H1	20.0	4.45 ± 0.10	69.2 ± 0.4	2.87 ± 0.12	0.65 ± 0.05	8.5 ± 0.5	18.8 ± 1.0
H2	80.0	5.75 ± 0.16	55.1 ± 0.3	7.93 ± 0.28	1.32 ± 0.03	8.4 ± 0.3	27.3 ± 1.0
H3	140.0	6.66 ± 0.14	50.0 ± 0.5	11.80 ± 0.10	2.30 ± 0.15	10.8 ± 0.5	25.1 ± 1.2
H4	190.0	10.03 ± 0.24	43.6 ± 0.3	11.50 ± 0.10	1.48 ± 0.10	8.4 ± 0.3	35.0 ± 0.8

Table 5.4 Composition of Tars Formed at 500°C (Initial Hydrogen to Coal Ratio Maintained Constant: 140 KPa/g: Final Pressure 2.5 - 13.2 MPa)

Composition of Tar

Toluene Tar (Wt.%)			THF Tar (Wt.%)		
Neutrals	Acids	Bases	Neutrals	Acids	Bases
90 ± 5	3 ± 0.3	4 ± 0.4	3 ± 0.25	93 ± 4	0.75 ± 0.1

Table 5.5 Variation of Yields of HPLC Fractions of Toluene Soluble Neutral Tars, Produced by Hydropyrolysis, with pressure

Experiment	Initial Hydrogen/ Coal Ratio KPa/g	Final Pressure MPa	Typical Compounds present in HPLC Fractions A - H and the Relative Yields of the HPLC Fractions							
			A	B	C	D	E	F	G	H
			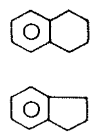	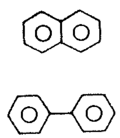	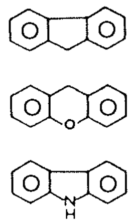	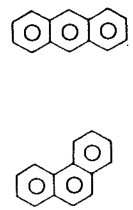	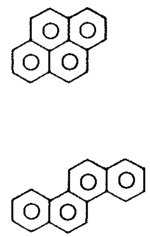	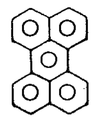	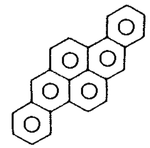	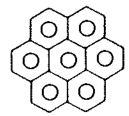
H1	20	4.45 ± 0.10	1	1	1	1	1	1	1	1
H2	80	5.75 ± 0.16	1.38	3.60	3.94	2.63	3.06	2.84	2.55	1.67
H3	140	6.66 ± 0.14	3.23	6.83	6.65	3.24	4.71	4.68	4.68	2.20
H4	190	10.03 ± 0.24	4.15	8.20	5.65	3.93	4.23	3.44	3.55	1.67
H5	140	2.50 ± 0.10	1	1	1	1	1	1	1	1
H6	140	4.50 ± 0.10	2.69	0.75	0.92	0.84	1.00	1.23	1.27	1.00
H7	140	6.66 ± 0.14	3.23	1.34	1.57	0.74	0.89	0.90	0.82	0.48
H8	140	13.20 ± 0.30	4.62	1.97	1.40	0.93	0.92	0.78	0.78	0.77

Table 5.6 Composition of Tar obtained from Pyrolysis under Hydrogen

Initial Hydrogen/Coal Ratio = 140 KPa/g

Final Pressure at 500°C = 6.66 ± 0.14 MPa

Toluene Soluble Neutral Fraction

Molecule	Relative Concentration
Indan	0.02
Methylindan	0.12
Tetrahydronaphthalene	0.05
Naphthalene	0.96
Ethylindan	0.03
Dimethylindan	0.04
Methyltetrahydronaphthalene	0.05
Methylnaphthalene	1
Biphenyl	0.33
Dihydrophenalene	0.35
Dimethyl/Ethylnaphthalene	0.66
Phenalene	0.05
Methylbiphenyl	0.30
Dimethylbiphenyl	0.09
Trimethylnaphthalene	0.12
Dibenzofuran	0.09
Ethylbiphenyl	0.06
Fluorene	0.40
Xanthene	0.05
Methyldibenzofuran	0.06

Table 5.6 Continued

Toluene Soluble Neutral Fraction - Continued

Molecule	Relative Concentration
Dihydrophenanthrene/Anthracene	0.08
Methylfluorene	0.21
Anthracene/Phenanthrene	0.40
Carbazole	0.03
Methylanthracene/Phenanthrene	0.08
Dihydropyrene	0.03
Pyrene	0.01
Methylpyrene	0.04
Benzanthracene	0.01
Chrysene	0.02
Alkanes $C_{11} - C_{24}$	Trace

Toluene Soluble Acidic Fraction

Molecule	Relative Concentration
Phenol	0.36
Methylphenol	0.87
Trimethylphenol	0.23
Ethyl/Dimethylphenol	1
Methylethylphenol	0.61
Diethylphenol	0.68
Methylindanol	0.36
Dimethyl indanol	0.02
Hydroxybiphenyl	0.21

Table 5.6 Continued

Toluene Soluble Basic Fraction

Molecule	Relative Concentration
Aniline	0.20
Methylaniline	0.27
Ethyl/Dimethyaniline	0.53
Quinoline	1
Methylquinoline	4.1
Tetrahydroquinoline	5.1
Ethyl/dimethylquinoline	3.8
Acridine	5.3
Methylacridine	1.0
Naphthalamine	0.30
Diphenylamine	0.53

THF Neutral Fraction

Molecule
Phenalene
Methylbiphenyl
Dimethylbiphenyl
Trimethylnaphthalene
Dibenzofuran
Ethylbiphenyl
Fluorene
Xanthene
Methyldibenzofuran
Dihydrophenanthrene/Anthracene
Methylfluorene

Table 5.6 Continued

THF Neutral Fraction - Continued

Molecule

Anthracene/Phenanthrene

Carbazole

Methylanthracene/Phenanthrene

Dihydropyrene

Pyrene

Methylpyrene

Benzanthracene

Chrysene

THF Soluble Acidic Fraction

Molecule

Catechol

Resorcinol

Hydroquinone

Naphthols

High Boiling Phenols

THF Soluble Basic Fraction

A broad unresolved peak was obtained by GC-MS

Table 5.7 Carbon, Hydrogen and Nitrogen Analyses for Cokes and Manvers Coal (As Received)

Coke from Experiment	Carbon %	Hydrogen %	Nitrogen %
H0	82.00 ± 0.05	2.80 ± 0.05	1.90 ± 0.10
H1	81.40 ± 0.20	3.00 ± 0.00	1.75 ± 0.05
H2	80.10 ± 0.70	2.75 ± 0.05	1.60 ± 0.00
H3	80.35 ± 0.85	2.95 ± 0.05	1.75 ± 0.05
H4	79.17 ± 0.50	2.85 ± 0.05	1.55 ± 0.05
H5	81.40 ± 0.40	2.95 ± 0.05	1.90 ± 0.10
H6	79.20 ± 0.20	2.95 ± 0.05	1.75 ± 0.05
H7	80.35 ± 0.85	2.95 ± 0.05	1.75 ± 0.05
H8	79.50 ± 0.20	2.90 ± 0.00	1.65 ± 0.05
Manvers Coal	78.60 ± 0.00	5.00 ± 0.10	1.60 ± 0.10

Table 5.8 Atomic H/C Ratios and Methanol Densities of Cokes

Initial Gas to Coal Ratio (KPa/g)	Final Pressure (MPa)	Atomic H/C Ratio	Methanol Density (g/cm^3 at 25^oC)
125 (Nitrogen)	0.1	0.41 ± 0.01	0.88 ± 0.03
4 - 190 (Hydrogen)	1.85 - 13.2	0.44 ± 0.01	1.54 (5) ± 0.2

Table 5.9 Microporities and Surface Areas of Cokes Produced under Hydrogen

Experiment	Initial Hydrogen/ Coal Ratio KPa/g	Final Pressure MPa	Surface Area m^2/g	Micropore Volume cm^3/g	Mean Equivalent Pore Radius $\bar{r}_e$ (nm)
Coal	-	-	162	0.061	0.75
H1	20	4.45 $\pm$ 0.10	97	0.033	0.69
H2	80	5.75 $\pm$ 0.16	57	0.019	0.69
H3	140	6.66 $\pm$ 0.14	61	0.021	0.70
H4	190	10.03 $\pm$ 0.24	34	0.011	0.68
H5	140	2.50 $\pm$ 0.10	103	0.037	0.73
H6	140	4.50 $\pm$ 0.10	68	0.023	0.70
H7	140	6.66 $\pm$ 0.14	61	0.021	0.70
H8	140	13.20 $\pm$ 0.30	33	0.011	0.69

Table 5.10 Variation in Percentage Gas Volumes at 500°C with Varying Initial Hydrogen/Coal Ratios

Experiment	Initial Hydrogen/ Coal Ratio KPa/g	Hydrogen	Methane	Ethene	Ethane	Propane	Butane
H1	20	51.40 ± 0.70	31.60 ± 0.60	2.35 ± 0.15	11.55 ± 0.25	2.10 ± 0.10	1.03 ± 0.03
H2	80	63.30 ± 2.00	20.40 ± 1.30	0.65 ± 0.05	11.70 ± 0.60	3.00 ± 0.30	1.15 ± 0.05
H3	140	69.25 ± 0.35	16.65 ± 0.25	0.60 ± 0.00	9.85 ± 0.05	2.65 ± 0.05	0.97 ± 0.03
H4	190	77.55 ± 1.05	11.60 ± 1.00	1.05 ± 0.05	6.45 ± 0.05	2.15 ± 0.05	1.05 ± 0.05

Table 5.11 Variation in Percentage Gas Volumes at 500°C with Final Pressure

(Initial Hydrogen/Coal Ratio Maintained Constant: 140 KPa/g)

Experiment	Final Pressure MPa	Hydrogen	Methane	Ethene	Ethane	Propane	Butane
H5	2.50 ± 0.10	77.40 ± 0.1	11.35 ± 0.15	1.85 ± 0.15	6.45 ± 0.05	1.25 ± 0.05	1.60 ± 0.02
H6	4.50 ± 0.10	74.80 ± 1.2	12.10 ± 0.40	1.90 ± 0.10	7.80 ± 0.60	1.90 ± 0.10	1.40 ± 0.04
H7	6.66 ± 0.14	69.25 ± 0.35	16.65 ± 0.25	0.60 ± 0.00	9.85 ± 0.05	2.65 ± 0.05	0.97 ± 0.03
H8	13.20 ± 0.30	65.90 ± 1.80	14.35 ± 0.65	2.20 ± 0.20	9.10 ± 0.60	6.65 ± 0.35	1.66 ± 0.01

Table 5.12 Yields of Gas in Grams per 100 Grams of Coal for Hydropyrolyses

Experiment	Final Pressure at 500°C MPa	Hydrogen	Methane	Ethene	Ethane	Propane	Butane
H1	4.45 ± 0.10	1.8 ± 0.1	8.9 ± 0.7	1.2 ± 0.0	6.1 ± 0.2	1.6 ± 0.0	1.1 ± 0.0
H2	5.75 ± 0.16	4.2 ± 0.5	10.9 ± 0.2	0.6 ± 0.0	11.7 ± 0.3	4.4 ± 0.1	2.2 ± 0.1
H3	6.66 ± 0.14	5.6 ± 0.3	10.8 ± 0.3	0.7 ± 0.0	12.0 ± 0.4	4.8 ± 0.1	2.3 ± 0.2
H4	10.03 ± 0.24	11.0 ± 0.6	13.2 ± 0.6	2.1 ± 0.0	13.8 ± 0.7	6.8 ± 0.2	4.3 ± 0.0
H5	2.50 ± 0.10	5.0 ± 0.3	5.8 ± 0.5	1.6 ± 0.0	6.2 ± 0.5	1.8 ± 0.0	3.0 ± 0.3
H6	4.50 ± 0.10	6.1 ± 0.7	7.8 ± 0.6	2.2 ± 0.1	9.4 ± 0.3	3.4 ± 0.2	3.4 ± 0.2
H7	6.66 ± 0.14	5.6 ± 0.3	10.8 ± 0.3	0.7 ± 0.0	12.0 ± 0.4	4.8 ± 0.1	2.3 ± 0.2
H8	13.20 ± 0.30	5.3 ± 0.5	9.2 ± 0.2	2.5 ± 0.1	10.9 ± 0.2	11.7 ± 0.2	3.9 ± 0.2

Table 5.13 Hydrogen Content of Gas in Grams per 100 Grams of Coal for Hydropyrolyses

Experiment	Final Pressure at 500°C MPa	Hydrogen	Methane	Ethene	Ethane	Propane	Butane
H1	4.45 ± 0.10	1.8 ± 0.1	2.2 ± 0.2	0.2 ± 0.0	1.2 ± 0.0	0.3 ± 0.0	0.2 ± 0.0
H2	5.75 ± 0.16	4.2 ± 0.5	2.7 ± 0.1	0.1 ± 0.0	2.4 ± 0.1	0.8 ± 0.0	0.4 ± 0.0
H3	6.66 ± 0.14	5.6 ± 0.3	2.7 ± 0.1	0.1 ± 0.0	2.4 ± 0.1	0.8 ± 0.0	0.4 ± 0.0
H4	10.03 ± 0.24	11.0 ± 0.6	3.3 ± 0.2	0.3 ± 0.0	2.8 ± 0.2	1.2 ± 0.0	0.8 ± 0.0
H5	2.50 ± 0.10	5.0 ± 0.3	1.4 ± 0.1	0.2 ± 0.0	1.1 ± 0.1	0.3 ± 0.0	0.5 ± 0.0
H6	4.50 ± 0.10	6.1 ± 0.7	2.0 ± 0.2	0.3 ± 0.0	1.8 ± 0.1	0.6 ± 0.1	0.6 ± 0.0
H7	6.66 ± 0.14	5.6 ± 0.3	2.7 ± 0.1	0.1 ± 0.0	2.4 ± 0.1	0.8 ± 0.0	0.4 ± 0.0
H8	13.20 ± 0.30	5.3 ± 0.5	2.3 ± 0.1	0.3 ± 0.0	2.2 ± 0.0	2.1 ± 0.0	0.7 ± 0.0

Table 5.14 Carbon Content of Gas in Grams per 100 Grams of Coal for Hydropyrolyses

Experiment	Final Pressure at 500°C MPa	Methane	Ethene	Ethane	Propane	Butane	Total Carbon in Gas
H1	4.45 ± 0.10	6.7 ± 0.5	1.0 ± 0.0	4.9 ± 0.2	1.3 ± 0.0	0.9 ± 0.0	14.8 ± 0.7
H2	5.75 ± 0.16	8.2 ± 0.1	0.5 ± 0.0	9.4 ± 0.2	3.6 ± 0.1	1.9 ± 0.1	23.6 ± 0.5
H3	6.66 ± 0.14	8.2 ± 0.2	0.6 ± 0.0	9.6 ± 0.3	3.9 ± 0.1	1.9 ± 0.2	24.2 ± 0.8
H4	10.03 ± 0.24	9.9 ± 0.4	1.8 ± 0.0	11.0 ± 0.6	5.5 ± 0.1	3.6 ± 0.0	31.8 ± 1.1
H5	2.50 ± 0.10	4.3 ± 0.3	1.4 ± 0.0	5.0 ± 0.3	1.4 ± 0.0	2.6 ± 0.3	14.7 ± 0.9
H6	4.50 ± 0.10	5.9 ± 0.5	1.8 ± 0.1	7.6 ± 0.2	2.8 ± 0.2	2.7 ± 0.2	20.8 ± 1.2
H7	6.66 ± 0.14	8.2 ± 0.2	0.6 ± 0.0	9.6 ± 0.3	3.9 ± 0.1	1.9 ± 0.2	24.2 ± 0.8
H8	13.20 ± 0.30	6.9 ± 0.1	2.1 ± 0.1	8.7 ± 0.0	9.6 ± 0.1	3.2 ± 0.2	30.5 ± 0.5

Table 5.15 Hydrogen Mass Balance in Grams per 100 Grams of Coal for Hydropyrolyses

Experiment	Final Pressure at 500°C MPa	Hydrogen in Water	Hydrogen in Tar based on Naphthalene	Hydrogen in Gas	Hydrogen in Coke	Total Hydrogen	Total Hydrogen Expected
H1	4.45 ± 0.10	0.9 ± 0.0	0.2 ± 0.0	5.9 ± 0.3	2.1 ± 0.0	9.1 ± 0.3	6.7
H2	5.75 ± 0.16	0.9 ± 0.0	0.6 ± 0.0	10.6 ± 0.7	1.5 ± 0.0	13.6 ± 0.7	11.7
H3	6.66 ± 0.14	1.2 ± 0.0	0.9 ± 0.0	12.0 ± 0.5	1.5 ± 0.0	15.6 ± 0.5	16.1
H4	10.03 ± 0.24	1.0 ± 0.0	0.8 ± 0.0	19.4 ± 1.0	1.2 ± 0.0	22.4 ± 1.0	20.6
H5	2.50 ± 0.10	1.1 ± 0.0	1.3 ± 0.0	8.5 ± 0.5	1.6 ± 0.0	12.5 ± 0.5	16.1
H6	4.50 ± 0.10	1.1 ± 0.1	1.0 ± 0.1	12.0 ± 1.1	1.5 ± 0.1	15.6 ± 1.4	16.1
H7	6.66 ± 0.14	1.2 ± 0.0	0.9 ± 0.0	12.0 ± 0.5	1.5 ± 0.0	15.6 ± 0.5	16.1
H8	13.20 ± 0.30	1.2 ± 0.1	0.9 ± 0.0	12.9 ± 0.6	1.3 ± 0.0	16.3 ± 0.7	16.1

Table 5.16 Carbon Mass Balance in Grams per 100 Grams of Coal for Hydropyrolyses

Experiment	Final Pressure at 500°C MPa	Carbon in Coke	Carbon in Tar based on Naphthalene	Carbon in Gas	Total Carbon	Total Carbon Expected
H1	4.45 ± 0.10	56.2 ± 0.5	3.3 ± 0.2	14.8 ± 0.7	74.3 ± 1.6	78.6
H2	5.75 ± 0.16	44.1 ± 0.6	8.7 ± 0.3	23.6 ± 0.5	76.4 ± 1.4	78.6
H3	6.66 ± 0.14	40.2 ± 0.8	13.2 ± 0.2	24.2 ± 0.8	77.6 ± 1.8	78.6
H4	10.03 ± 0.24	34.1 ± 0.5	12.2 ± 0.2	31.8 ± 1.1	78.1 ± 1.8	78.6
H5	2.50 ± 0.10	46.1 ± 0.6	19.7 ± 0.6	14.7 ± 0.9	80.5 ± 2.1	78.6
H6	4.50 ± 0.10	41.8 ± 1.0	15.0 ± 0.3	20.8 ± 1.2	77.6 ± 2.5	78.6
H7	6.66 ± 0.14	40.2 ± 0.8	13.2 ± 0.2	24.2 ± 0.8	77.6 ± 1.8	78.6
H8	13.20 ± 0.30	34.0 ± 0.2	13.4 ± 0.3	30.5 ± 0.5	77.9 ± 1.0	78.6

Table 5.17 Hydrogen Consumption

Experiment	Grams of Coal Used	Initial Hydrogen/Coal Ratio (KPa/g)	Final Pressure (at 500°C) MPa	Wt. of Initial Hydrogen Gas in Autoclave (grams)	Wt. of Hydrogen Gas after Pyrolysis (grams)	Hydrogen* Consumed in Grams	Hydrogen Consumed Per Gram of Coal
H1	50	20	4.45 ± 0.10	0.84	0.90	-0.06	-0.0012
H2	25	80	5.75 ± 0.16	1.67	1.05	0.62	0.025
H3	25	140	6.66 ± 0.14	2.78	1.40	1.38	0.055
H4	25	190	10.03 ± 0.24	3.90	2.75	1.15	0.046
H5	6.25	140	2.50 ± 0.10	0.70	0.31	0.39	0.062
H6	12.5	140	4.50 ± 0.10	1.39	0.76	0.63	0.050
H7	25	140	6.66 ± 0.14	2.78	1.40	1.38	0.055
H8	50	140	13.20 ± 0.30	5.57	2.65	2.93	0.059

* Calculated from the difference in the molecular hydrogen present at the beginning and end of the pyrolysis.

CHAPTER SIX

THE PYROLYSIS OF MANVERS COAL IN AN ATMOSPHERE OF DEUTERIUM

CHAPTER SIX

THE PYROLYSIS OF MANVERS COAL IN AN ATMOSPHERE OF DEUTERIUM

6.1 Introduction

Previously (chapter 5), Manvers coal has been pyrolysed to 500^{o}C in atmospheres of hydrogen. Whereas gas yields increased with pressure and with the ratio of hydrogen to coal, tar yields ceased to increase above an initial ratio of 140 KPa of hydrogen per gram of coal and were larger at lower than at higher pressures. The coal was pyrolysed rather slowly and as liberated fluid material diffused through the pyrolysing system further reactions occurred and consequently the tars evolved were highly aromatic and the effects of pressure on tar composition were similar to those of raising the temperature of pyrolysis.

Pyrolysis of coals involves the transfer of hydrogen atoms from one part of their structure to another[43] but although the variation in the yields of products and the properties of the cokes from the hydropyrolysis of Manvers coal has been described in detail, information about the redistribution of hydrogen has been lacking. There was no way of labelling the hydrogen or of distinguishing between hydrogen which was initially part of the coal and hydrogen originating in the external atmosphere. Therefore, Manvers coal has been pyrolysed in an atmosphere of deuterium in order to obtain greater insight into the mechanism of hydropyrolysis. In particular it was hoped to distinguish between direct hydrogenation (deuteration!) of the coal and the products of pyrolysis and the 'shuttling' of hydrogen atoms between different parts of the pyrolysing coal.

Fu and Blaustein[44] investigated the reactions of coal in deuterium oxide in plasmas. Franz and his colleagues[45] have used deuterated solvents in studies of the liquefaction mechanism of coals. Gaines and Yürüm[33] studied the pyrolysis of a partially deuterated coal and a partially deuterated lignite and found evidence of extensive scrambling of the hydrogen and deuterium atoms during pyrolysis. Their conclusions were confirmed and significantly extended by Wilson and Vassallo[46]. Kershaw and Barrass[47] and particularly Heredy and his colleagues[48] studied the pyrolysis of coals in deuterium gas. Kershaw and Barrass[47] analysed the deutero methanes and the tars which were formed. They observed that nearly half the aromatic hydrogen in the tars was deuterium and that in the substituents to the aromatic rings deuterium was located preferentially bonded to the α carbon. Heredy's work[48] confirmed the latter observations though there was no comment on the amount of deuterium which became directly attached to the aromatic ring. He found incorporation of deuterium into the pyrolysis products to decrease in the order char,tar,gas. Recently Rose et al[49] have studied the pyrolysis of a deuterated benzylated coal.

The present experiments have been conducted in the stainless steel autoclave previously described (chapter 3) and Manvers coal was pyrolysed to 500^{o}C in the absence of a solvent. The conditions chosen, a deuterium:coal ratio of 140 KPa/g and a total final pressure of 2.64 ± 0.07 MPa, were close to those known to give maximum yields of tar. In some experiments Manvers coal was pyrolysed in the presence of 5% of pyrite or of 5% of tetralin to determine whether these compounds, often used as catalysts in liquefaction studies, had any effect on the distribution of hydrogen amongst the products.

6.2 Experimental

The autoclave was flushed first with nitrogen then with deuterium. 6.25g of dry coal was added, the autoclave closed and the deuterium pressure adjusted to 0.86 MPa. The stirred autoclave was heated at 4.2°C/min to 500°C and the final temperature was maintained for two hours. Table 6.1 shows the experimental conditions adopted for pyrolyses in deuterium. Typical graphs of the rate of increase of pressure versus temperature during the pyrolyses are shown in figure 6.1. After cooling all products were analysed. The complete pyrolysis procedure, the general methods of analysis and the detailed analysis of the coal can be found in chapter 3.

In the present experiments emphasis was given to the analysis of the cokes by infra red spectrometry using a Perkin Elmer Model 683 fitted with a Harrick DRA 35P diffuse reflectance module. Diffuse reflectance spectra of mixtures containing approximately 5% of coke in KBr, crushed to -100 μm +50 μm, were measured in atmospheres of nitrogen. The powders were loosely close packed in a disk of 0.5 cm depth.

Toluene and THF soluble tars were analysed by gas chromatography - mass spectrometry as described previously (chapter 3),

Table 6.1 Experimental Conditions for Deuterium Pyrolyses

Average rate of heating	=	$4.2^{o}C\ min^{-1}$
Final coal pyrolysis temperature	=	$500^{o}C$
Heat soak time at $500^{o}C$	=	2 hours
Weight of coal used	=	6.25g
Initial deuterium to coal ratio	=	140 KPa/g

Catalyst used(5% - wt% of coal)	Final Pressure at $500^{o}C$ MPa
none	2.64 ± 0.07
tetralin	2.74 ± 0.10
pyrite	2.64 ± 0.03

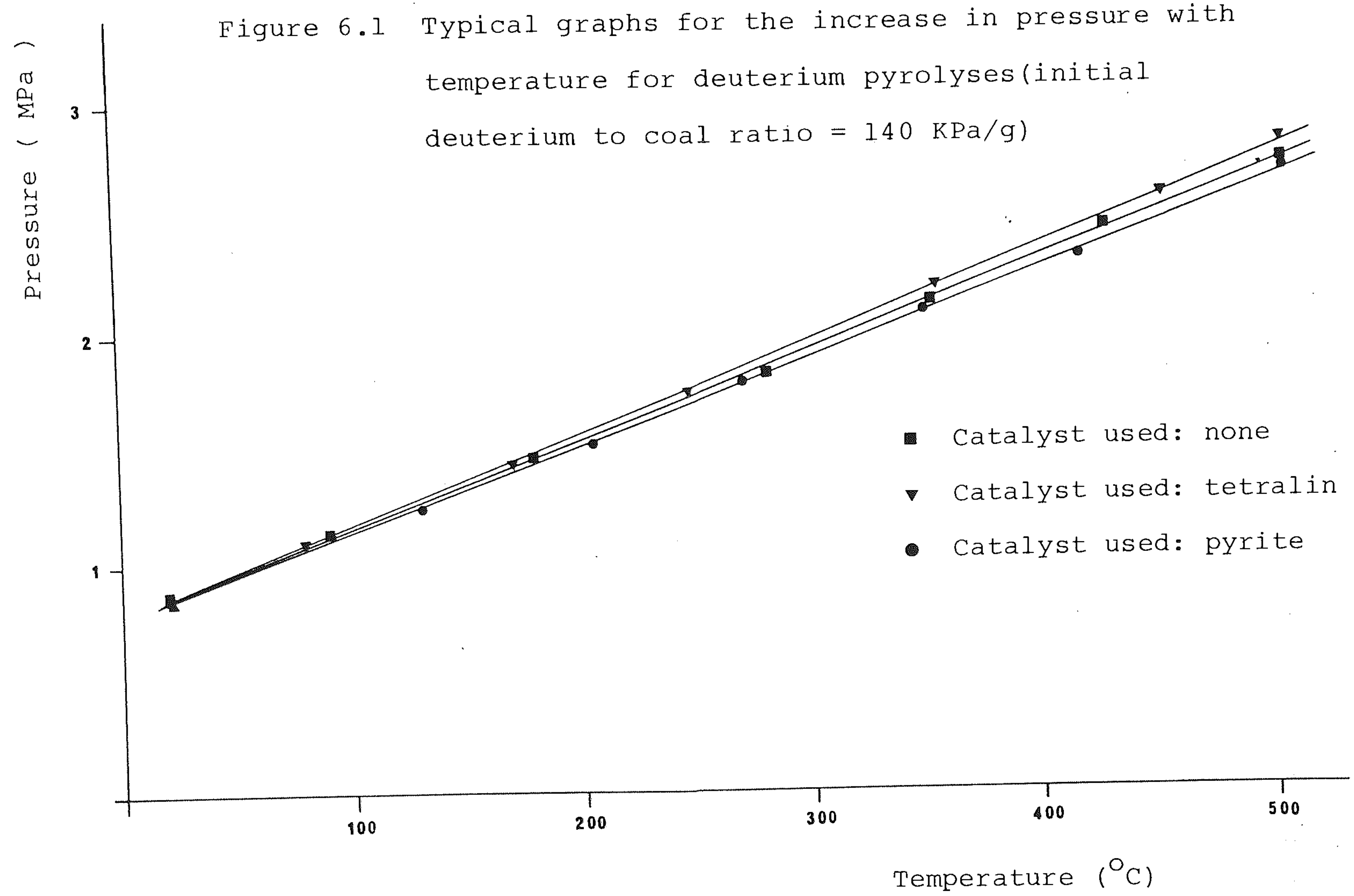

Figure 6.1 Typical graphs for the increase in pressure with temperature for deuterium pyrolyses(initial deuterium to coal ratio = 140 KPa/g)

but the tars were not separated into acidic, basic and neutral components lest this changed the deuterium distributions.

Gases were analysed by mass spectrometry using a modified MS9 at an ionising energy of 16 eV. This was sufficient to ensure the formation of molecular ions from hydrocarbons with very little accompanying fragmentation. The resolution of the mass spectrometer was sufficient to permit identification of deuterated families such as CH_4^+, CH_3D^+, $CH_2D_2^+$ etc. by their accurate mass numbers, and their distinction from such ions as O^+, OH^+, H_2O^+, $^{13}CH_4$ etc.

6.3 Results and Discussion

6.3.1 General remarks about yields

Yields from pyrolysis in deuterium (table 6.2) and general analyses of the products were similar to those obtained when pyrolyses were conducted under the same conditions under hydrogen. There was neither evidence for significant deuteration of the coal nor of a significant isotope effect on the yields and one may suppose that the deuterium pyrolyses can be compared with the previous hydropyrolyses. The detailed analyses of the gases revealed traces of benzene, toluene and xylenes not noticed in the previous hydropyrolyses (figure 6.2).

6.3.2 Infra red spectra of cokes

Figure 6.3 shows a typical diffuse reflectance spectrum of the semicoke obtained from pyrolyses to 500°C in deuterium. Infra

Table 6.2 Pyrolyses in Deuterium

Initial deuterium/coal ratio = 140 KPa/g; final temperature 500°C

Products (g) from 100g of coal + 5g of catalyst

Catalyst	Final Pressure MPa	Coke	Liquor	Toluene Soluble Tar	THF Soluble Tar	Gas (by difference)
none	2.64 ± 0.07	61.5 ± 0.1	8.7 ± 0.4	10.6 ± 0.4	7.0 ± 0.2	12.2
tetralin	2.74 ± 0.10	62.6 ± 0.3	9.1 ± 0.4	11.9 ± 0.6	7.0 ± 0.3	14.4
		Δ 1.1	0	1.3	0	2.2
pyrite	2.64 ± 0.03	66.3 ± 0.7	8.8 ± 0.5	10.2 ± 0.5	5.9 ± 0.5	13.8
		Δ 4.8	0	0	-1.1	1.6

Δ = g gain or loss caused by catalyst

Figure 6.2 Part of a mass spectrum of deuterated gas showing the presence of benzene, toluene and xylene

Molecule	m/e
Benzene	78
Toluene	92
Xylene	106

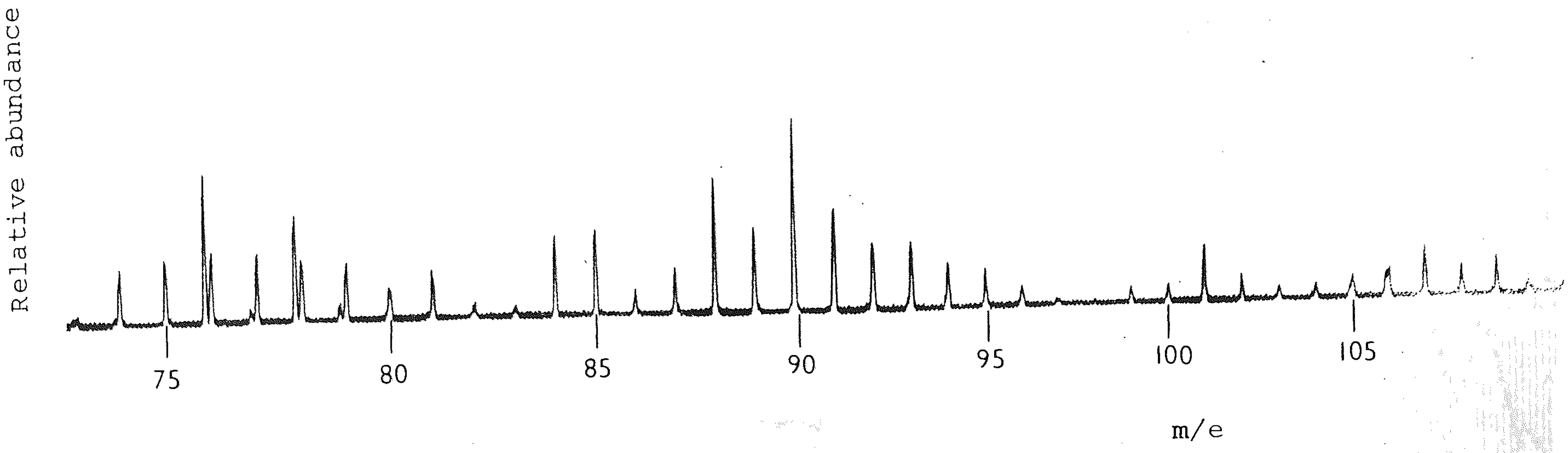

Figure 6.3

Diffuse Reflectance Infra Red Spectrum Of Deuterated Semicoke

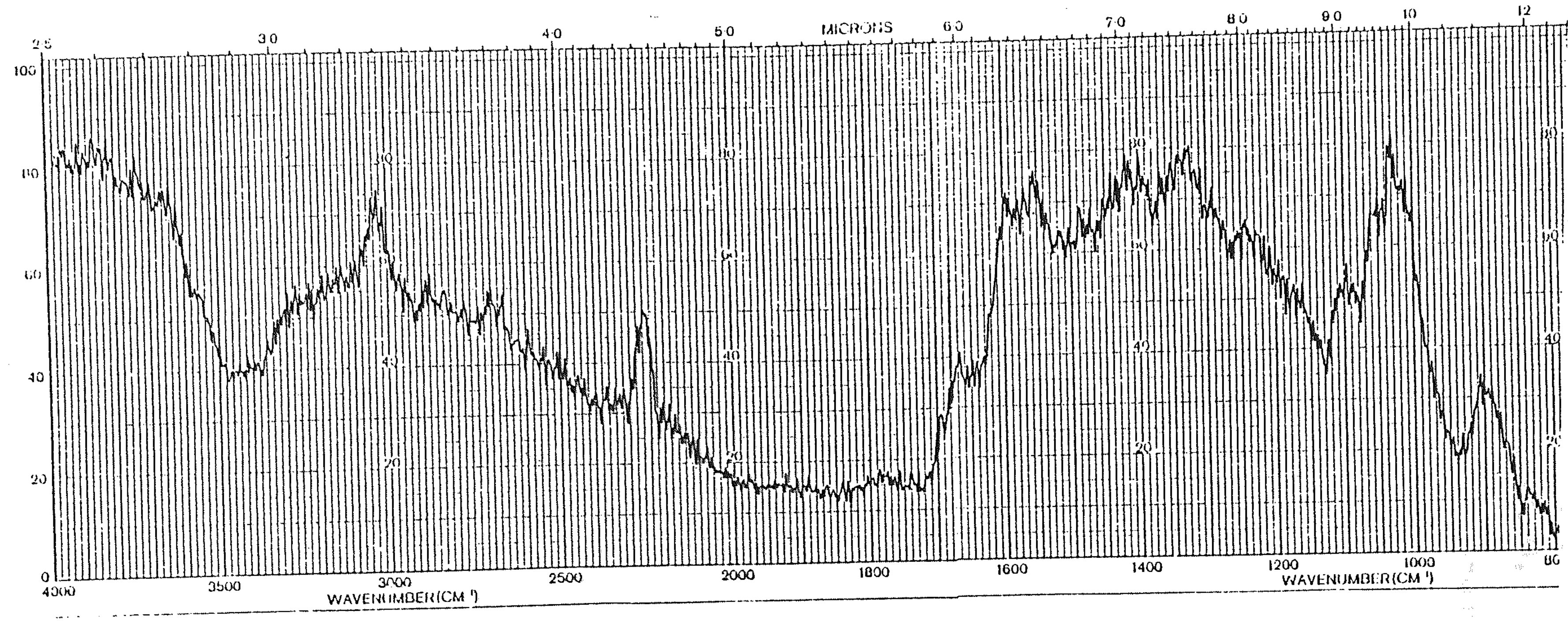

red spectra of coals (a spectrum of Manvers coal is given in figure 6.4) obtained by this technique have reasonably straight baselines parallel to the x-axis due to scattering, mainly by potassium bromide, occurring uniformly throughout the range of wavelengths[50]. The sloping baseline in the 4000 - 1800 cm^{-1} region given by the semicoke may be due, therefore, to the persistence of electronic absorption down to these comparatively low energies. The inverted absorption by the O-H stretching vibration around 3500 cm^{-1} was due to a small amount of moisture in the potassium bromide used in the reference spectrum. Figure 6.3 shows sharp absorption due to aromatic C-H stretching vibrations centred at 3030 cm^{-1} and broader and much weaker absorption near 2890 cm^{-1} due to aliphatic C-H vibrations. Sharp absorption at 2260 cm^{-1} was absent in similar spectra of hydropyrolysis cokes and is close to the absorption of aromatic C-D stretching vibrations in deuterated benzene, toluene and pyridine[51]. The absorption can therefore be assigned confidently to aromatic C-D stretching vibrations in the cokes. There was little deuterium in aliphatic groups. Broad absorption at 1600, 1450 and 1350 cm^{-1} was pronounced. In that stretching vibrations suggest little aliphatic hydrogen to be present much of the absorption at 1450 cm^{-1} must be due to aromatic ring vibrations[33]. Comparison of the intensity of the C-H and C-D absorptions indicates that the ratio of deuterium to hydrogen in the cokes was about 0.4 . This was lower than the ratio found by Heredy[48] who pyrolysed at 400°C and at considerably higher pressures than have been used here, both factors which might be expected to have raised the deuterium ratio. More importantly the ratio of 0.4

Figure 6.4

Diffuse Reflectance Infra Red Spectrum Of Manvers Coal

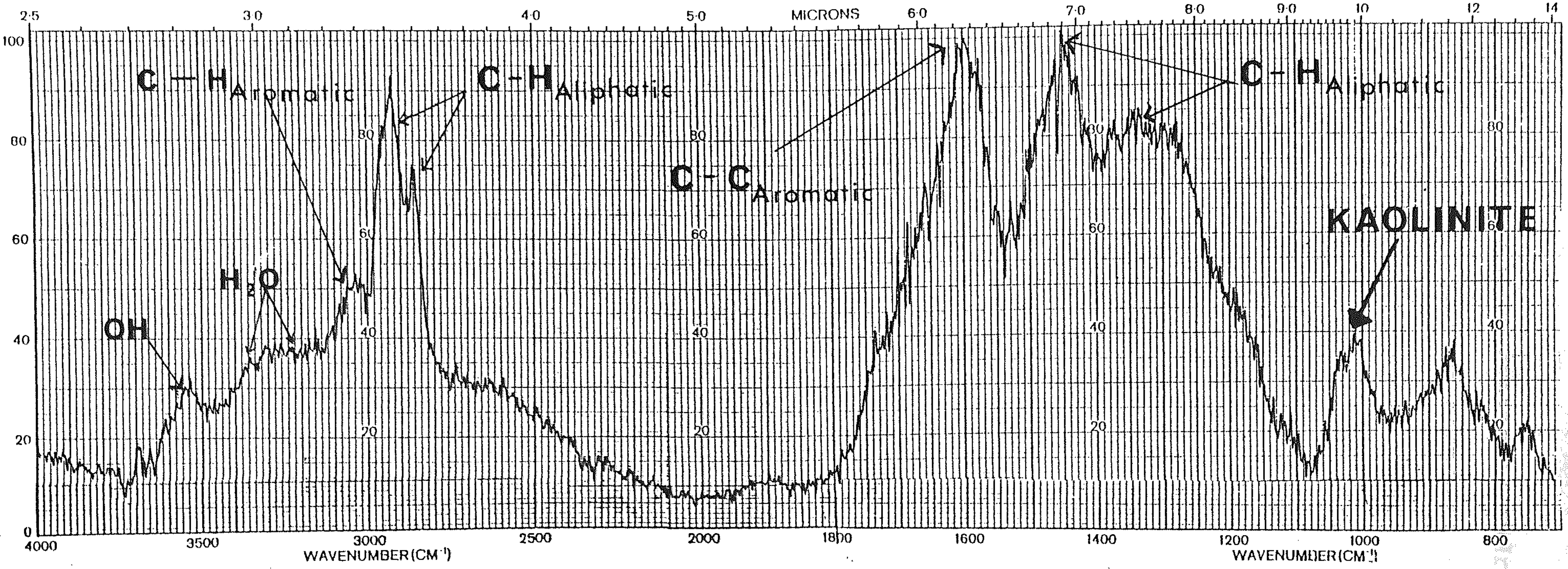

is much less than the ratio of deuterium to available hydrogen present during the pyrolysis. The hydrogen to carbon ratios of cokes prepared under identical pressures of nitrogen and hydrogen were very similar. That is, the presence of hydrogen did not hydrogenate the cokes but increased the yield of volatile products. This was also true when hydrogen was supplied by partial reduction of the initial coal[33]. One concludes that the deuterium present in the cokes had not been introduced by addition but by exchange with existing aromatic hydrogen. Mechanisms for exchange of deuterium with aromatic systems are, of course, well established. That exchange was incomplete suggests either that under the conditions of the pyrolysis exchange was slow or that deuterium was unable to penetrate easily into the pyrolysing solid.

6.3.3 Deuterated Tars

Examination of the tars showed that the 40m, OV-1 coated, glass capillary column used for gas chromatography failed to resolve the different deuterated species and, for example, all the deuterated naphthalenes had about the same retention time and gave a single, rather broad peak on the chromatogram. Appendix 3 shows the mass spectra of the material eluted from near the maximum of typical gas chromatogram peaks. It will be seen that several deuterated species were present in each peak. To make further progress we have concentrated on 'key' ions in the mass spectra. In the mass spectrum of the parent (non deuterated) compound these selected ions were accompanied only by ions of low abundance (intensity not more than 10% of that of the key ions) at neighbouring mass numbers. From the mass spectrum of the material eluted at the maximum of the appropriate GC peak one may readily calculate the relative concentrations of the different deuterated species from the relative intensities of the higher mass number neighbours of the key ion. For example, comparison of the peak heights at mass numbers 115 - 122 gave the relative intensities of the ions $C_9H_7^+$ to $C_9D_7^+$ obtained from the deuterated methyl naphthalenes. These calculations assume the probabilities of fragmentation and ionisation of a deuterated molecule to be independent of the number of deuterium atoms. The results of the calculations for twelve compounds selected as typical of those occurring in the tar are shown in table 6.3. It is seen that the tar molecules were often highly deuterated, the ratio of deuterium to hydrogen varying from 1 to 2.6 . The ratio varied from one compound to another in a manner which suggests that eventually the formation of the compounds may have to be considered individually. The high levels of deuterium imply that, as with the cokes, most deuterium atoms entered the compounds by exchange with hydrogen atoms through the intermediacy of π electron complexes. Table 6.3 compares the observed distribution of deuterium and hydrogen atoms with that given by a random scrambling of these atoms. A random scrambling distribution would be obtained if the hydrogen and deuterium atoms were in thermodynamic equilibrium and differences in C-H and C-D bond energies could be neglected. The distribution of deuterium and hydrogen in the twelve compounds considered was in fact in reasonable agreement with the random scrambling prediction. The agreement was particularly good for dibenzofuran and for the C_3 phenol. It

Table 6.3 Relative Deuterium Distributions of Twelve Compounds Present in Deuterated Tar

MS: Distribution from mass spectrum.

RS: Calculated distribution if random scrambling of deuterium and hydrogen atoms occurred and the ratio of deuterium to hydrogen was that quoted in the final column.

Parent Compound	Distribution	Ions										Overall D/H Ratio
C_3 Phenol		$C_8H_9O^+$	$C_8H_8DO^+$	$C_8H_7D_2O^+$	$C_8H_6D_3O^+$	$C_8H_5D_4O^+$	$C_8H_4D_5O^+$	$C_8H_3D_6O^+$	$C_8H_2D_7O^+$	$C_8HD_8O^+$	$C_8D_9O^+$	
	MS	3	6	14	48	92	100	66	28	8	0	1.08
	RS	1	5	22	57	93	100	71	32	8	1	1.07
C_2 Phenol		$C_7H_7O^+$	$C_7H_6DO^+$	$C_7H_5D_2O^+$	$C_7H_4D_3O^+$	$C_7H_3D_4O^+$	$C_7H_2D_5O^+$	$C_7HD_6O^+$	$C_7D_7O^+$			
	MS	3	4	32	74	100	89	29	3			1.32
	RS	1	8	34	75	100	79	34	6			1.32
Methylindan		$C_9H_9^+$	$C_9H_8D^+$	$C_9H_7D_2^+$	$C_9H_6D_3^+$	$C_9H_5D_4^+$	$C_9H_4D_5^+$	$C_9H_3D_6^+$	$C_9H_2D_7^+$	$C_9HD_8^+$	$C_9D_9^+$	
	MS	0	18	25	31	63	89	100	40	14	0	1.18
	RS	0	3	17	47	85	100	78	39	11	1	1.18

Table 6.3 Continued

Parent Compound	Distribution	Ions										Overall D/H Ratio
β - Methyl-naphthalene		$C_9H_7^+$	$C_9H_6D^+$	$C_9H_5D_2^+$	$C_9H_4D_3^+$	$C_9H_3D_4^+$	$C_9H_2D_5^+$	$C_9HD_6^+$	$C_9D_7^+$			
	MS	0	8	23	61	82	100	54	14			1.64
	RS	0	4	22	60	100	98	53	12			1.65
α - Methyl-naphthalene	MS	0	5	16	51	62	100	45	14			1.75
	RS	0	3	18	54	95	100	57	14			1.75
Dimethyl-naphthalene *		$C_{11}H_9^+$	$C_{11}H_8D^+$	$C_{11}H_7D_2^+$	$C_{11}H_6D_3^+$	$C_{11}H_5D_4^+$	$C_{11}H_4D_5^+$	$C_{11}H_3D_6^+$	$C_{11}H_2D_7^+$	$C_{11}HD_8^+$	$C_{11}D_9^+$	
	MS	0	0	5	16	67	70	100	72	34	6	1.72
	RS	0	0	5	19	50	87	100	73	31	6	1.73
Dimethyl-naphthalene	MS	0	0	0	29	46	98	100	78	31	5	1.72
	RS	0	1	5	19	50	87	100	73	31	6	1.72
Dimethyl-naphthalene	MS	4	5	21	28	60	90	100	55	29	6	1.40
	RS	0	2	10	33	71	100	93	56	19	3	1.40
Dimethyl-naphthalene	MS	0	0	10	21	44	92	100	46	14	0	1.47
	RS	0	1	8	30	67	100	98	61	22	3	1.48

* Four isomeric dimethylnaphthalenes were distinguished on the gas chromatogram. These are listed in the table in increasing order of retention times.

Table 6.3 Continued

Parent Compound	Distribution	Ions											Overall D/H Ratio
Dibenzo-furan		$C_{11}H_7^+$	$C_{11}H_6D^+$	$C_{11}H_5D_2^+$	$C_{11}H_4D_3^+$	$C_{11}H_3D_4^+$	$C_{11}H_2D_5^+$	$C_{11}HD_6^+$	$C_{11}D_7^+$				
	MS	0	0	13	43	81	100	52	18				1.94
	RS	0	0	13	45	88	100	64	17				1.96
Methyl-fluorene		$C_{13}H_9^+$	$C_{13}H_8D^+$	$C_{13}H_7D_2^+$	$C_{13}H_6D_3^+$	$C_{13}H_5D_4^+$	$C_{13}H_4D_5^+$	$C_{13}H_3D_6^+$	$C_{13}H_2D_7^+$	$C_{13}HD_8^+$	$C_{13}D_9^+$		
	MS	0	0	9	24	52	73	100	55	19	5		1.55
	RS	0	1	7	26	62	97	100	66	25	4		1.55
Pyrene		$C_{16}H_{10}^+$	$C_{16}H_9D^+$	$C_{16}H_8D_2^+$	$C_{16}H_7D_3^+$	$C_{16}H_6D_4^+$	$C_{16}H_5D_5^+$	$C_{16}H_4D_6^+$	$C_{16}H_3D_7^+$	$C_{16}H_2D_8^+$	$C_{16}HD_9^+$	$C_{16}D_{10}^+$	
	MS	12	13	19	64	50	83	100	76	45	16	0	1.09
	RS	0	3	13	39	76	100	91	56	23	5	1	1.09

was less satisfactory for pyrene. Agreement can be improved by assuming that two populations of molecule were present each of which enjoyed random scrambling, the ratios of the two hypothetical populations being adjusted to give agreement with the observed experimental results.

The agreement between the observed distribution of deuterium and hydrogen in the twelve compounds and the predictions of random scrambling suggests that the distribution of hydrogen was controlled by thermodynamics rather than by kinetics. A typical random scrambling calculation for dibenzofuran is given in appendix 3.

6.3.4 Deuterium in Liquor

Polar hydroxyl groups undergo hydrogen-deuterium exchange very readily. The refractive index measurements showed the deuterium:hydrogen ratio of liquor from which ammonia and hydrogen sulphide had been removed was 1.1 . One had expected a rather higher proportion of deuterium but impurities in the liquor may have caused errors in the interpretation of the refractive index measurement.

6.3.5 Deuterated Gases

Table 6.4 shows the relative proportions of the deuterated gases and compares these with the corresponding predictions of random scrambling. In fact there is a good agreement between the observed distribution of methanes and the random scrambling distribution. This is the third occasion[33,46] on which it has been shown that the formation of methane by low temperature pyrolysis has been found to be controlled by thermodynamics and it begins to look as if the result may be general. The distributions of the other hydrocarbon gases show deviations from random scrambling, the proportions of di- (and higher) deuterated to singly deuterated species being consistently higher than predicted. Nevertheless, the concentration ratios (singly deuterated compound)^2/ (non deuterated compound) (dideuterated compound) are nearly the same for ethane, propane and butane. This expression is the ratio of the equilibrium constants for the reactions

$$D_2 + RCH_3 \rightleftharpoons RCH_2D + HD$$

and

$$D_2 + RCH_2D \rightleftharpoons RCHD_2 + HD$$

and the results therefore suggest the possibility that thermodynamic equilibrium, had been established during pyrolysis[46,52] the deviation from random scrambling being a consequence of the

Table 6.4 Relative percentages of the volumes of deuterated gases

(Initial deuterium to coal ratio = 140 KPa/g and the final pressure, at 500°C, = 2.64 ± 0.07 MPa)

Deuterated Methanes

	CH_4	CH_3D	CH_2D_2	CHD_3
MS	48.6	37.9	13.5	-
RS	49	39	11	1

Deuterated Ethenes

	C_2H_4	C_2H_3D	$C_2H_2D_2$	C_2HD_3
MS	49.5	24.9	17.4	8.2
RS	49	39	11	1

Deuterated Ethanes

	C_2H_6	C_2H_5D	$C_2H_4D_2$
MS	61.6	27.9	10.5
RS	60	33	7

Deuterated Propanes

	C_3H_8	C_3H_7D	$C_3H_6D_2$	$C_3H_5D_3$
MS	48.3	31.1	14.9	5.7
RS	42	40	15	3

Deuterated Butanes

	C_4H_{10}	C_4H_9D	$C_4H_8D_2$
MS	45.1	34.5	20.4
RS	43	41	16

MS : Values obtained by mass spectrometry

RS : Values predicted if there had been random scrambling of appropriate amounts of hydrogen and deuterium atoms.

greater stability of C-D compared to C-H bonds.

It has usually been supposed that gaseous hydrocarbons are evolved during the pyrolysis of coals from the aliphatic portion of the structure[1,53]. Thus the formation of methane from alkyl groups during hydropyrolysis may be represented by the equations

$$RCH_2CH_3 + X_2 \rightleftharpoons RCH_2X + CH_3X$$

$$RCH_2X + X_2 \rightleftharpoons RX + CH_2X_2 ,$$

where X_2 represents deuterium or hydrogen, whilst the formation of other hydrocarbon gases may accord with such equations as

$$R(CH_2)_3CH_3 + X_2 \rightleftharpoons RCH_2X + CH_3CH_2CH_2X$$

$$R(CH_2)_3CH_2X + X_2 \rightleftharpoons RCH_2X + CH_2XCH_2CH_2X .$$

Such a naive description hides the complexity of the free radical chains which occur. The weakest bonds are those β to the aromatic rings[54] and the carbon-carbon bonds in extended aliphatic side chains[55]. Rose et al[49] emphasise the importance of methyl radicals as intermediates in methane formation during the pyrolysis of benzylated coal. Initiation of pyrolysis will be followed by simultaneous radical chains in the gas phase, in the fluid phase and on the surface of the coal-coke. The relative importance of these reactions will vary with the temperature and the pressure of pyrolysis and, indeed, in the pyrolyses (table 5.11) the yields of methane,

ethane and butane showed a slightly complicated dependence on pressure. In addition to the pyrolysis of aliphatic side chains gas is formed in the presence of hydrogen or deuterium by the cracking of fluid material and, especially at elevated temperatures, by the direct hydrogenation of the solid coke (see for example reference 56 and table 4.2) and these reactions result in some methane being formed from aromatic carbon atoms. The deuterium distributions suggest that this system of reactions yields a thermodynamic distribution of hydrogen atoms.

The most important result of table 6.4 is that the ratio of hydrogen to deuterium involved in the capping of radicals which is given approximately by the $(CH_4):(CH_3D)$, $(C_2H_6):(C_2H_5D)$, $(C_3H_8):(C_3H_7D)$ and $(C_4H_{10}):(C_4H_9D)$ ratios is shown to have been about 1.25 - 2.25 to 1 . In other words hydrogen was more involved in the breaking of alkyl chains and the capping of radicals than was deuterium. This, despite the fact that at the beginning of the pyrolysis there was more than twice as much deuterium in the autoclave as gas than there was hydrogen in the coal.

If one considers a simplified model in which hydrogen is generated in the centre of the coal and diffuses, reacting as it goes, to the outside where there is a hydrogen pressure, P_o , then it is evident that the concentration of hydrogen at any point within the coal is the sum of two independent terms. Each term satisfies the diffusion equation; the first, due to the formation of hydrogen, satisfies boundary conditions of being zero at the external surface of the coal and equal to the generating function at the centre of the coal, whilst the second gives the concentration of hydrogen in the coal due to the external pressure, being zero initially. For the second term the average concentration of hydrogen at time t in a sphere of coal of radius a due to an external pressure P_o is given by

$$P_o\left[1 - 6/\pi^2\left(\exp(-\alpha t) + {}^1/_4\exp(-4\alpha t) + {}^1/_9\exp(-9\alpha t) + \ldots\right)\right]$$

where $a^2\alpha/\pi^2$ is the coefficient of diffusion[57]. This expression illustrates the obvious point that an increase in the external hydrogen (deuterium) pressure increases the concentration of hydrogen within the pyrolysing coal. Such a line of argument leads one to expect that this extra hydrogen would produce an increased yield of volatile material during pyrolsis and at 500°C the yield of volatile material did in fact increase with hydrogen pressure, the relationship appearing to be linear above 4.5 MPa (see table 5.2). At the beginning and end of pyrolysis deuterium diffuses through pores, accordingly αt is large and the average pressure of deuterium in the solid due to the external atmosphere is close to P_o. Manvers being a coking coal, plasticity was developed during pyrolysis and a coherent coke resulted. The diffusion constant for the passage of deuterium in plastic material can be estimated using the Stokes-Einstein equation given in chapter 2, page 12. This is many orders of magnitude smaller than the diffusion constant for travel through the micropore system[58] (see tables 2.1b and 2.6), αt will be small and the average pressure within the bed due to the external pressure will be significantly smaller tnan P_o. The surprise is not that relatively little deuterium participated in hydrocarbon gas formation but that any was effective at all. Heat entered from the outside of the bed towards the centre and consequently it will have been the edge of the bed which first pyrolysed and became plastic. The formation of plastic material would tend to seal the bed from the external deuterium and slow down the emergence of hydrogen from the bed. The hydrogen within the bed, unable to escape rapidly, participates in localised reactions within the coal. Molecular hydrogen emerges from pyrolysing coal only after 'resolidification' has diminished plasticity. Thus it seems that a major effect of pressure is to determine the rates of diffusion within the pyrolysing system. It should be recalled that the result of pyrolysis in hydrogen is to modify and generally increase the maximum fluidity generated[59] and to reduce the accessible micropore volume in the resulting coke (see table 5.9). Thus the effect of pressure on the rates of diffusion will be somewhat complicated.

The recognition that relatively little deuterium entered the pyrolysing coal suggests that the highly deuterated tar molecules must have been formed by exchange either in the vapour phase at the upper temperatures of pyrolysis or in the outer layer of the plastic phase.

6.3.6 Pyrolyses with Pyrite and Tetralin

Mixtures of Manvers coal with 5% of pyrite and with 5% of tetralin were also pyrolysed in deuterium under standard autoclave conditions. Yields are shown in table 6.2 (page 130). Although the yields were changed slightly by the presence of the additives the deuterium to hydrogen ratios found in the cokes, the twelve selected tar compounds and the hydrocarbon gases were , within experimental error, unchanged.

Pyrite has been used frequently in liquefaction experiments to promote transport of hydrogen from one part of the system to another[60,61,62]. Mössbauer studies of the cokes showed that in the present experiments the pyrite had become converted to clumps of pyrrhotite during pyrolysis. This implies that some sulphur had been 'lost' by the pyrite, presumably as hydrogen (deuterium) sulphide. Table 6.2 indicates that this was accompanied by the cracking of some of the THF soluble tar but there appears to have been no effect on the distribution of hydrogen or deuterium during pyrolysis. The deuterium to hydrogen ratios of liquor (1.1), tar molecules (1 to 2) and cokes (0.4) were unchanged by the presence of pyrite. The relative percentage of the volumes of deuterated gas were also unchanged. Diffuse reflectance infra red spectra of deuterated semicokes (a typical spectrum is given in figure 6.5) were unchanged by the presence of pyrite.

Figure 6.5 Diffuse Reflectance Infra Red Spectrum of a Deuterated Semicoke Produced in the Presence of Pyrite

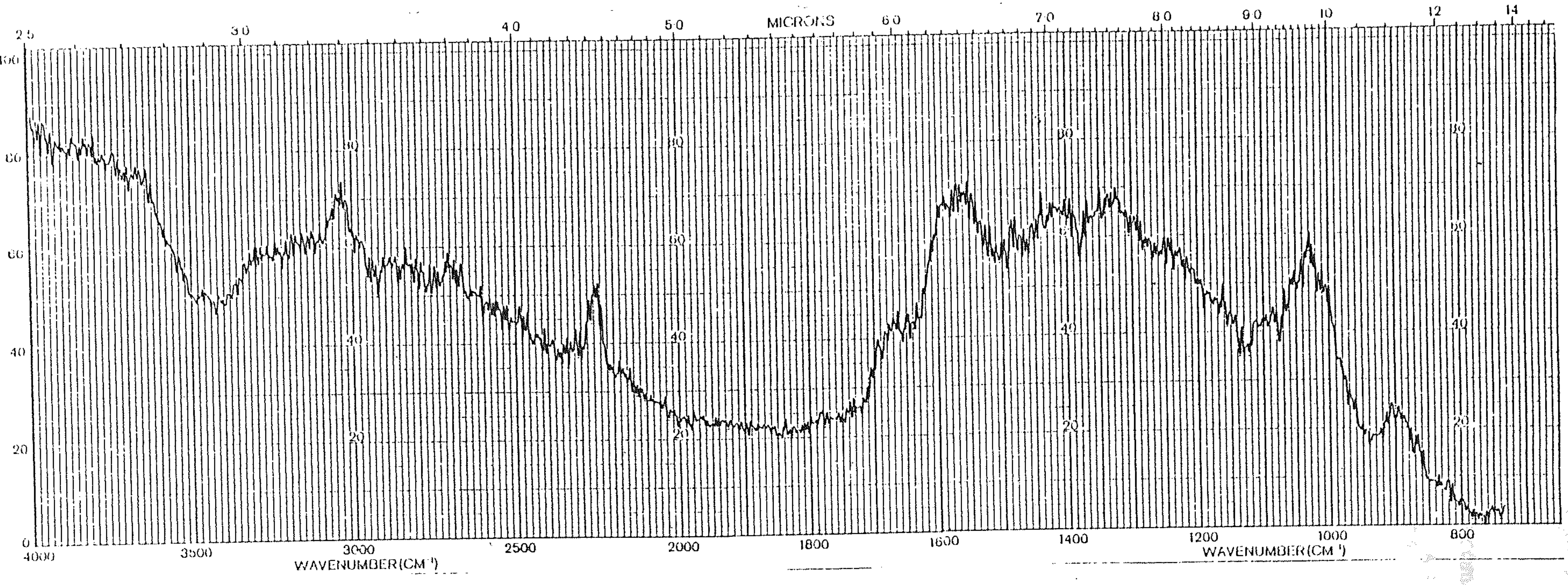

Tetralin has often been used as a hydroaromatic solvent in investigations of liquefaction mechanisms[63,64,65]. Table 6.2 indicates that in the present experiments the presence of tetralin increased the yields of coke , tar and gas. The toluene soluble tar became exceptionally rich in naphthalene (table 6.5) and it seems therefore that the tetralin did indeed contribute hydrogen to the pyrolysis. The relative percentage of the volumes of deuterated gas were unchanged by the presence of tetralin as were the deuterium to hydrogen ratios of the tar (1 to 2), liquor (1.1) and coke (0.4). Diffuse reflectance infra red spectra of deuterated semi-cokes (a typical spectrum is given in figure 6.6) produced in the presence of tetralin showed that they were similar to those produced in the absence of a catalyst (figure 6.3, page 132).

The catalytic hydrogenation of coal is always difficult in as much as it is difficult to spread a potential catalyst uniformly throughout the coal structure. The major product of all the pyrolyses of Manvers coal has been a semicoke with an atomic H/C ratio of a third. Whereas aromatic material readily exchanges hydrogen via π complexes, there appears to be no pathway for the ready hydrogenation of the coke structure. Under the pyrolysis conditions used here hydrogenation of the coke was always slow and the catalysis of this reaction presents a challenge.

The inability of two known liquefaction catalysts to induce a greater extent of deuteration is entirely consistent with

Table 6.5 Relative concentration of selected molecules found in deuterated tar

Initial deuterium to coal ratio = 140 KPa/g

Final pressure range at 500°C = 2.64 to 2.74 MPa

Molecule*	Relative Concentration		
	Catalyst: none	Catalyst: tetralin	Catalyst: pyrite
Phenol	6.3	2.6	2.0
Methylphenol	10.1	12.7	4.9
C_2 Phenol	1.3	2.3	0.9
Naphthalene	9.0	22.6	9.7
Dimethylindene	0.4	1.4	0.3
Methyltetralin	1.4	2.3	0.6
Methylnaphthalene	7.6	9.9	6.0
Biphenyl	1.0	1.2	1.0
Dihydrophenalene	1.4	2.0	1.1
Dimethylnaphthalene	1.6	5.1	3.7
Methylbiphenyl	1.1	1.9	1.2
Dibenzofuran	0.7	1.5	1.7
Fluorene	2.1	2.4	2.8
Methylfluorene	0.4	0.4	0.4
Anthracene/Phenanthrene	2.6	1.5	5.8

* The relative concentration of the molecule includes deuterated species.

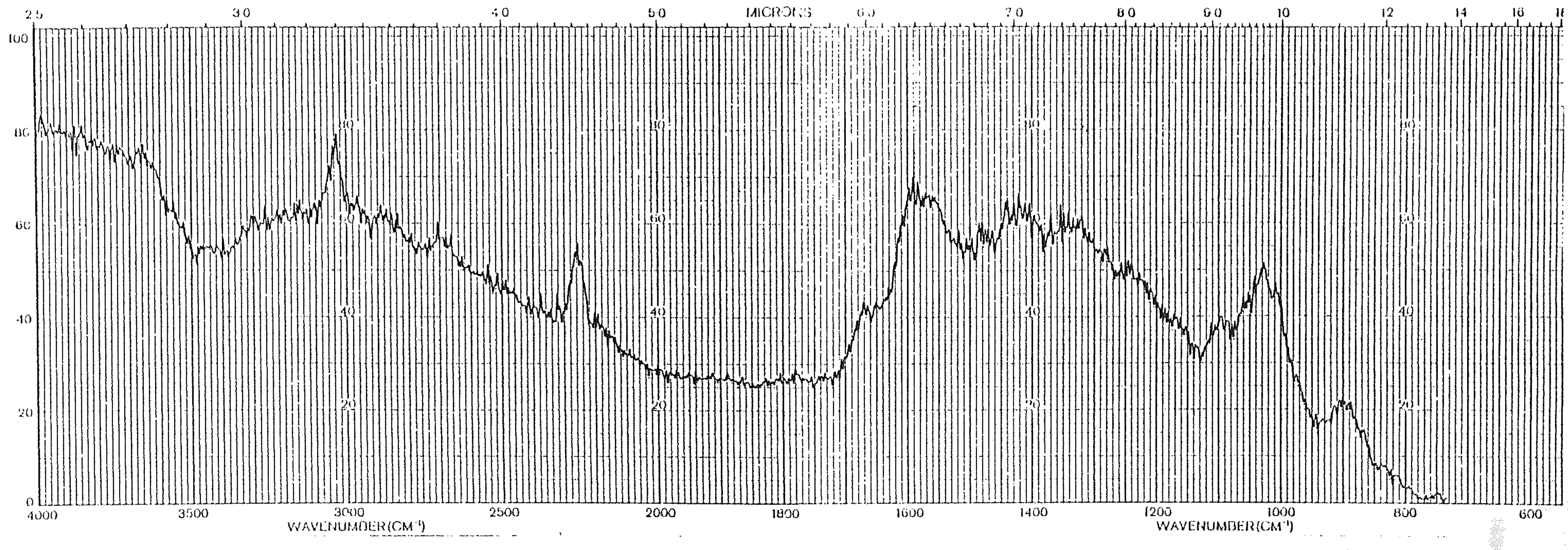

Figure 6.6 Diffuse Reflectance Infra Red Spectrum of a Deuterated Semicoke Produced in the Presence of Tetralin

and goes someway towards confirming the mechanism of deuteration that has been proposed in section 6.3.5, page 146: that the rate and extent of deuteration is controlled by its ability to diffuse through the fluid coal and this is unaffected by the catalysts. Any deuterium which does enter the pyrolysis zone rapidly equilibriates in the thermodynamic sense with the hydrogen atoms in its vicinity and this is a situation which cannot be improved upon by catalysis.

CHAPTER SEVEN

CONCLUSION AND SUGGESTIONS FOR FURTHER WORK

CHAPTER SEVEN

CONCLUSION AND SUGGESTIONS FOR FURTHER WORK

7.1 Conclusion

When Manvers coal was pyrolysed to 500°C the major product was a semicoke having an elemental hydrogen:carbon ratio of a third. This ratio remained roughly constant whether the coal was pyrolysed in nitrogen or in hydrogen. As the initial pressure of hydrogen was increased hydropyrolysis resulted in increasing yields of volatile products. More hydrogen was present in gaseous hydrocarbons than in the other products of hydropyrolysis and this proportion increased with the initial pressure of hydrogen though the total amount of hydrogen consumed per gram of coal from the atmosphere remained constant.

When the pyrolyses were performed under the same conditions in an atmosphere of deuterium the deuterium to hydrogen ratios in the semicokes, in selected tar molecules, in the liquor and in the gaseous hydrocarbons were 0.4, 1 to 2, 1.1 and 0.16 respectively. These were unaffected by the presence of 5% of added pyrite or tetralin and the problem of catalysing the hydrogenation of carbonaceous solids is challenging.

The relative proportions of deuterated methanes were consistent with the random scrambling of deuterium and hydrogen atoms and the results suggest that this may also be true of the distributions of deuterated ethanes, propanes and butanes. In other words the experimental evidence suggests that the most important gas forming reactions were rapid and resulted in a distribution of molecules which was controlled by the structure of the initial coal and by thermodynamics. At the beginning of pyrolysis there were more than twice as many deuterium atoms present as gaseous deuterium than there were hydrogen atoms combined in the coal. Nevertheless the analyses indicate that the deuterium was much less effective than the hydrogen in capping radicals . During pyrolysis the development of plasticity produced semi-permeable material through which deuterium and hydrogen diffused very slowly thereby partially isolating the pyrolysing material from the external deuterium (or hydrogen in hydropyrolysis) and causing the hydrogen released by pyrolysis to participate in local reactions before it could escape from the coal. The major effects of an external pressure of hydrogen or deuterium appear to arise through increasing the concentration of hydrogen or deuterium within the pyrolysing coal and delaying the diffusion of hydrogen and hydrocarbons from the coal. The effects are in a sense self enhancing. The sealing of the system by the plastic material and the increased concentration of hydrogen generates yet more fluid material so that the micropore structure collapses or becomes blocked, transport within the pyrolysing mass is further slowed and local reactions occur to an even greater extent. Under nitrogen pressures the concentration of hydrogen is lower and plastic material cracks to gases and solid rather than yielding smaller molecules of tar. This description is clearly consistent with the fact that hydropyrolysis gave a strong, swollen coke whilst pyrolysis under nitrogen gave a coke which was barely coherent.

The rather high deuterium to hydrogen ratios observed in selected tar molecules suggest that deuterium became incorporated through exchange with hydrogen atoms in the aromatic rings. The distributions of deuterated species were close to those predicted by random scrambling of deuterium and hydrogen atoms.

7.2 Suggestions for further work

Further investigation of a range of solid fuels to confirm the observations that have been reported would yield a substantial clarification of the mechanism of pyrolysis and hydropyrolysis at slow rates of heating.

Comparison of the hydropyrolysis of a coking and a non-coking coal (or a lignite) would be interesting because the latter does not become plastic during pyrolysis and therefore hydrogen and the products of pyrolysis would be able to diffuse relatively faster. Hence, a greater tar and gas yield would be expected.

Faster rates of heating should also be studied since they diminish secondary reactions, the cracking of tar to give gas, and produce tar of much higher molecular weight.

APPENDIX 1

Thermodynamic Calculations: a worked example

Table 2, page 163, represents thermodynamic data (ΔH_R, ΔS_R and ΔG_R) for selected reactions. Consider the following reaction taken from table 2:

$$C_{14}H_{12}\,(s) \longrightarrow C_{14}H_{10}\,(s) + H_2\,(g)$$

9,10-Dihydrophenanthrene → Phenanthrene

The various thermodynamic quantities for this and other reactions in table 2 have been calculated in the manner shown below.

	$\Delta H^o_{f,298}$ KJ/mol	ΔS^o_{298} J/mol K
H_2 (g)	0	130.56
$C_{14}H_{12}$ (s)	66.3	229.40
$C_{14}H_{10}$ (s)	116.20	215.06

All necessary heats of formation and entropy data for selected molecules are given in appendix 1, table 1. The heat of formation for some molecules in their solid state has not been cited in the literature and therefore as a good approximation, the heat of formation in the liquid state of the molecule has been used instead.

Calculation Of Enthalpy Of Reaction, $\Delta H_{R,298}$

$$\Delta H_{R,298} = \Sigma(\Delta H^{o}_{f,298}(\text{products})) - \Sigma(\Delta H^{o}_{f,298}(\text{reactants}))$$

$$= (\Delta H^{o}_{f,298}(C_{14}H_{10}(s) + \Delta H^{o}_{f,298}(H_2(g))) - (\Delta H^{o}_{f,298}(C_{14}H_{12}(s)))$$

$$= (116.20 + 0) - (66.3)$$

$$= 49.90 \text{ KJ/mole}$$

Calculation Of Entropy Of Reaction, $\Delta S_{R,298}$

$$\Delta S_{R,298} = \Sigma(\Delta S^{o}_{298}(\text{products})) - \Sigma(\Delta S^{o}_{298}(\text{reactants}))$$

$$= (\Delta S^{o}_{298}(C_{14}H_{10}(s) + \Delta S^{o}_{298}(H_2(g))) - (\Delta S^{o}_{298}(C_{14}H_{12}(s)))$$

$$= (215.06 + 130.56) - (229.4)$$

$$= 116.22 \text{ J/mole K}$$

Calculation Of Gibbs Free Energy, $\Delta G_{R,298}$ and $\Delta G_{R,800}$

$$\Delta G = \Delta H - T\Delta S \quad \text{and} \quad \Delta G_{R,298} = \Delta H_{R,298} - T\Delta S_{R,298}$$

$$\Delta G_{R,298} = (49.90) - (298 \times 116.22 / 1000)$$

$$= 15.26 \text{ KJ/mole}$$

Assuming that ΔH_R and ΔS_R vary little with temperature then:

$$\Delta G_{R,800} = \Delta H_{R,298} - T\Delta S_{R,298}$$

$$= (\ 49.90\ ) - (\ 800 \times 116.22\ /\ 1000\ )$$

$$= -\ 43.07\ \text{KJ/mole}$$

Calculation of Gibbs Free Energy at 800 K and 10 Atmospheres

The value obtained for $\Delta G_{R,800}$(I atm) needs to be corrected for pressure effects as follows:

$$\Delta G = \pm\ 2.303\ n\ R\ T\ \log_{10}(P_2/P_1) \qquad \text{Joules}$$

Where:
P_2 = 10 atmospheres
P_1 = 1 atmosphere
R = 8.314 J/mole K
T = 800 K
n = number of moles of gas that are under going a volume increase (+) or a volume decrease (-), when we consider the reaction going from left to right.

$$\Delta G_{800,P_2} = \Delta G_{800,P_1} + \Delta G$$

In the present reaction involving the dehydrogenation of 9,10-Dihydrophenanthrene there is a volume increase and therefore,

$$G = + 2.303\ n\ R\ T\ \log_{10}\ (P_2/P_1) \qquad \text{Joules}$$

and $n = 1$

$$\Delta G = + 19.14 \times 800 \times \log_{10}\ (10/1)$$

$$= 19.14 \times 800 \times 1$$

$$= 15.3\ \text{KJ/mole}$$

and

$$\Delta G_{R,800,10\ atm} = \Delta G_{R,800,1\ atm} + \Delta G$$

$$= - 43.07 + 15.3$$

$$= - 27.77\ \text{KJ/mole}$$

Similarly, $\Delta G_{R,800}$ at 100 atmospheres is:

$$\Delta G = - 2.303\ R\ T\ \log_{10}(P_2/P_1)$$

P_2 = 100 atmospheres

P_1 = 1 atmosphere

$$\Delta G = - 30.6\ \text{KJ/mole}$$

and $$\Delta G_{R,800,100\ atm} = \Delta G_{800,1\ atm} + \Delta G$$

$$\Delta G_{R,800,100\ atm} = -\ 43.07 \quad + \quad 30.6$$

$$= -\ 12.47\ KJ/mole$$

Similarly, $\Delta G_{R,800,1000\ atm} = +\ 2.83\ KJ/mole$

Table 1

Thermodynamic Data

Molecule	$\Delta H^{o}_{f,298}(g)$ KJ/mole	$\Delta H^{o}_{f,298}(l/s)$ KJ/mole	$\Delta S^{o}_{298}(g)$ J/mole K	$\Delta S^{o}_{298}(s)$ J/mole K
Hydrogen[66]	0		130.56	
Water[66]	-241.82		188.71	
Methane[66]	-74.85		186.27	
Ethane[66]	-83.85		229.12	
Propane[66]	-104.68		270.20	
Phenol[67]	-94.10	-165.10(s)	328.40	149.4
Toluene[66]	50.17	12.18(l)	320.13	189.3
Naphthalene[66]	150.58	78.53(s)	333.15	167.4
Benzene[66]	82.93	49.08(l)	269.45	147.0
Tetralin[66]	26.61	-28.58(l)	369.64	200.4
Biphenyl[67]	172.80	96.65(s)	348.53	205.85
Diphenylmethane[67]	151.50	88.91(l)	319.03	154.8
Phenanthrene[66]	207.10	116.20(s)	394.50	215.06
Anthracene[66]	227.69	129.20(s)	385.92	207.15
Diphenylethane[67,70]	116.3	44.06(s)	463.65	269.45
n-Hexadecane[67,68]	-373.34	-454.3 (l)	778.30	450.8
n-Octadecane[67]	-414.55	-568.69(s)	856.21	496.64
n-Propylbenzene[66]	7.90	-38.30(l)	398.40	261.3
Cyclohexane[66]	-123.13	-156.23(l)	298.23	204.1
9,10-Dihydro-phenanthrene[69]	155.4	66.3 (s)	416.3	229.4
Diphenylether[71]	71.12	-32.1 (s)		233.9

Table 2 Thermodynamic Analysis of Selected Reactions

Reaction	$\Delta H_{R,298}$ 1 Atm KJ/mole	$\Delta S_{R,298}$ 1 Atm J/mol K	$\Delta G_{R,298}$ 1 Atm KJ/mole	$\Delta G_{R,800}$ 1 Atm KJ/mole	$\Delta G_{R,800}$ 10 Atm KJ/mole	$\Delta G_{R,800}$ 100 Atm KJ/mole	$\Delta G_{R,800}$ 10^3 Atm KJ/mole
$CH_3CH_2CH_3(g) + H_2(g) \rightarrow C_2H_6(g) + CH_4(g)$	-54.02	14.63	-58.38	-65.72	-65.72	-65.72	-65.72
$nC_{18}H_{38}(s) + H_2(g) \rightarrow nC_{16}H_{34}(s) + C_2H_6(g)$	30.54	52.72	14.83	-11.63	-11.63	-11.63	-11.63
$C_6H_5CH_2CH_2C_6H_5(s) + H_2(g) \rightarrow 2C_6H_5CH_3(s)$	-19.70	-21.41	-13.32	-2.57	-17.87	-33.17	-48.47
$C_6H_5CH_2CH_2CH_3(s) + H_2(g) \rightarrow C_2H_6(g) + C_6H_5CH_3(s)$	-115.73	18.41	-121.21	-130.46	-130.46	-130.46	-130.46
$C_6H_5OC_6H_5(s) + H_2(g) \rightarrow C_6H_5OH(s) + C_6H_6(s)$	-83.92	-68.06	-63.64	-29.47	-44.77	-60.07	-75.37
$C_6H_5OH(s) + H_2(g) \rightarrow C_6H_6(s) + H_2O(g)$	-27.64	55.75	-44.25	-72.24	-72.24	-72.24	-72.24
$C_6H_5CH_2C_6H_5(s) + H_2(g) \rightarrow C_6H_5CH_3(s) + C_6H_6(s)$	-27.65	50.94	-42.83	-68.40	-83.70	-99.00	-114.30
$C_6H_6(s) + 3H_2(g) \rightarrow C_6H_{12}(s)$	-205.31	-334.58	-105.60	62.35	16.45	-29.45	-75.35
$C_6H_5C_6H_5(s) + H_2(g) \rightarrow 2C_6H_6(s)$	1.51	-42.41	14.15	35.44	20.14	4.84	-10.46
$C_6H_5OC_6H_5(s) + H_2O(g) \rightarrow 2C_6H_5OH(s)$	-56.28	-123.81	-19.38	42.77	27.47	12.17	-3.13
Tetralin(s) $\rightarrow$ Naphthalene(s) + $2H_2(g)$	107.11	228.12	39.13	-75.38	-44.78	-14.18	16.42
9,10-Dihydrophenanthrene(s) $\rightarrow$ Phenanthrene(s) + $H_2(g)$	49.90	116.22	15.26	-43.07	-27.77	-12.47	2.83

Atm: Atmosphere (s)

APPENDIX 2

Carbon Dioxide Adsorption Isotherm Data For Manvers Coal

Temperature = 298 K

Sample Weight = 0.9630 g

Free Space = 27.8253 cm^3

Saturation Vapour Pressure of CO_2, P_o = 48237.21 mm Hg

Equilibrium Pressure, P_e (mm Hg)	Volume Adsorbed, V (cm^3/g)	Elapsed Time (hours)
5.52	0.26	2.116
11.35	0.50	2.571
17.39	0.72	2.913
31.82	1.20	3.413
47.66	1.65	3.823
71.50	2.24	4.142
110.98	3.05	4.437
178.44	4.17	4.710
223.56	4.82	4.983
289.92	5.61	5.268
378.26	6.67	5.678
426.61	7.17	5.882
494.99	7.80	6.098
573.62	8.44	6.337
669.10	9.11	6.531
783.88	9.80	6.793

Best Fit To Dubinin-Astakhov Equation

$\ln(V)$	$(\ln(P_o/P_e))^{1.78}$
2.28	12.43
2.21	13.29
2.13	14.16
2.05	15.00
1.97	15.88
1.90	16.61
1.72	18.27
1.57	19.95
1.43	21.46
1.11	24.81
0.81	28.10
0.50	31.29
0.18	34.61
-0.33	39.86
-0.69	43.76
-1.35	50.70

Limiting Micropore Volume, V_o = 0.06 cm^3/g

Characteristic Energy, E = 9.26 KJ/mole

Modal Equiv. Pore Radius, r_e = 0.67 nm

Frequency of the mode, f_{mode} = 0.17 cm^3/g nm

Mean Equiv. Pore Radius, $\bar{r}_e$ = 0.75 nm

Micropore Surface Area, S_{micro} = 162 m^2/g

Carbon Dioxide Adsorption Isotherm Data For A Nitrogen Coke,N3 (Initial Nitrogen to coal ratio = 4 KPa/g and the Final Pressure = 1.90 ± 0.05 MPa)

Temperature = 298 K

Sample weight = 1.1520 g

Free Space = 27.5804 cm^3

Saturation Vapour Pressure of CO_2, P_o = 48237.21 mm Hg

Equilibrium Pressure, P_e (mm Hg)	Volume Adsorbed, V (cm^3/g)	Elapsed Time (hours)
7.34	0.61	26.158
11.13	0.91	27.557
15.36	1.20	28.456
30.92	2.20	30.026
47.45	3.10	31.710
65.21	3.94	32.836
101.03	5.32	33.781
163.98	7.26	34.702
216.23	8.51	35.351
282.05	9.81	35.920
371.00	11.27	36.454
423.44	12.03	36.841
490.35	12.85	37.171
569.23	13.70	37.558
664.22	14.60	37.922
776.31	15.49	38.218

Best Fit To Dubinin-Astakhov Equation

ln (V)	$(\ln(P_o/P_e))^{2.21}$
2.74	22.97
2.68	24.93
2.62	26.95
2.55	29.00
2.49	31.09
2.42	33.04
2.28	37.29
2.14	41.68
1.98	46.54
1.67	55.76
1.37	64.88
1.13	72.00
0.79	82.19
0.18	100.48
-0.09	109.58
-0.49	121.98

Limiting Micropore Volume, V_o	= 0.06	cm^3/g
Characteristic Energy, E	= 11.62	KJ/mole
Modal Equiv. Pore Radius, r_e	= 0.63	nm
Frequency of the mode, f_{mode}	= 0.23	cm^3/g nm
Mean Equiv. Pore Radius, $\bar{r}_e$	= 0.69	nm
Micropore Surface Area, S_{micro}	= 181	m^2/g

Carbon Dioxide Adsorption Isotherm Data for a Hydrogen Coke, H3 (Initial hydrogen to coal ratio = 140 KPa/g and the Final Pressure = 6.66 ± 0.14 MPa)

Temperature = 298 K

Sample Weight = 1.0020 g

Free Space = 27.7213 cm^3

Saturation Vapour Pressure of CO_2, P_o = 48237.21 mm Hg

Equilibrium Pressure, P_e (mm Hg)	Volume Adsorbed V (cm^3/g)	Elapsed Time (hours)
8.17	0.07	27.694
15.88	0.17	28.991
23.18	0.29	30.857
33.80	0.45	32.870
49.69	0.67	34.884
74.54	0.98	36.910
116.05	1.35	38.138
182.23	2.02	40.050
225.76	2.38	41.233
293.52	2.85	42.337
385.83	3.27	42.837
427.10	3.56	43.349
497.43	3.96	43.998
577.53	4.25	44.373
671.55	4.60	44.760
788.52	4.96	45.158

Best Fit To Dubinin-Astakhov Equation

ln (V)	$(\ln(P_o/P_e))^{2.41}$
1.60	30.22
1.53	33.14
1.45	36.03
1.38	39.03
1.27	42.24
1.18	44.46
1.05	50.77
0.87	57.30
0.70	62.97
0.30	75.95
-0.02	90.10
-0.40	104.30
-0.80	118.95
-1.24	134.38
-1.77	150.97
-2.66	182.91

Limiting Micropore Volume, V_o = 0.02 cm^3/g

Characteristic Energy, E = 11.03 KJ/mole

Modal Equiv. Pore Radius, r_e = 0.64 nm

Frequency of the mode, f_{mode} = 0.08 cm^3/g nm

Mean Equiv. Pore Radius, $\bar{r}_e$ = 0.70 nm

Micropore Surface Area, S_{micro} = 61 m^2/g

APPENDIX 3

Mass spectra of twelve deuterated compounds

Four isomeric dimethylnaphthalenes were distinguished on the gas chromatogram. These are given in the appendix in increasing order of retention times.

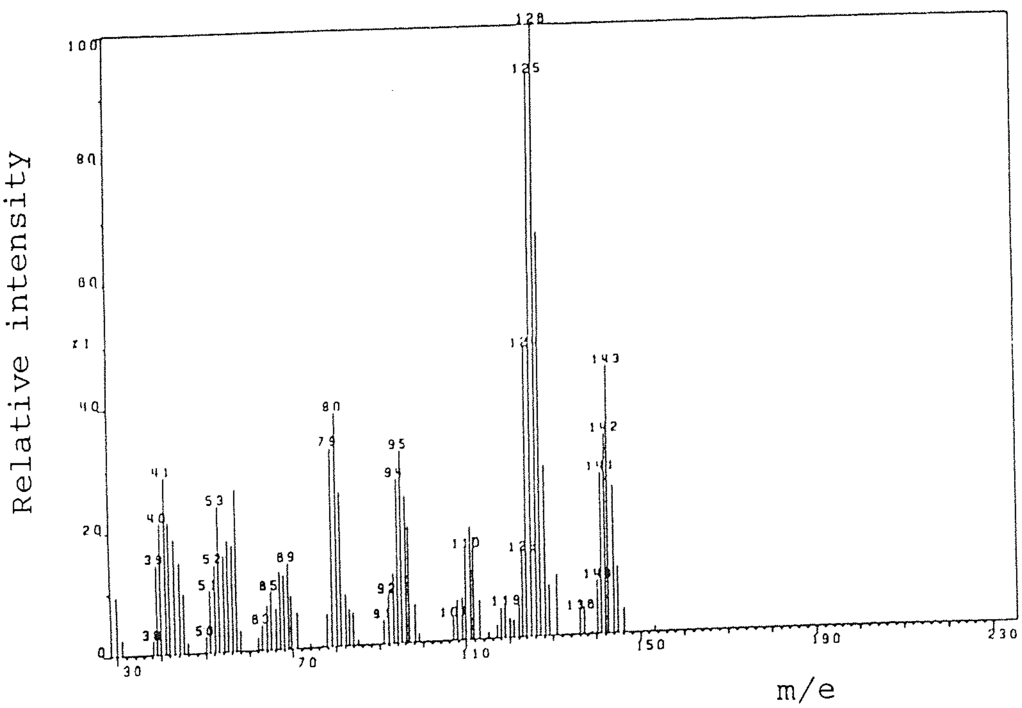

Deuterated C_3 Phenol

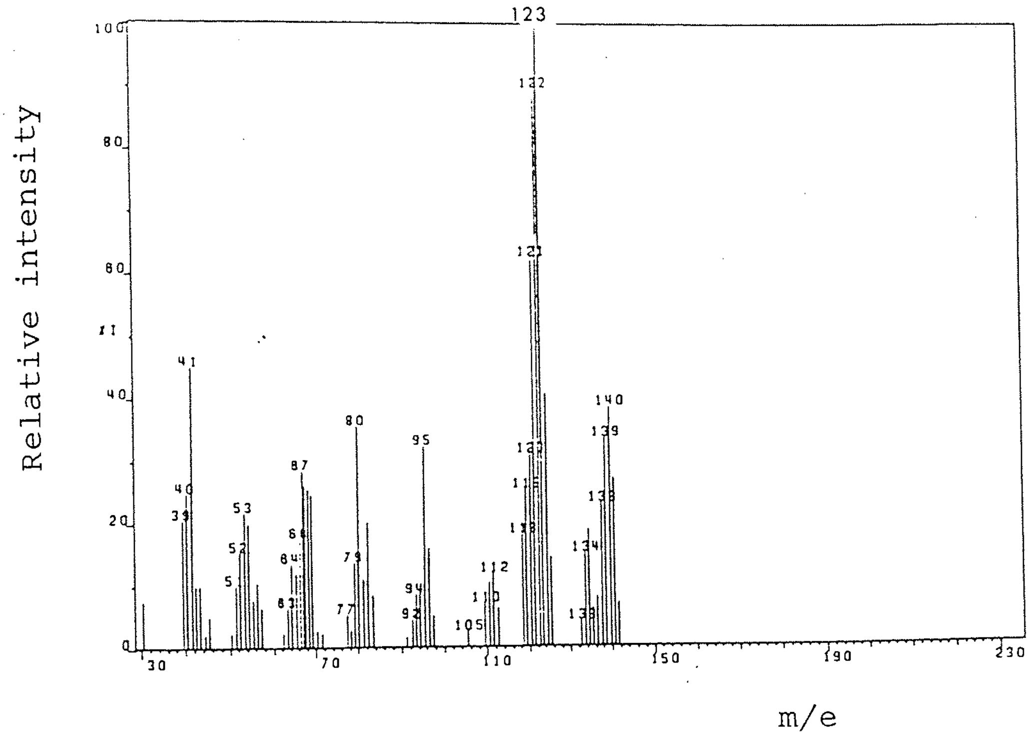

Deuterated Methylindan

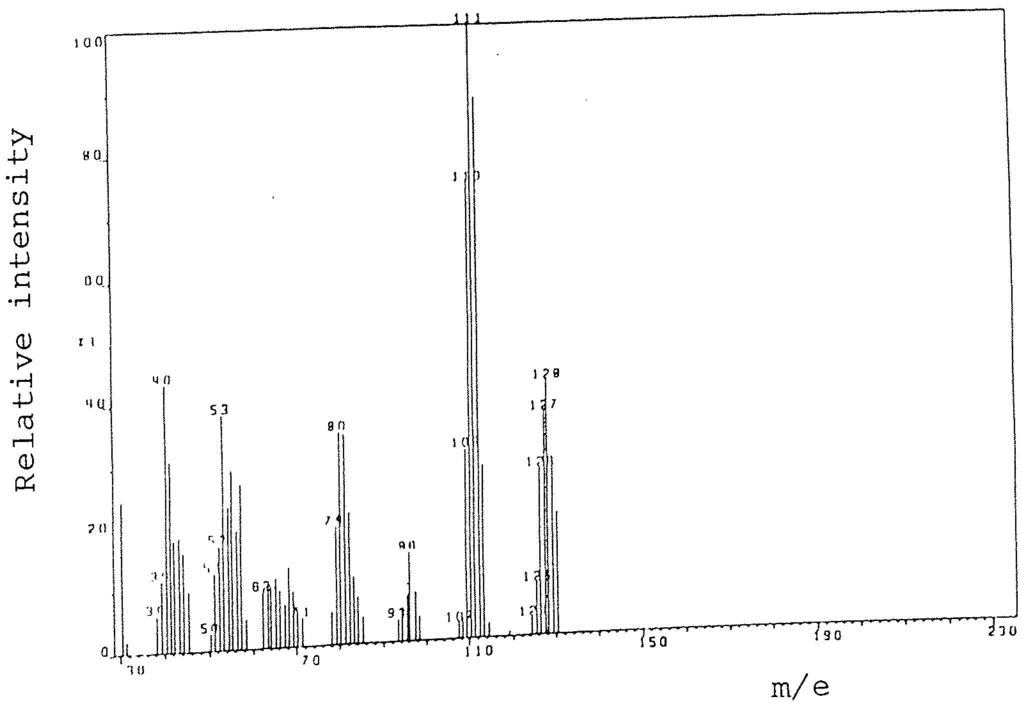

Deuterated C_2 Phenol

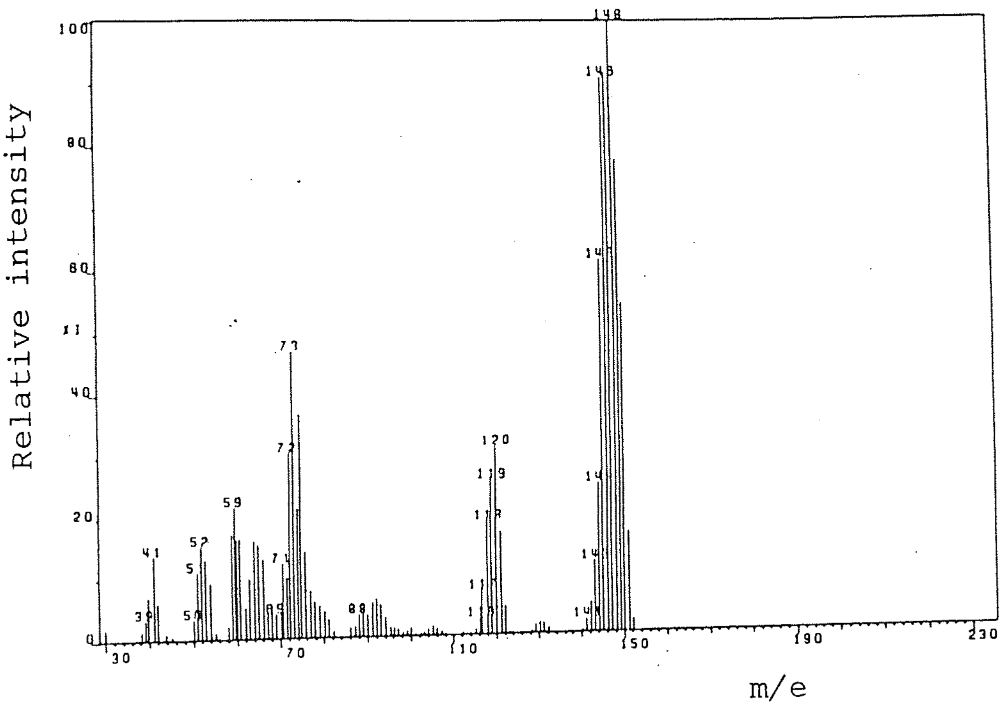

Deuterated β-Methylnaphthalene

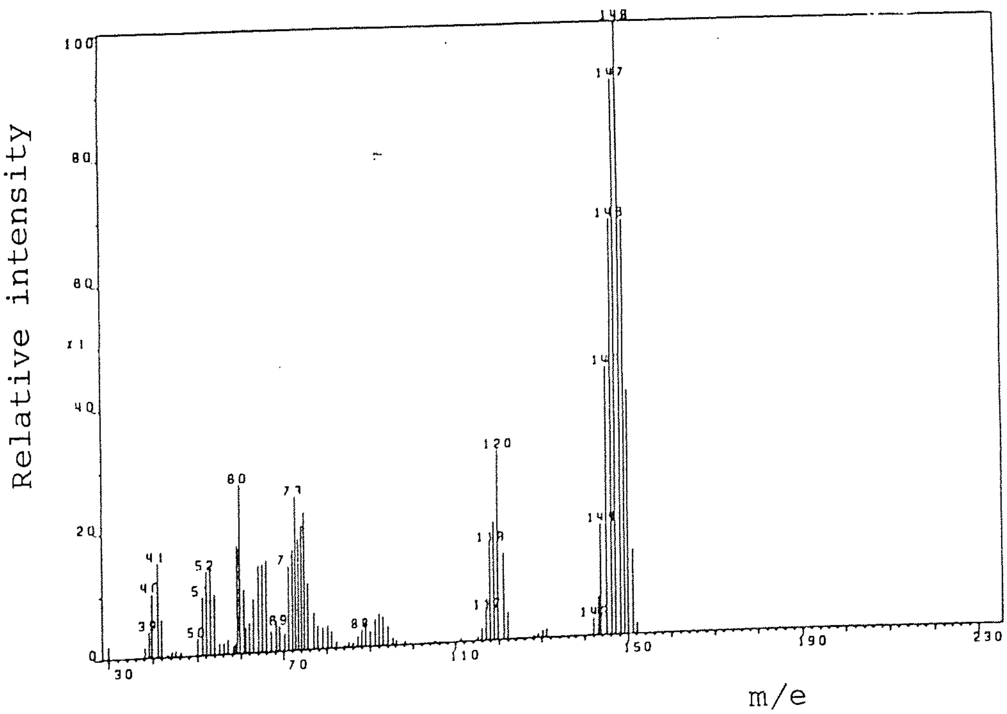

Deuterated α-Methylnaphthalene

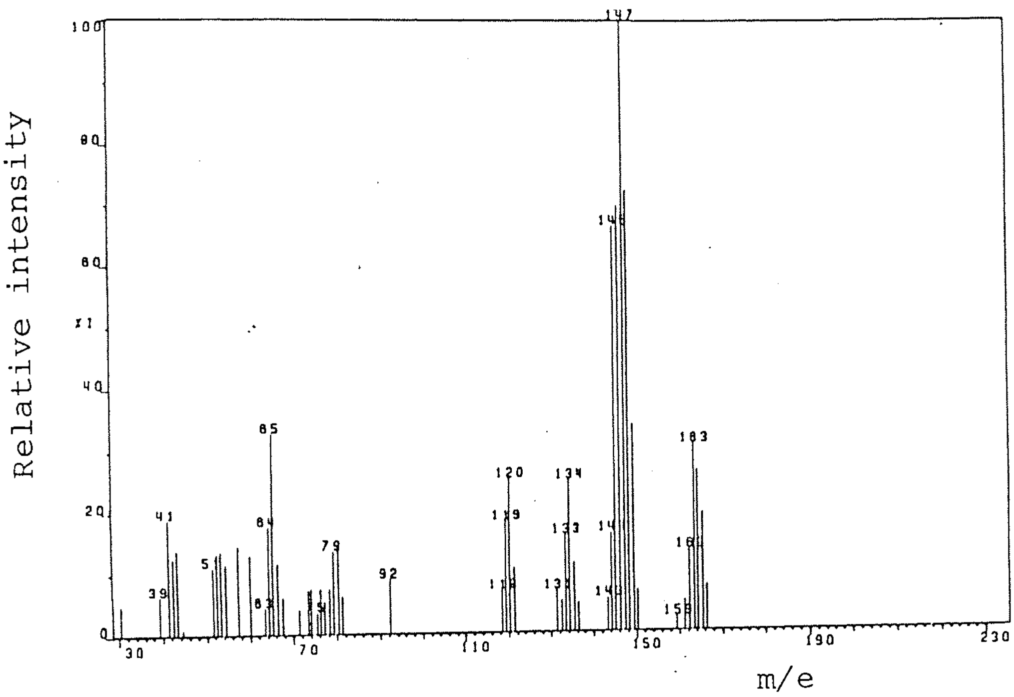

Deuterated Dimethylnaphthalene

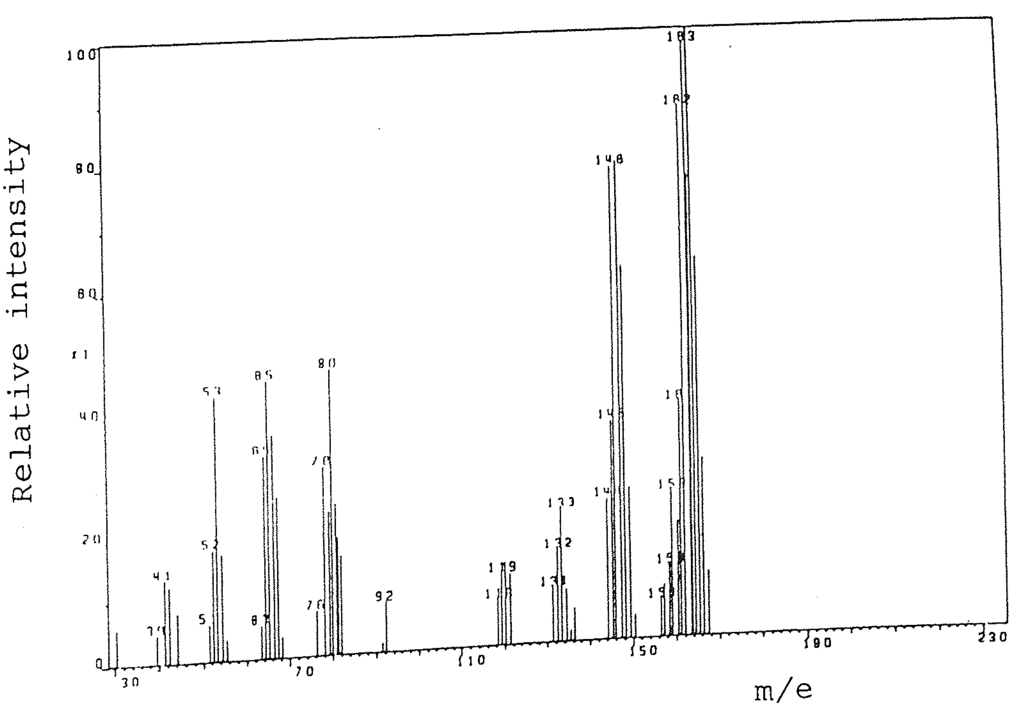

Deuterated Dimethylnaphthalene

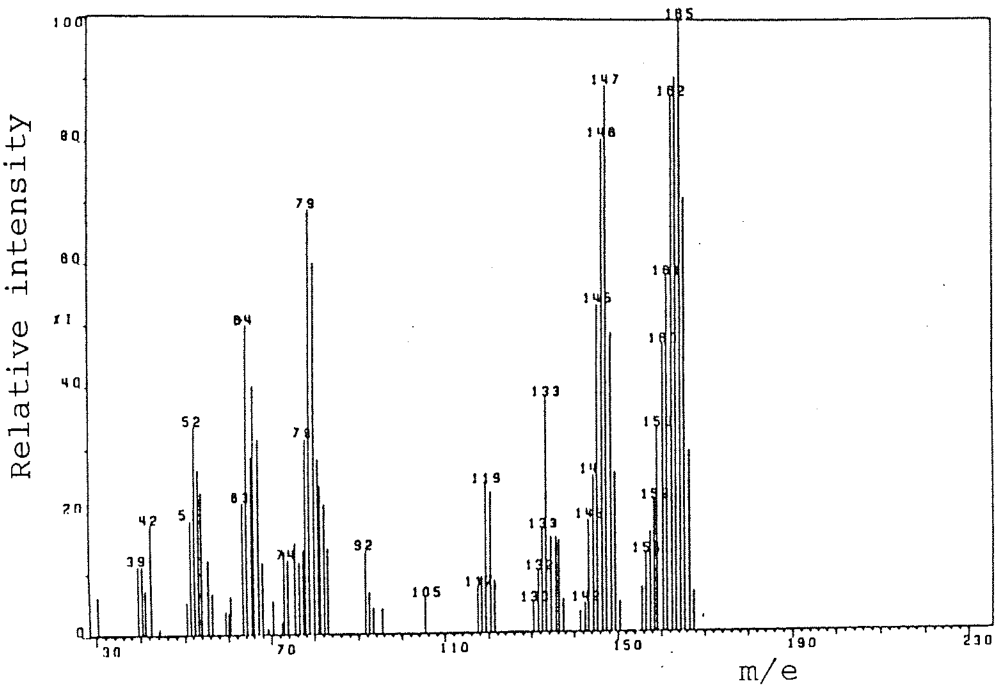

Deuterated Dimethylnaphthalene

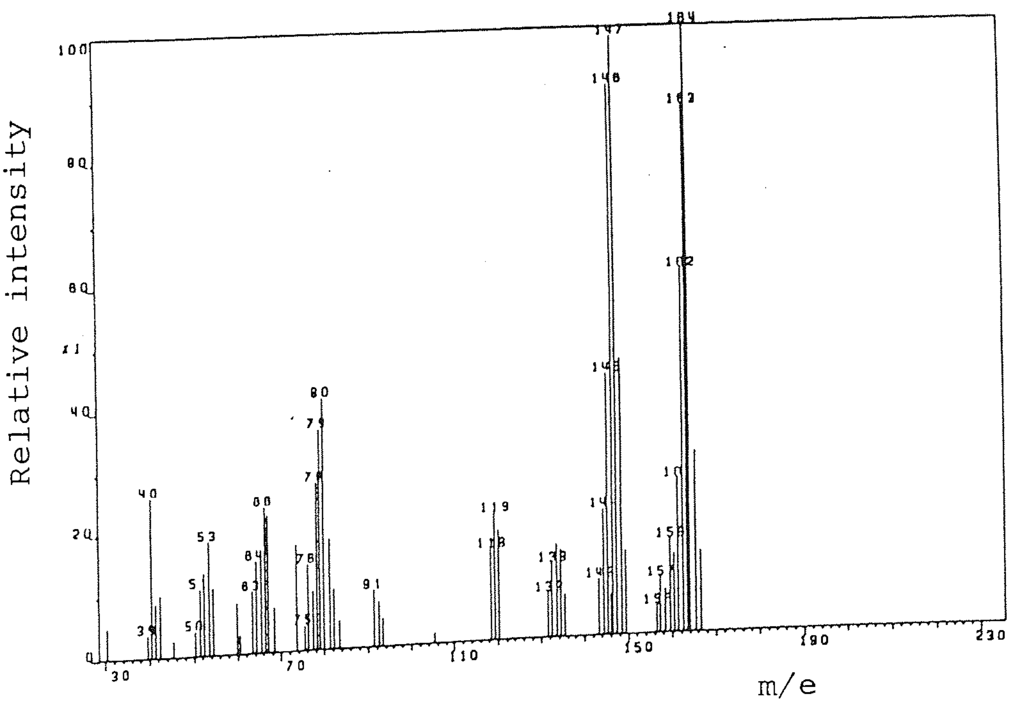

Deuterated Dimethylnaphthalene

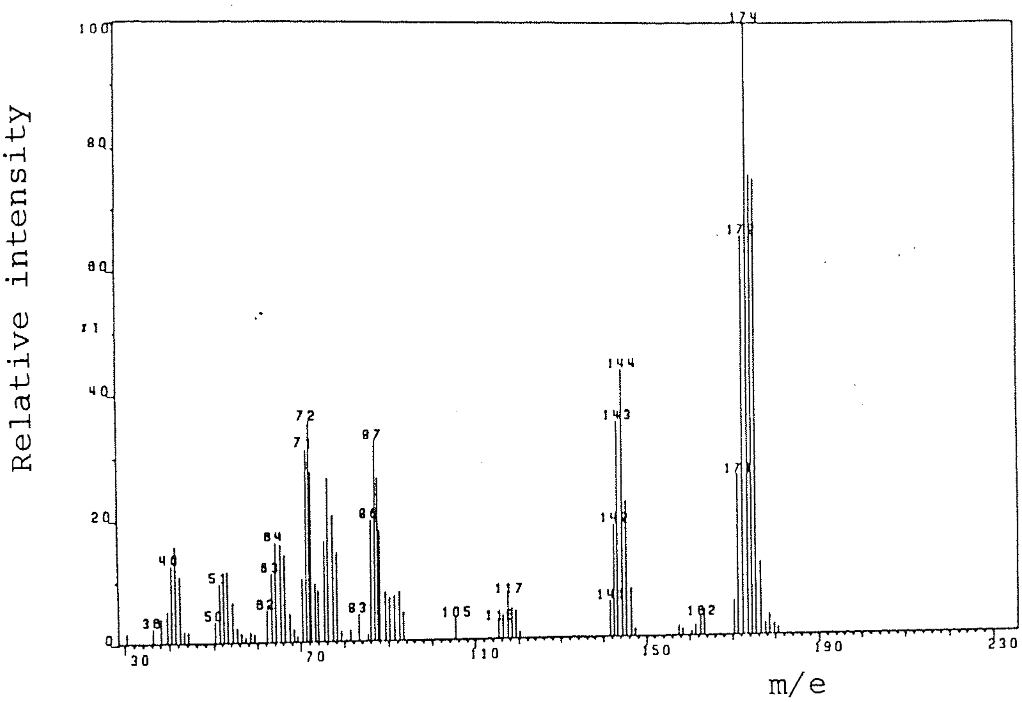

Deuterated Dibenzofuran

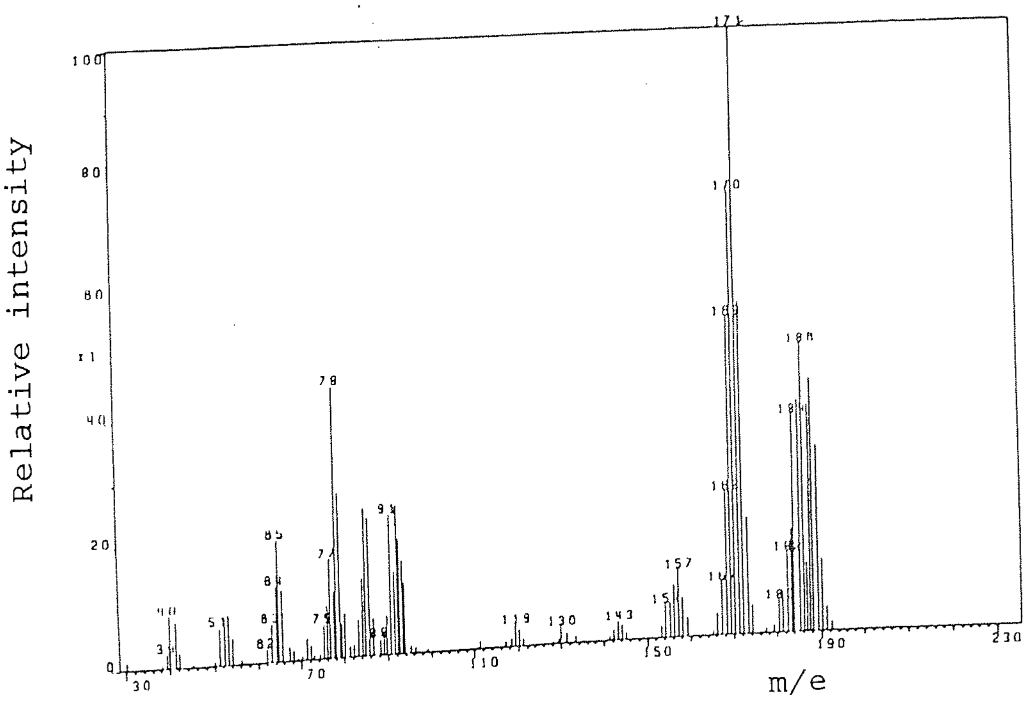

Deuterated Methylfluorene

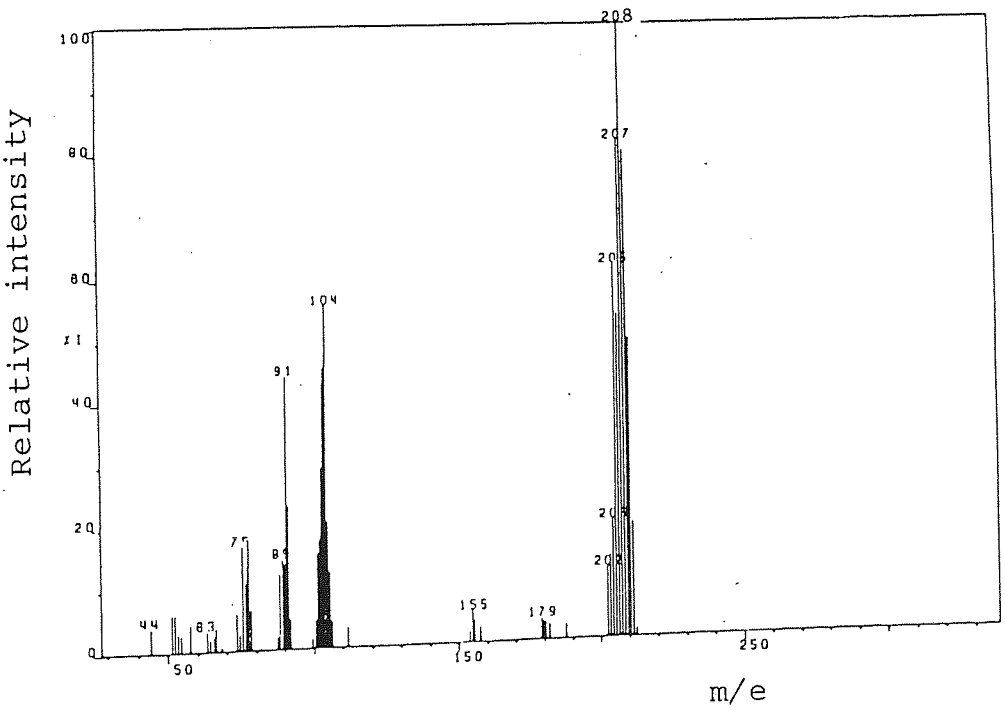

Deuterated Pyrene

Random scrambling calculation for dibenzofuran

In the mass spectrum of non deuterated dibenzofuran the peak at mass number 139 was due to the 'key' ion $C_{11}H_7^+$, and this ion was accompanied only by ions of low abundance (intensity not more than 10% of the key ion) at neighbouring mass numbers.

Consider the mass spectrum of deuterated dibenzofuran given in this appendix. From this mass spectrum one may readily calculate the relative concentrations of the different deuterated species from the relative intensities of the higher mass number neighbours of the key ion. For example, comparison of the peak heights at mass numbers 141 - 146 gave the relative intensities of the ions $C_{11}H_5D_2^+$(13), $C_{11}H_4D_3^+$(43), $C_{11}H_3D_4^+$(81), $C_{11}H_2D_5^+$(100), $C_{11}H\ D_6^+$(52) and $C_{11}D_7^+$(18). Relative intensities of these ions are given in brackets.

The relative proportions of deuterium atoms, D, and hydrogen atoms, H, in the ions were calculated by multiplying the relative intensity of each ion by the deuterium or hydrogen fraction in the ion. For the ion $C_{11}H_5D_2^+$, D is equal to 3.71 (13 x 2/7) and H is equal to 9.29 (13 x 5/7). Table 1 shows the D and H values for all the ions. The total relative amount of deuterium in the ions, D', is equal to 202.43 and the total relative amount of hydrogen in the ions, H', is equal to 104.57. Hence the overall deuterium to hydrogen ratio is 1.94.
Consider the formation of $C_{11}H_5D_2^+$. If we consider the random scrambling of 202 deuterium atoms and 104 hydrogen atoms then

Table 1 Deuterium(D) and Hydrogen(H) values of ions

Ion	Relative Intensity from mass spectrum	D	H
$C_{11}H_5D_2^+$	13	3.71	9.29
$C_{11}H_4D_3^+$	43	18.43	24.57
$C_{11}H_3D_4^+$	81	46.29	34.71
$C_{11}H_2D_5^+$	100	71.43	28.57
$C_{11}H\ D_6^+$	52	44.57	7.43
$C_{11}D_7^+$	18	18	0

the number of ways (combinations) in which we can pick 5 hydrogen atoms and 2 deuterium atoms is given by the expression H'(H'-1)(H'-2)(H'-3)(H'-4) D'(D'-1) / 5! 2! , where H'is equal to 104 and D' is equal to 202. A similar treatment was applied to the other ions and the results are given in table 2. Table 2 shows that the relative distribution (relative number of combinations) of ions calculated from the random scrambling of hydrogen and deuterium atoms is very similar to the distribution obtained from the mass spectrum of dibenzofuran.

Table 2 Random Scrambling of Hydrogen and Deuterium Atoms

Ion	Number of ways (combinations) in which the appropriate number of hydrogen and deuterium atoms can be picked	Relative number of combinations	Relative intensity from mass spectrum
$C_{11}H_5D_2^+$	$\frac{H'(H'-1)(H'-2)(H'-3)(H'-4)\ D'(D'-1)}{5!\ 2!} = 1.87 \times 10^{12}$	13	13
$C_{11}H_4D_3^+$	$\frac{H'(H'-1)(H'-2)(H'-3)\ D'(D'-1)(D'-2)}{4!\ 3!} = 6.40 \times 10^{12}$	45	43
$C_{11}H_3D_4^+$	$\frac{H'(H'-1)(H'-2)\ D'(D'-1)(D'-2)(D'-3)}{3!\ 4!} = 1.26 \times 10^{13}$	88	81
$C_{11}H_2D_5^+$	$\frac{H'(H'-1)\ D'(D'-2)(D'-2)(D'-3)(D'-4)}{2!\ 5!} = 1.43 \times 10^{13}$	100	100
$C_{11}H\ D_6^+$	$\frac{H'\ D'(D'-1)(D'-2)(D'-3)(D'-4)(D'-5)}{6!} = 9.10 \times 10^{12}$	64	52
$C_{11}\ D_7^+$	$\frac{D'(D'-1)(D'-2)(D'-3)(D'-4)(D'-5)(D'-6)}{7!} = 2.45 \times 10^{12}$	17	18

$D' = 202$

$H' = 104$

REFERENCES

1. Dicker, P.H., Gaines, A.F. and Stanley, L., Journal of Applied Chemistry, 1963, 13, 455

2. Buravas, S., Gaines, A.F., Hasadsri, T., Prasertwitayakij, A. and Sucharitakul, N., Fuel, 1970, 49, 180

3. Petrakis, L., Grandy, D.W. and Jones, G.L., Fuel, 1982, 61, 21

4. Retcofsky, H.L., Stark, J.M. and Friedel, R.A., Analytical Chemistry, 1968, 40, 1699

5. Van Krevelen, D.W., Huntjens, F.J. and Dormans, H.N.M., Fuel, 1956, 35, 462

6. Finlayson, P.C. and Macrae, J.C., Residential Conference on Science in the use of Coal, 15-17 April, 1958, C-15 , Published by the institute of Fuel. Gaines, A.F., Loc. Cit., C-58

7. Lynch, L.J. and Webster, D.S., Fuel, 1979, 58, 235

8. Howard, J.B., Chemistry of coal utilization, edited by Elliott, M.A., 2nd supplementary volume, page 665, Wiley-Interscience, 1981

9. Gavalas, G.R., Coal Pyrolysis (coal and science technology), Elsevier, 1982

10. Adkins, H. and Reid, W.A., Journal of American Chemical Society, 1941, 63, 741

11. Hooper, R.J., Battaerd, H.A.J. and Evans, D.G., Fuel, 1979, 58, 132

12. Berkovitch, I. and McCulloch, A., Fuel, 1946, 25, 41

13 Halleux, A., Delavarenne, S. and Tschamler, H., Nature, 1961, 190, 437

14. Halleux, A. and de Greef, H., Fuel, 1963, 42, 185

15. Carson, D.W. and Ignasiak, B.S., Fuel, 1980, 59, 757

16. Kroÿer, C., Darsuw, G., Fuhr, K. and Erdöl, u., Kohle, 1965, 181, 701

17. Alemany, L.B., Handy, C.I. and Stock, L.M., American Chemical Society, Division of Fuel Chemistry preprints, 1979, 24, 156

18. Alemany, L.B., Advanced Chemical Series, Coal Structure, Edited by Gorbaty, M.L. and Ouchi, K., American Chemical Society, 1981, 192, 207

19. Ignasiak, B.S. and Gawlak, M., Fuel, 1977, 56, 216

20. Howard, J.B., Chemistry of Coal Utilization, Edited by Elliott, M.A., 2nd Supplementary Volume, page 753, Wiley-Interscience, 1981

21. Furfari, S., Annales des Mines de Belgique, 1981, 12, 1069

22. Cyprès, R. and Furfari, S., Fuel, 1981, 60, 768
Cyprès, R. and Furfari, S., Fuel, 1982, 61, 721

23. Geoffrey, F., James, R.G., Ladner, W.R. and Newman, J.O.H., Fuel, 1984, 63, 897

24. Gavalas, G.R., Coal Pyrolysis (coal and science technology), Elsevier, page 77, 1982

25. Van Krevelen, D.W. and Schuyer, J., Coal Science, Elsevier, page 289, 1957

26. Gieseler, K., Glückauf, 1934, 70, 178

27. Lowry, H.H., Chemistry of Coal Utilization, Supplementary Volume 1, page 159, Wiley-Interscience, 1983

28. Atkins, P.W., Physical Chemistry, Oxford university press, 2nd edition, page 884, 1982

29. Gavalas, G.R., Coal Pyrolysis (coal and science technology), Elsevier, page 104, 1982

30. Gavalas, G.R., Coal Pyrolysis (coal and science technology), Elsevier, page 111, 1982

31. Howard, J.B., Chemistry of Coal Utilization, Edited by Elliott, M.A., 2nd Supplementary Volume, page 727, Wiley-Interscience, 1981

32. I.P. Standards for Petroleum and its products, Institute of Petroleum, London, Part 1, page 812, 1964

33. Gaines, A.F. and Yürüm, Y., Fuel, 1976, 55, 129

34. Medek. J., Fuel, 1977, 56, 132

35. Spitzer, Z., Bíba, V. and Kadlec, O., Carbon, 1976, 14, 153

36. International Critical Tables (of numerical data, physics, chemistry and technology), McGraw-Hill, New York, Chief Editor: Washburn, E.W., Volume 3, page 127

37. Kubelka, P. and Munk, F., Zeifschrift Fur Technische Physik, 1931, 12, 593

38. Kubelka, P., Journal of Optical Society of America, 1948, 38, 448

39. Aristoff, E., Rieve, R.W. and Shalit, H., Chemistry of Coal Utilization, Edited by Elliott, M.A., 2nd Supplementary Volume, page 983, Wiley-Interscience, 1981

40. Organic Electronic Spectral Data, Edited by Kamlet, M.J., Interscience Publishers, New York, Volume 1, 1946 - 1952

41. Organic Electronic Spectral Data, Edited by Wheeler, O.H. and Kaplan, L.A., Interscience Publishers, New York, Volume 3, 1956 - 1957

42. Walker, P.L., Analytical Methods for Coal and Coal Products, Edited by Karr, C., Academic Press, Volume 1, page 132, 1978

43. Dryden, I.G.C., Journal of the Institute of Fuel, 1957, 30, 193

44. Fu, Y.C. and Blaustein, R.D., Chemistry and Industry, 1967, 1257

45. Franz, J.A., Fuel, 1979, 58, 405
Franz, J.A. and Camaioni, D.M., Fuel, 1980, 59, 803
Franz, J.A. and Camaioni, D.M., Fuel, 1984, 63, 990

46. Wilson, M.A. and Vassallo, A.M., Proceedings of International Conference on Coal Science, Düsseldorf, page 338, 1981

47. Kershaw, J.R. and Barrass, G., Fuel, 1977, 56, 455

48. Skowronski, R.P., Heredy, L.A. and Ratto, J.J., Preprints, American Chemical Society, Division of Fuel Chemistry, 1978, 23(4), 155

Ratto, J.J., Heredy, L.A. and Skowronski in Coal Liquefaction Fundamentals, American Chemical Society, Symposium Series, 1980, 139, 347

Skowronski, R.P., Ratto, J.J., Goldberg, I.B. and Heredy, L.A., Fuel, 1984, 63, 440

49. Rose, G.R., Zabransky, R.F., Stock, L.M., Huang, C.B., Srinivas, V.R. and Tze, K., Fuel, 1984, 63, 1339

50. Gaines, A.F., Proceedings of NATO A.S.I. on New Spectroscopic Methods in Coal Science, Nova Scotia, 1984

51. Mecke, R. and Langenbucher, F., Infra red Spectra of Selected Chemical Compounds, Heyden and Sons, 1961

52. Jones, L.H. and McDowell, R.S., Journal of Molecular Spectroscopy, 1959, 3, 632

53. Wen, C.Y. and Lee, E.S., Coal Conversion Technology, Addison Wesley, 1979, pages 63 and 67

54. Benson, S,W., Foundations of Chemical Kinetics, McGraw-Hill, page 670, 1980

55. Gaines, A.F. and Page, F.M., Journal of Chemical Research (M), page 2624, 1980

56. Dent, F.J., Blackburn, W.H. and Millett, H.C., Institute of Gas Engineers, Communication 190, 1938

57. Carslaw, H.S. and Jaeger, J.C., Conduction of Heat in Solids, Oxford University Press, 2nd Edition, page 234, 1959

58. Gavalas, G.R., Coal Pyrolysis (coal and science technology), Elsevier, page 105, 1982

Schaub, G., Peters, W.A. and Howard, J.B., Proceedings of International Conference on Coal Science, Dusseldorf, page 229, 1981

59. Kaiho, M. and Toda, V., Fuel, 1979, 58, 397

60. Mukherjee, D.K. and Chowdhury, P.B., Fuel, 1976, 55, 4

61. Given, P.H., Cronauer, D.C., Spackman, W., Lovell, H.L. and Bimas, B., Fuel, 1975, 54, 34

62. Guin, J.A., Tarver, A.R., Lee, J.M., Lo, L. and Curtis, C.W., Industrial Engineering Chemical Process Design and Development, 1979, 18(3), 371

63. Neavel, R.C., Fuel, 1976, 55, 237

64. Petrakis, L. and Grandy, D.W., Nature, 1981, 289, 476

65. Chien, P.L., Tsai, M.-C., Kapoor, A. and Weller, S.W., International Conference on Coal Science, August 1983, Pittsburgh, USA

66. API 44 Tables, Selected Values of Properties of Hydrocarbons and related compounds, Volume vi, Tables P, 1978 - 1983

67. Karapet'Yants, M.Kh. and Karapet'Yants, M.K., Handbook of Thermodynamic Constants of Inorganic and Organic Compounds, Ann Arbor-Humphrey Science Publishers, London, 1970

68. Landolt - Bornstein, Tables 4. Teil, Kalorische Zustandsgrossen, 1961, page 285

69. Lee, S.H., Journal of Chemical Thermodynamics, 1979, 11, 469

70. Benson, S.W. and Buss, J.H., Journal of Physical Chemistry, 1957, 61, 104

71. Landolt - Bornstein, Tables 4. Teil, Kalorische Zustandsgrossen, 1961, page 331